Departments of Pathology and Urology

Research Program in Systems Oncology (ONCOSYS)

University of Helsinki and Helsinki University Hospital

Helsinki, Finland

Doctoral Program in Clinical Research (KLTO).

Building Blocks of Prostate Cancer Diagnostics

Kevin Sandeman

Doctoral Dissertation

With the approval of the Faculty of Medicine at the University of Helsinki, this dissertation is presented for public discussion in Biomedicum, Haartmaninkatu 3, Lecture Hall 2, on November 10th, 2023, at 13:00.

Helsinki 2023

Supervised by

Tuomas Mirtti, MD, PhD, Adjunct Professor

Medicum and Research Program in Systems Oncology

Department of Pathology, HUS Diagnostic Center

University of Helsinki and Helsinki University Hospital

Helsinki, Finland

Antti Rannikko, MD, PhD, Professor

Department of Urology

HUS, Clinicum and Research Program in Systems Oncology

University of Helsinki and Helsinki University Hospital

Helsinki, Finland

Reviewed by

Pirkko-Liisa Kellokumpu-Lehtinen, MD, PhD, Professor, Emerita

Department of Oncology

University of Tampere

Tampere, Finland

Leena Latonen, PhD, Docent

Institute of Biomedicine

University of Eastern Finland

Kuopio, Finland

Opponent

GJLH (Arno) van Leenders, MD, PhD, Associate Professor

Department of Pathology

Erasmus MC

Rotterdam, Netherlands

Publisher: University of Helsinki / Series: Dissertationes Universitatis Helsingiensis 59/2023

ISBN 978-951-51-9456-5 (print) // ISBN 978-951-51-9457-2 (online)ISSN 2954-2898 (print) // ISSN 2954-2952 (online)

PunaMusta, Joensuu 2023

To Yuma, Miku and Sae

Contents

Abbreviations 5

List of original publications 8

Author's contributions 9

Abstract 11

Sammanfattning 12

1 Introduction 13

2 Literature review 15

2.1 The Prostate 15

2.2 Prostate cancer 16

2.2.1 Definition 16

2.2.2 Molecular properties and genetic alterations 17

2.2.3 Risk factors 18

2.2.4 Incidence, prevalence, and mortality 18

2.2.5 Histology 18

2.3 Diagnosis of prostate cancer 19

2.3.1 Screening 19

2.3.2 Digital rectal examination and transrectal ultrasound 20

2.3.3 Magnetic resonance imaging 20

2.3.4 PSMA positron emission tomography 21

2.3.5 Prostate biopsy 21

2.3.6 Grading and staging 22

2.4 Artificial Intelligence algorithms 28

2.4.1 Validation of Artificial Intelligence algorithms 29

2.4.2 Clinical digital pathology 30

2.5 Management of prostate cancer 31

2.5.1 Overview 31

2.5.2 Active surveillance and watchful waiting 34

2.5.3 Radiotherapy 35

2.5.4 Radical prostatectomy 35

2.5.5 Hormonal therapy 36

2.5.6 Immunotherapies 37

2.6 Disease prediction 39

2.6.1 Nomograms 39

2.6.2 Biomarkers in prostate cancer 41

3 Aims of the study 43

4 Materials and methods 44
4.1 Data sources and ethics statement 44
4.2 Study settings 44
4.2.1 Study I-III 44
4.2.2 Study IV 47
4.3 Statistics 49
5 Results 51
5.1 Study I 51
5.2 Study II 56
5.3 Study III 60
5.4 Study IV 66
6 Discussion 72
6.1 Study I 72
6.2 Study II 74
6.3 Study III 75
6.4 Study IV 75
7 Conclusions 77
8 Acknowledgments 78
9 References 80
10 Original publications 100

Abbreviations

177Lu-PSMA-617	lutetium-177 prostate-specific membrane antigen-617
ABI	Abiraterone
ADC	apparent diffusion coefficient
ADT	androgen deprivation therapy
AI	artificial intelligence
AJCC	American Joint Committee on Cancer
AMACR	a-methylacyl-CoA racemase
APA	Apalutamide
APCC	Advanced Prostate Cancer Consensus Conference
AR	androgen receptor
ARSI	androgen receptor signaling inhibitor
AS	active surveillance
AU ROC	area under the receiver operating characteristic
BCR	biochemical recurrence
BMI	body mass index
BPH	benign prostate hyperplasia
BRCA 1 and 2	Breast Cancer genes 1 and 2
Bx	prostate biopsies
CAPRA	Cancer of the Prostate Risk Assessment
CI	confidence interval
CNN	convolutional neural network
csPCa	clinically significant prostate cancer
ctDNA	circulating tumor DNA (Deoxyribonucleic Acid)
DCE	dynamic contrast-enhanced
DHT	Dihydrotestosterone
DL	deep learning
DRE	digital rectal examination
DSS	disease-specific survival
DWI	diffusion-weighted imaging
EAU	European Association of Urology
EBRT	external beam radiotherapy
ED	erectile dysfunction
ENZ	Enzalutamide
EPE	extraprostatic extension
ERG	v-ets avian erythroblastosis virus E26 oncogene homolog gene
ERSPC	European Randomised Study of Screening for Prostate Cancer
ETS	Erythroblast Transformation Specific
FAP	Fibroblast Activated Protein
FDA	United States Food and Drug Administration
FFPE	formalin-fixed paraffine-embedded
GG	Gleason Grade
GGG	Gleason Grade Group
GnRH	gonadotropin-releasing hormone
GS	Gleason Score
H&E	hematoxylin and eosin
HGPIN	high-grade prostatic intraepithelial neoplasia

HR	hazard ratio
HUS	Helsinki university hospital
HUSLAB	Helsinki University Hospital Laboratory Services
IDLE	indolent lesion of epithelial origin
IHC	Immunohistochemistry
LA	Lymphadenectomy
LHRH	luteinizing hormone-releasing hormone
LIS	laboratory information system
lncRNA	long non-coding RNA
LNM	lymph node metastasis
mCRPC	(metastatic) castration-resistant prostate cancer
mCSPC	(metastatic) castration-sensitive prostate cancer
MDM	multidisciplinary meetings
MFS	metastases-free survival
MLH1	MutL Homolog 1
MMR	mismatch repair
mpMRI	multiparametric magnetic resonance imaging
MRI	magnetic resonance imaging
MSH2	MutS Homolog 2
MSH6	MutS Homolog 6
MSKCC	Memorial Sloan Kettering Cancer Center
NPV	negative predictive value
NS	node status
OS	overall survival
PACS	picture archiving and communication system
PAD	pathological anatomical diagnosis
PARPi	poly ADP-ribose polymerase inhibition
PCa	prostate cancer
PET	positron-emission tomography
PHI	Prostate Health Index
PI-RADS	Prostate Imaging Reporting and Data System
PLCO	Prostate, Lung, Colorectal and Ovarian cancer screening study
PLND	pelvic lymph node dissection
PMS2	Postmeiotic Segregation Increased 2
PPV	positive predictive value
PRECISE	Prostate Cancer Radiological Estimation of Change in Sequential Evaluation
PSA	prostate-specific serum antigen
PSMA	prostate-specific membrane antigen
pT	pathologic stage
PTEN	Phosphatase and Tensin Homolog
RALP	robot-assisted laparoscopic prostatectomy
ROC AUC	receiver operating characteristics area under the curve
ROI	region of interest
RP	radical prostatectomy
rPFS	radiographic progression-free survival
RT	Radiotherapy
SMA	alpha-smooth muscle actin
SRT	salvage radiotherapy

SVI	seminal vesicle invasion
T2WI	T2-weighted imaging
TCGA	Cancer Genome Atlas
TMA	tissue microarray
TME	tumor microenvironment
TMPRSS2	transmembrane protease serine 2
TNM	Tumor Lymph Nodes Metastasis Classification of Malignant Tumors
TRUS	transrectal ultrasound
UI	urinary incontinence
UICC	Union for International Cancer Control
WSI	whole slide image
WW	watchful waiting

List of original publications

This thesis includes the following original publications:

I. **Sandeman K*,** Eineluoto JT*, Pohjonen J, Erickson A, Kilpeläinen TP, Järvinen P, Santti H, Petas A, Matikainen M, Marjasuo S, Kenttämies A, Mirtti T, Rannikko A. Prostate MRI added to CAPRA, MSKCC and Partin cancer nomograms significantly enhances the prediction of adverse findings and biochemical recurrence after radical prostatectomy. PLoS One. 2020 Jul 9;15(7):e0235779. Doi: 10.1371/journal.pone.0235779. PMID: 32645056; PMCID: PMC7347171. This article was used in the thesis by Juho Eineluoto.

II. Eineluoto JT, **Sandeman K**, Pohjonen J, Sopyllo K, Nordling S, Stürenberg C, Malén A, Kilpeläinen TP, Santti H, Petas A, Matikainen M, Pellinen T, Järvinen P, Kenttämies A, Rannikko A, Mirtti T. Associations of PTEN and ERG with Magnetic Resonance Imaging Visibility and Assessment of Non-organ-confined Pathology and Biochemical Recurrence After Radical Prostatectomy. Eur Urol Focus. 2021 Nov;7(6):1316-1323. Doi: 10.1016/j.euf.2020.06.016. Epub 2020 Jun 30. PMID: 32620540. This article was used in the thesis by Juho Eineluoto.

III. Teijo Pellinen*, **Kevin Sandeman***, Sami Blom, Riku Turkki, Annabrita Hemmes, Katja Välimäki, Juho Eineluoto, Anu Kenttämies, Stig Nordling, Olli Kallioniemi, Antti Rannikko, and Tuomas Mirtti. Stromal FAP Expression is Associated with MRI Visibility and Patient Survival in Prostate Cancer. Cancer Res Commun; 2(3) March 2022. Doi: 10.1158/2767-9764.CRC-21-0183

IV. **Kevin Sandeman,** Sami Blom, Ville Koponen, Anniina Manninen, Juuso Juhila, Antti Rannikko, Tuomas Ropponen and Tuomas Mirtti. AI model for prostate biopsies predicts cancer survival. Diagnostics. 2022; 12(5):1031. doi.org/10.3390/diagnostics12051031

*These authors contributed equally to this work

Author's contributions

Study I

Conceptualization
Data curation
Formal analysis
Visualization
Writing the original draft, review & editing

Declaration of Contributions
Kevin Sandeman made significant individual contributions to the joint publication as a team member. His roles included conceptualization, data curation, formal analysis, visualization, and writing. Kevin's skills as a physician focused on pathology enabled us to gather data from radiology and pathology reports. He was also responsible for data curation and analysis with visualization of the findings and writing of the article. Through his work, Kevin Sandeman had a significant impact on this article.

Study II

Conceptualization
Acquisition of data
Analysis and interpretation of data
Drafting of the manuscript
Critical revision of the manuscript for important intellectual content

Declaration of Contributions
Kevin Sandeman made significant individual contributions to the joint publications as a team member. His roles included conceptualization, data acquisition, analysis and interpretation, manuscript writing, and revision. Kevin's skills as a physician focused on pathology enabled us to prepare tissue samples (tissue microarrays) from the radiology findings. He was also responsible for data curation and analysis with visualization of the findings. Through his work, Kevin Sandeman had a significant impact on this article.

Study III

Resources
Data curation
Software
Formal analysis
Validation
Investigation
Methodology
Writing the original draft

Study IV

Conceptualization
Data curation
Formal analysis
Investigation

Methodology
Visualization
Writing the original draft, review, and editing

Study I and II have been included in an earlier dissertation (Juho T. Eineluoto, title: Characteristics of multiparametric magnetic resonance imaging in prostate cancer diagnostics and active surveillance) and are included here with permission of the first author (permission granted 26.09.2023)

Abstract

The most prevalent cancer in men is prostate cancer (PCa). Diagnostic methods currently detect most PCa at an early stage, but the diagnosis of many PCa cases that are clinically insignificant raises concerns about the need for aggressive intervention in all cases. The increased use of multiparametric magnetic resonance imaging (mpMRI) with structured reporting based on Prostate Imaging Reporting and Data System (PI-RADS) and targeted immunohistochemical stains have improved the identification of clinically significant PCa.

Studies I-III compared mpMRI visibility of lesions with histopathological findings in radical prostatectomy (RP) specimens. Study I focused on enhancing preoperative risk assessment tools, such as clinical parameters, Cancer of the Prostate Risk Assessment (CAPRA) score, Memorial Sloan Kettering Cancer Center (MSKCC) nomograms, and Partin tables, with the addition of mpMRI visibility. Study II examined the risk of biochemical recurrence (BCR) and evaluated the significance of Phosphatase and Tensin Homolog (PTEN) and ETS-related gene (ERG) biomarker expression. Study III examined the tumor microenvironment (TME) of these lesions. In Study IV, we developed an artificial intelligence (AI) algorithm to diagnose and grade prostate cancer in prostate biopsies and reported its performance as a comparison with pathologists' diagnoses and with BCR.

The main results for study I, were that models with mpMRI improved the prediction of postoperative adverse findings such as non-organ confined disease and survival analysis for BCR. Study II confirmed better survival time for BCR and less non-organ-confined disease for mpMRI-invisible lesions. Lesions visible on mpMRI were found to have a more frequent loss of PTEN expression. Study III found lesions with high stromal FAP (Fibroblast Activated Protein) expression in mpMRI had a higher risk of BCR. The presence of a large number of stromal FAP-positive cells was linked to a change in PTEN status in these visible lesions. In study IV, an AI algorithm detected and graded prostate cancer on a par with those of pathologists and predicted adverse staging and the risk for BCR.

The main conclusion is that mpMRI visible lesions are associated with signs of higher biological aggressiveness. Aggressiveness is expressed in clinical and biomarker adverse findings such as BCR, non-organ confined disease, altered PTEN, and stromal FAP status. AI algorithms can support clinicians in detecting and grading prostate cancer for biopsies with an added risk stratification value for BCR and higher staging.

Sammanfattning

Den vanligaste cancern hos män är prostatacancer (PCa). Diagnostiska metoder upptäcker för närvarande de flesta PCa i ett tidigt skede, men diagnosen av många kliniskt obetydliga PCa-fall väcker frågor kring behovet av aggressiva ingrepp för alla fall. Den ökade användningen av multiparametrisk magnetisk resonanstomografi (mpMRI) med strukturerad rapportering baserad på Prostate Imaging Reporting and Data System (PI-RADS) och riktade immunhistokemiska färgningar har förbättrat upptäckten av kliniskt signifikant PCa.

Studier I-III jämförde mpMRI-synlighet av lesioner med histopatologiska fynd i radikala prostatektomi (RP) fall. Studie I fokuserade på att förbättra preoperativa riskbedömningsverktyg, såsom kliniska parametrar, Cancer of the Prostate Risk Assessment (CAPRA) -score, Memorial Sloan Kettering Cancer Center (MSKCC) -nomogram och Partin-tabeller, genom komplementering med mpMRI-synlighet. Studie II undersökte risken för biokemiskt återfall (BCR) och utvärderade betydelsen av PTEN och ERG biomarköruttryck. Studie III undersökte den mikroskopiska tumörmiljön (TME) för dessa lesioner. I studie IV utvecklade vi en artificiell intelligens (AI) -algoritm för att diagnostisera och gradera prostatacancer i prostatabiopsier och rapporterade dess prestanda i jämförelse med patologernas diagnos och BCR.

Som huvudresultat för studie I förbättrade modeller med mpMRI förutsägelsen av postoperativa negativa fynd, såsom lokalt avancerad sjukdom och överlevnadsanalys för BCR. Studie II bekräftade bättre överlevnadstid för BCR och mindre lokalt avancerad sjukdom för mpMRI-osynliga lesioner. Lesioner synliga på mpMRI visade sig ha en mer frekvent förlust av PTEN-uttryck. Enligt studie III hade lesioner med högt stromalt FAP (Fibroblast Activated Protein) -uttryck i mpMRI en högre risk för BCR. Förekomsten av ett stort antal stromala FAP-positiva celler kopplades till en förändring i PTEN-status i dessa synliga lesioner. I studie IV upptäckte och graderade en AI-algoritm prostatacancer i nivå med patologer och förutsåg ogynnsam stadieindelning och risk för BCR.

Huvudslutsatsen är att mpMRI-synliga lesioner är förknippade med tecken på högre biologisk aggressivitet. Aggressiviteten uttrycks i kliniska och biomarkörsfynd som BCR, lokalt avancerad sjukdom, förändrad PTEN och stromal FAP-status. AI-algoritmer kan stödja patologerna I upptäckt och gradering av PCa på mellannålsbiopsier med en utökad riskstratifieringsvärde för BCR och högre stadieindelning.

1 Introduction

Prostate cancer (PCa) is the second most common cancer in men worldwide, with an incidence of 37.5 and a mortality of 8.1 per 100,000 in developed countries[1]. In Finland, the lifetime risk for a man to develop PCa is 14.5% and to die of PCa is 4% [2].

The diagnosis of PCa typically involves a combination of prostate-specific antigen (PSA) testing, digital rectal examination (DRE), and prostate biopsy (Bx). Neither elevated PSA nor tumorous findings on DRE are specific for cancer, however. On the other hand, negative findings of these parameters do not exclude malignancy, not even aggressive malignancies[3]. Clinical treatment decisions are typically based on the microscopic diagnosis of PCa that are graded according to the Gleason score (GS) on biopsies[4]. A further grouping of the Gleason scores resulted in the Gleason Grade Group (GGG) that supported a more evident division into clinically relevant groups[5]. Sampling clinically significant prostate cancer (csPCa) with biopsies can be challenging, whereas indolent, clinically insignificant cancer in Bx is a common finding that should result in the patient's active surveillance (AS).

The outcome of individual PCa patients is determined by combining pathological GGG of biopsy results with other PCa-related factors, such as PSA levels, PSA doubling time, clinical stage, age, and biopsy-detected tumor volume. This information has been used to develop predictive tools such as Partin tables, Memorial Sloan Kettering Cancer Center (MSKCC) nomograms, and Cancer of the Prostate Risk Assessment (CAPRA) scores to enhance the accuracy of predictions[6–8].

A combination of mpMRI and either Likert evaluation or a structured Prostate Imaging Reporting and Data Sytem (PI-RADS) has been proposed to improve the accuracy of PCa diagnosis, particularly for csPCa[9–11]. mpMRI aids in directing biopsies toward index lesions[12]. However, a proportion of the lesions are sometimes undetected[13–15]. Cellularity is associated with diffusion-weighted imaging (DWI)-determined apparent diffusion coefficients (ADC), PI-RADS values, and thus by MRI visibility, although the findings are somewhat inconsistent[16–18]. It is worth mentioning that the mpMRI of csPCa often has tumor-linked desmoplastic stroma, which indicates that the MRI results may be significantly influenced by the tumor's microenvironment (TME), structure, and composition[19]. However, the molecular and cellular differences between the TME of MRI true-positive and MRI false-negative lesions and benign prostate tissue have not been thoroughly investigated.

Immunohistochemical biomarkers have shown potential for defining csPCa. Loss of Phosphatase and Tensin Homolog (PTEN) expression, which as a tumor suppressor gene, is associated with adverse events at prostatectomy[20–23]. In contrast to PTEN, expression of the v-ets avian erythroblastosis virus E26 oncogene homolog gene (ERG) could be associated with a worse outcome, according to certain studies[20,22,24]. Clinically, the added value of these findings still has to be addressed.

After deep learning and convolutional neural networks emerged, AI algorithms were able to obtain promising results for detecting and grading PCa on scanned slides[25]. Nevertheless, the clinical integration and validation of these algorithms are slow as many laboratories lack digital pathology resources or the capacity for workflows to apply these solutions.

This dissertation aims to contribute to the understanding of the accuracy and nature of mpMRI-diagnosed lesions from a histopathological perspective. AI-based methods for predicting the individual the PCa patient's prognosis have been developed and are also assessed.

The pathological definition and description of mpMRI under and over-diagnosed lesions are necessary to specify the real diagnostic value of mpMRI. Study I focused on the predictive role of mpMRI diagnostics in combination with actual nomograms. Study II emphasizes the PTEN and ERG status of mpMRI-detected or missed lesions. Study III concentrates on the cellular and tumor

environment composition of mpMRI-detected or mpMRI missed lesions. Study IV focuses on the performance of AI for detecting and grading PCa of biopsies with an emphasis on survival after robot-assisted laparoscopic prostatectomy (RALP).

2 Literature review

2.1 The Prostate

The prostate is an accessory gland in the male urogenital system. It lies under the bladder neck and surrounds the urethra. Five prostatic zones define its microanatomy: a) 25% constitutes a central zone, b) an anterior fibromuscular zone, which covers the front side as an apron, c) a transitional zone that is prone to benign prostatic hyperplasia, d) 70% that constitutes a peripheral glandular region and, e) a periurethral gland region (Figure 1).

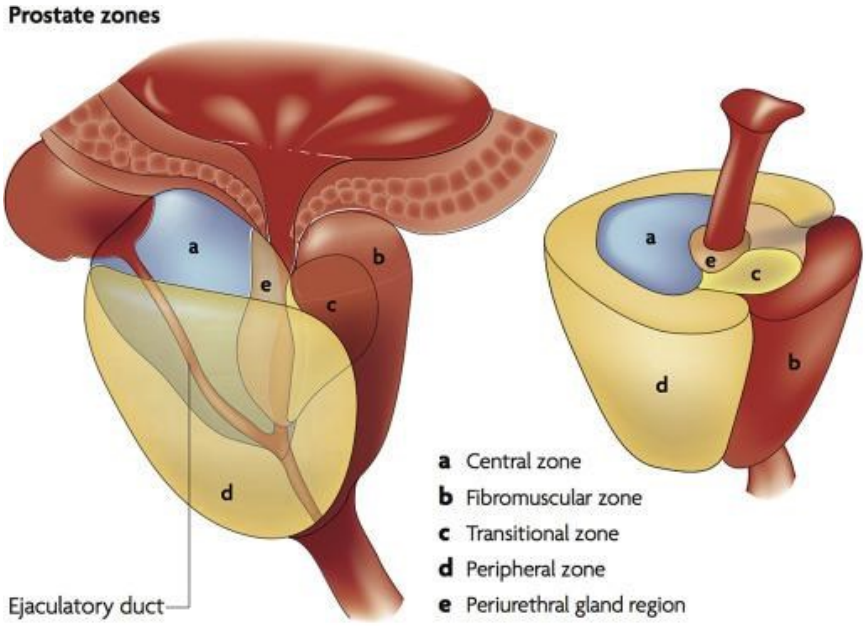

Figure 1. Zonal anatomy of the prostate. Reprint with permission from Springer Nature[26].

The histology of the benign prostate gland has three components: glandular tissue, stroma and immune cells. The glandular structures are embedded in the stromal component, which are infiltrated by immune cells as part of inflammatory and malignant processes.

The glands are composed of two cell types. First: the columnar secretory cells, which are responsible for producing and secreting the components of prostatic fluid, and which contributes to semen. Second: the basal cells, which are adjacent to the basement membrane and which provide structural support to the glandular epithelium. The basal cells are typically smaller than the columnar cells and they have a flattened shape. Basal cells are typically present in benign conditions but absent in a well-differentiated adenocarcinoma[27]. The stroma of the prostate gland consists of fibrous tissue and smooth muscle cells. It provides support and structure to the glandular tissue. A modest presence of immune cells, primarily lymphocytes, is considered normal regardless of age. These lymphocytes, mainly T cells, are more abundant in the stroma than in the epithelium (Figure 2)[28].

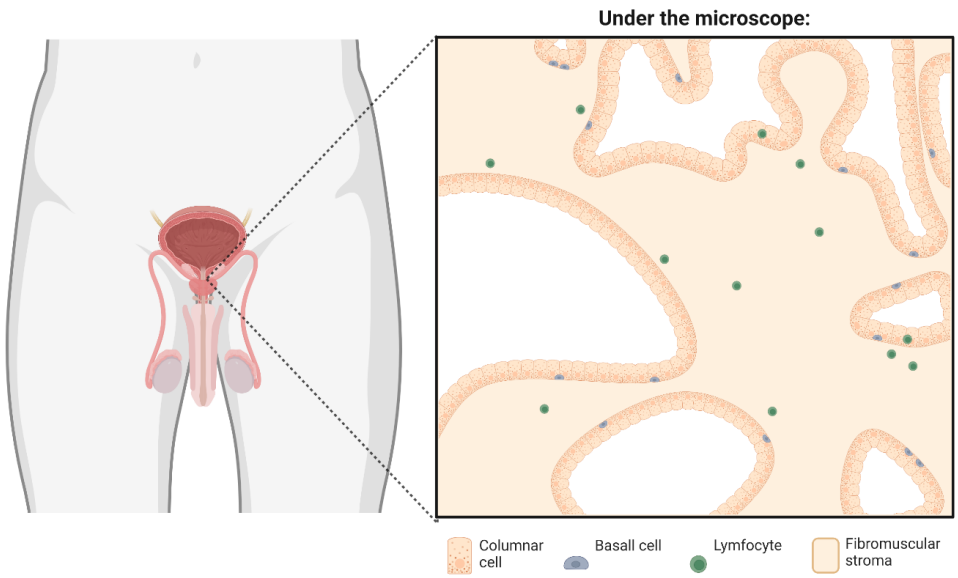

Figure 2. Normal prostatic histology. Left: Overview of male reproductive anatomy. Right: Normal prostatic histology.

The development of the prostate gland starts in the ninth embryonic week. The fetal testes start androgen production around fetal week ten. The development is anatomically completed around week 36 of gestation[29–31]. Until puberty and androgen-induced growth, the prostate maintains its size[32].

During ejaculation, semen is produced as a mixture of components from various anatomical entities. The ejaculate starts as immature sperm in the testis and when matured the sperm are blended with seminal vesicle fluid and prostatic secretion, predominantly containing PSA produced by the prostatic epithelia[33]. The serine protease cleavage action by PSA, among other kallikreins, is crucial for fruitful reproduction[34]. Another essential molecule is prostate-specific membrane antigen (PSMA), a protein on the surface of prostate cells. It functions as a transmembrane glutamate carboxypeptidase, which helps break down glutamate, a neurotransmitter involved in the signaling between nerve cells[35].

2.2 Prostate cancer

2.2.1 Definition

PCa that arises in the prostatic secretory epithelium, is the most prevalent malignancy of the prostate gland. PCa is most commonly an acinar adenocarcinoma with the pathognomonic histological feature of the basal cell layer absence.

The latest WHO Classification of Tumors morphologically distinguishes PCa patterns, subtypes, and variants. PCa patterns of acinar adenocarcinoma, such as atrophic, cystic, pseudohyperplastic, foamy gland and mucinous are differential diagnoses as they can mimic benign histological changes, and their associated Gleason grade (GG) determines their prognostic significance. Particular PCa subtypes are prostatic intraepithelial neoplasia–like, plasmacytoid (signet ring–like), sarcomatoid, and

pleomorphic giant cell adenocarcinoma[36]. In contrast, the term variants is reserved for genomic changes[37].

Ductal adenocarcinoma is believed to be more than a subtype of acinar adenocarcinoma because of its typical clinical conduct and metastatic pattern. Its morphology is defined by papillarity and complex cribriform glands covered by columnar pseudostratified epithelium[38].

2.2.2 Molecular properties and genetic alterations

Crucial genetic changes encompass the fusion of transmembrane protease serine 2 (TMPRSS2) with Erythroblast Transformation Specific (ETS) family oncogenes, the amplification of the MYC oncogene, and the deletion or mutation of PTEN and TP53 in all stages of prostate cancer. More severe cases also involve amplification or mutation of the androgen receptor (AR). Additionally, germline or somatic mutations in DNA damage repair genes, such as breast cancer genes 1 and 2 (BRCA1 and BRCA2) and mismatch repair (MMR)-related genes, increase the likelihood of developing PCa[39–41].

The most common fusion involves TMPRSS2 with ERG. This genetic alteration with the TMPRSS2-ERG fusion protein that acts as an active transcription factor is identified in nearly half of the prostate cancer biopsy samples obtained from Caucasian men[42,43]. ERG is a member of the ETS transcription factor family and it regulates gene expression, cell growth, and division. Overexpression of ERG can lead to uncontrolled cell growth and the development of PCa[21,24]. Furthermore, ERG overexpression is associated with a more aggressive form of the disease and an increased risk of recurrence and progression[44,45]. In addition to ERG, other non-ERG ETS transcription factor family genes, such as ETV1, ETV4, ETV5, or FLI1, can also fuse with TMPRSS2. These non-ERG ETS fusions are present in approximately one out of seven prostate cancers. Although they may be less common, they are clinically significant and should not be overlooked when mainly focusing solely on ERG expression[46].

PTEN is a tumor suppressor gene that is involved in regulating cell growth and division. PTEN gene expression can be altered or lost, thereby decreasing the amount of PTEN protein produced. PTEN is frequently missing or altered in PCa, which can contribute to the disease's development and progression[20–23]. PTEN loss or mutation is also associated with a more aggressive form of PCa, and patients with PTEN loss/mutation are at higher risk for recurrence and progression of the disease[20–22,24,44,45]. PTEN gene alterations are found in more than 12-17% of localized and metastatic castration-sensitive prostate cancer (mCSPC) tumors. However, these alterations are particularly enriched in metastatic castration-resistant prostate cancer (mCRPC), which is present in over 40% of tumors[47,48].

The human chromosome 8, locus 8q24 contains the MYC gene, which codes for the MYC protein, a potent regulator of gene expression. Nuclear MYC protein overexpression is an early alteration in most PCa[49]. TP53 mutations result in the dysfunction of a tumor suppressor protein, p53, and are uncommon in localized disease (8%) but more common in mCSPC (27%) and mCRPC (50%)[47,48]. AR-related mutations are regarded as part of disease progression into mCRPC as androgen deprivation therapy (ADT) resistance occurs, which is induced by ADT. These mutations collectively occur in more than 70% of patients with mCRPC in contrast to only 2-6% mCSPC with AR gene alterations[48,50]. An example of resistance mechanisms in PCa is AR-V7, a splice variant of the AR that lacks the ligand-binding domain, which is the receptor region that interacts with androgens. As a result, AR-V7 is constitutively active, meaning it can promote the growth and survival of PCa cells even in the absence of androgens. This variant is associated with resistance to ADT[51].

2.2.3 Risk factors

The main risk factors for PCa are age, ethnicity, and family history of PCa. The population prevalence of high-risk PCa rises from 1.4% at age 65 to 5.2% at age 75[52]. The probability of PCa is also increased for men with two affected brothers to 13.6% at the age of 75[52]. Hereditary PCa is related to a younger start, though the disease's mortality does not differ from the non-hereditary variant[53,54]. Ethnicity is a primary risk factor, as a review showed PCa in 51% of African-American and 36% of Caucasian men in their seventies. In comparison, PCa appeared in only 21% of Asian men[55].

African American men have a two-fold increased risk of localized or de novo metastatic prostate cancer and death compared to Caucasian American men, even when given equal access to care in the Veteran Administration cohort[56]. Black men with metastatic prostate cancer are more likely to have specific mutations than Caucasian and Asian men. These mutations, including those in the androgen receptor and DNA-repair genes, are considered "clinically significant" as they can affect prognosis, response to therapy, and enrollment in clinical trials and precision oncology studies. This suggests that biological factors may play a role in these disparities[57]. Although many adjustable environmental and medical factors have been proposed, there are no clear recommendations for particular precautionary conduct[58].

2.2.4 Incidence, prevalence, and mortality

PCa is prevalent among men worldwide as it accounts for 14% of all cancer diagnoses. The incidence varies geographically, with the highest rates in Western countries[1]. The higher PCa rate in the Western world may be due to the widespread use of PSA testing, subsequent diagnoses, and an aging population. In Finland, 5034 new PCa cases were reported, and 928 deaths due to PCa were registered, resulting in the highest cancer incidence (182.7/100 000) and the second highest mortality (37.6/100 000) for any cancer in 2020. In the same year, PCa prevalence reached 58,500 cases. Of all PCa cases, 94% remained alive during follow-up 2018-2020. Historically, the incidence of PCa in Finland increased during the 1990s and reached its highest point in 2004. The incidence is comparable to that observed in the 1990s during which the mortality rate began to decrease. However, survival rates for PCa plateaued at over 90% around 2010. The comparison between the periods 2010-2014 and 2015-2019 showed a decline in incidence by 7% and in mortality by 12% [59].

2.2.5 Histology

Light microscopy examination of hematoxylin and eosin (H&E) stained tissue sections is crucial for diagnosing PCa and making treatment choices. Prostatic acinar adenocarcinoma originates in the secretory cells of the prostate and accounts for 95% of all PCa cases[60]. The diagnosis of adenocarcinoma is made by assessing three criteria: the glandular structure, the absence of basal cells, and the characteristics of the nuclei in the epithelial cells lining the glands (Table 1)[60–62]. Minor criteria can also confirm a more malignant diagnosis.

Primary criteria (all primary criteria must be fulfilled)
Malignant glands infiltrating the stroma AND An absence of basal cells (typically) AND Nuclear features, including enlargement and hyperchromasia
Minor criteria (non-obligatory but useful)
Cytoplasmic features, including amphophilic or abundant pale cytoplasm with straight luminal borders Prominent nucleoli Atypical luminal contents, crystalloids, blue-tinged mucin, and amorphous pink secretion Perineural invasion, particularly circumferential, and intraneural invasion (specific but not sensitive) Mucinous fibroplasia (specific but not sensitive) Glomerulations (specific but not sensitive)

Table 1. Criteria for histological diagnosis of prostate adenocarcinoma. Reprint with permission from WHO Permissions [60].

When uncertainty exists, the lack of basal cells can be determined by using immunohistochemical stains for basal cell markers such as 34βE12, CK5/6, or p63[63]. A pathologist should be aware of the potential absence of basal cells in small, atypical benign glands. In addition, a-methylacyl-CoA racemase (AMACR) combined with basal cell markers assists in diagnosing PCa[64–67]. Approximately 80% of limited prostatic adenocarcinomas show expression of AMACR cytoplasmic staining on needle biopsy. Additionally, AMACR is not solely specific for adenocarcinoma and high-grade prostatic intraepithelial neoplasia (HGPIN), as some benign lesions can also exhibit positivity[68–70].

2.3 Diagnosis of prostate cancer

2.3.1 Screening

Screening refers to the systematic examination of asymptomatic men. PCa screening is disputed among urologists without a clear consensus on its need and execution[71]. However, a new council recommendation from the European Commission extended organized national cancer screening programs to PCa[72].

PSA measurement is used for the screening of PCa. PSA is a prostate-specific protein, and its increase can result from age-related prostatic growth, benign prostate hyperplasia (BPH), prostatitis, or PCa[73]. The rate of change in PSA levels (0.75 µg/L per year) was significantly greater in PCa cases compared with control subjects and subjects with BPH[74]. Pre-PSA era patients had excellent prognoses despite the lack of follow-up and repeated biopsies for cT1a prostate cancers[75–77], which could support lesser need for biopsies for incidental low-risk PCa findings. Although screening reduces mortality, it also generates overdiagnosis, false alarms, and complications from biopsies and therapy[78].

The most referred large randomized clinical trials are the Prostate, Lung, Colorectal and Ovarian cancer screening (PLCO) study[79] and the European Randomised Study of Screening for Prostate Cancer (ERSPC) study[80]. The PLCO study did not find any improvement in overall survival (OS) or PCa-specific survival. On the other hand, the ERSPC confirmed a 50% PCa mortality reduction and 41% metastasis reduction due to PSA testing after a follow-up of 14 years[80]. However, no screening study has demonstrated an apparent effect on overall survival[78,81–83].

In the case of screening, the recommended method is to determine the PSA baseline and plan the follow-up interval on the baseline[80]. The European Association of Urology (EAU) guidelines state that the decision for early PSA testing should be made between the patient and their physician after

evaluating the benefits and risks of the test[84]. The recommendation is to use a risk-adapted approach to identify men at risk of developing PCa, starting at age 50 and based on individual life expectancy. Men at higher risk should be offered screening from age 45, and those with a confirmed BRCA mutation (especially BRCA2) should be screened from age 40. Multiparametric magnetic resonance imaging (mpMRI) is recommended to minimize unnecessary biopsies. However, a combination of targeted and systematic biopsies should be performed when needed. Tissue-based biomarkers are not currently recommended for routine use[85].

2.3.2 Digital rectal examination and transrectal ultrasound

Digital rectal examination (DRE) is used to detect abnormal prostatic masses that can be a sign of PCa. A comparative study between different screening techniques showed that PSA detected 75% and DRE 56% of PCa cases. The combined use of these methods increased the detection of organ-confined disease to 78% over DRE alone[86].

Transrectal ultrasonography (TRUS) is the first-line modality to visualize the prostate. TRUS can be used to diagnose prostate size and lesions quickly. Because of TRUS's limitations in the differential diagnosis between malignant and benign prostate lesions Therefore, biopsies are recommended for the histological diagnosis, according to the clinical judgment of the urologist[87,88].

2.3.3 Magnetic resonance imaging

2.3.3.1 Prostate mpMRI

Prostate mpMRI has substantially improved the detection rate of PCa [9,12]. Prostate mpMRI utilizes a 1.5- or 3-Tesla magnetic field. Most centers apply a 3-Tesla magnetic field for prostate mpMRI. An endorectal probe with a 1.5 Tesla magnetic field is recommended according to the ESUR guidelines [89]. mpMRI is the standard modality for prostate MRI, as it creates a 3D image of the prostate by combining the following: T2-weighted (T2WI), diffusion-weighted, dynamic contrast-enhanced images, and occasionally magnetic resonance spectroscopy.

A systematic review reported that mpMRI detects clinically significant prostate cancer (csPCa) with considerable variation in rates among studies[9]. The accuracy, sensitivity, and specificity ranges were 44–87%, 58–96%, and 23–87%, respectively. As mpMRI has a lower sensitivity for clinically nonsignificant PCa, it is suggested as the primary method for screening in cases of elevated PSA. It is believed that the use of mpMRI thereby reduces the overdiagnosis of PCa[9]. The GÖTEBORG prostate cancer screening 2 trial showed that mpMRI-directed targeted biopsy for screening and early detection in persons with elevated PSA levels lowered the risk of overdiagnosis by half at the cost of delaying detection of intermediate-risk tumors in only a small proportion of patients[77]. Any mpMRI-detected lesion with a PI-RADS score of over 3 should be biopsied, preferably with targeted biopsies for histological confirmation[90]. Moreover, the accuracy of the targeted biopsies depends on the radiologist's and urologist's experience[91].

The Prostagram study showed in 2021 that a short mpMRI protocol of approximately 15 minutes without contrast enhancement could find csPCa. The use of this technique showed no overdiagnosis of clinically insignificant cancer[92]. The EAU guidelines support mpMRI for triage before prostate biopsies but not for screening of PCa[93]. Negative mpMRI results and low clinical suspicion of PCa can result in the omission of biopsies after shared decision-making with the patient[93]. Positive mpMRI results with PI-RADS equal to or higher than 3 should require prostate biopsies, according to the guidelines[93]. mpMRI prior to prostate biopsies can result in grade migration toward clinically

significant PCa due to better targeting of the lesions compared to standard biopsy series[94,95]. Hence, patients with MRI-visible PCa could have better outcomes than those with only standard biopsies. This reflection should be weighed into risk classification and treatment decisions.

2.3.3.2 Prostate Imaging Reporting and Data System

The PI-RADS is a standard system for reporting the results of MRI examinations of the prostate[10]. It is a system for grading the likelihood that an abnormal finding on prostate mpMRI is cancer. The PI-RADS score ranges from 1 to 5 and evaluates the appearance of prostate tissue on mpMRI images, with a higher score indicating a higher probability of PCa.

The PI-RADS score guides further testing and treatment decisions for men with suspected prostate cancer[10]. PI-RADS version 1 had limitations due to the lack of a uniform structure and clear threshold for csPCa[96]. An update resulted in the second version of PI-RADS with clear recommendations for technical parameters and instructions for reporting and sectoring[10]. The sensitivity of PI-RADS version 2 was found to be 0.89 (95% CI: 0.86-0.92), and its specificity was 0.73 (95% CI: 0.60-0.83)[15]. It had a higher sensitivity than version 1, with a pooled sensitivity of 0.95 versus 0.88 (p = 0.04) [15,97]. PI-RADS version 2.1 has been introduced in the anticipation that the latest modifications would improve the inter-reader variability and simplify the assessment of MRI even further[98].

2.3.3.3 Likert

The Likert scoring system for mpMRI is an overall clinical impression without specific characteristics per sequence. The system is used by radiologists to rate the overall impression of individual lesions or total cases into five scores that combine mpMRI findings with clinical data. The technique is applied as screening, AS, follow-up, and post-treatment monitoring[99,100]. The Likert scoring system performed equally or better compared to PI-RADS for any PCa[11]. The Prostate Cancer Radiological Estimation of Change in Sequential Evaluation (PRECISE) panel recommends using a Likert score to assess the likelihood of progression in suspected lesions during AS with sequential mpMRI[100].

2.3.4 PSMA positron emission tomography

PSMA positron emission tomography (PET) is an imaging modality that is used to stage advanced PCa. A radioactive tracer combined with a PSMA antibody binds to the PSMA of PCa cells and emits gamma rays, which are registered by a detector to produce an image[35]. The role of PSMA-PET is to help diagnose and stage prostate cancer and monitor the response to treatment. It can detect small amounts of prostate cancer cells, even in areas where traditional imaging tests may not be able to visualize them. In patients with mCRPC, PSMA expression is exceptionally high, and PSMA-positive lesions are present in most cases[35].

2.3.5 Prostate biopsy

2.3.5.1 Systematic biopsy

The need for prostate biopsies should be determined based on the PSA level, suspicious DRE, the patient's biological age, his potential comorbidities, and the therapeutic consequences[84]. Transrectal or perineal ultrasound-guided 18-Gauge core needle biopsy is the standard technique to retain tissue for histological diagnosis[101]. Usually, 10 to 12 biopsy cores from apex to base, according to a template, are taken to enhance the possibility of cancer detection. This approach also leads to an overdetection of non-clinically significant PCa compared to mpMRI-targeted biopsies[102].

2.3.5.2 Targeted biopsy

Urologists target specific regions of interest (ROI) as defined by radiologists based on mpMRI findings. This technique has enhanced the csPCa detection rates[12,103]. Currently, two techniques for targeted biopsy are being clinically implemented. The first cognitive technique involves the urologist's evaluation of the mpMRI lesions, followed by TRUS-guided biopsies taken from the suspected area[104]. The second technique combines the mpMRI examination data by fusing it in real-time during the TRUS examination to guide the biopsy needle directly to the lesions[12]. Both techniques seem equal in detecting csPCa, though more comparative studies will ascertain a possible superiority to one technique[105,106].

The approach for mpMRI-guided biopsies can be transrectal or transperineal. Both techniques have similar PCa detection rates, although the transperineal method detected better apical and anterior lesions[107,108]. Furthermore, transperineal biopsies are associated with a lower infection risk than transrectal biopsies, which is an essential consideration in the era of antibiotic resistance. Therefore, despite the slightly increased discomfort associated with transperineal biopsies, they are gaining acceptance as a safer and more effective approach for mpMRI-guided biopsies[109].

From a histopathological point of view, three comparative studies between the GS of systematic biopsy cores and RP specimens showed that GS 6 had some genetic overlap with high-grade PCa, such as TMPRSS2:ERG fusion, PTEN loss, and BRCA mutation. In these studies, GS 6 of biopsies were confirmed as a nonlethal, non-metastasizing disease, upgraded in 35% of the RP specimens. GS 3 + 4 = 7 got an upgrade in 25%, whereas GS 4 + 3 = 7 was downgraded in 40% of the RP cases. An increased percentage of GS 5-6 cancer per core predicted an upgrade at RP[110–112]. Pathology errors, borderline grades, and sampling errors were assumed as the leading causes for up- and downgrading at RP, whereas targeted biopsies were suggested to diminish sampling errors.

2.3.6 Grading and staging

2.3.6.1 Gleason score and ISUP grade grouping

Since 1966, the most crucial predictive marker in PCa has been the histopathological diagnosis according to the Gleason grading system (Figure 3), which makes the pathologist's role more important in choosing the proper care option[4]. The GS is defined by the histological differentiation of malignant glands and is reported as two numbers[4]. The first number represents the most common grade pattern in the specimen. The second number signifies the grade pattern with the worst outcome or the second most common grade pattern for biopsies. In prostatectomy specimens, the grade patterns are reported in the order of their proportion of total cancer area, starting from the highest proportion. The Gleason sum is the sum of the first two grade patterns[4]. The GG with the GS is an inherent component of the morphological diagnosis since GS-derived ISUP International Society of Urological Pathology (ISUP) grade groups may be diverse (i.e., grade group 4).

In 2005, ISUP adjusted the original criteria for Gleason scoring to conform to the PSA-era knowledge about PCa behavior[113]. The consensus meeting changes focused mainly on the relationship between GG 3 and 4 as the most critical predictive grades, especially in identifying active surveillance patients. In 2010, cribriform differentiation was always graded as GG 4 (Figure 3 and Figure 4), followed by glomeruloid differentiation in 2014[5].

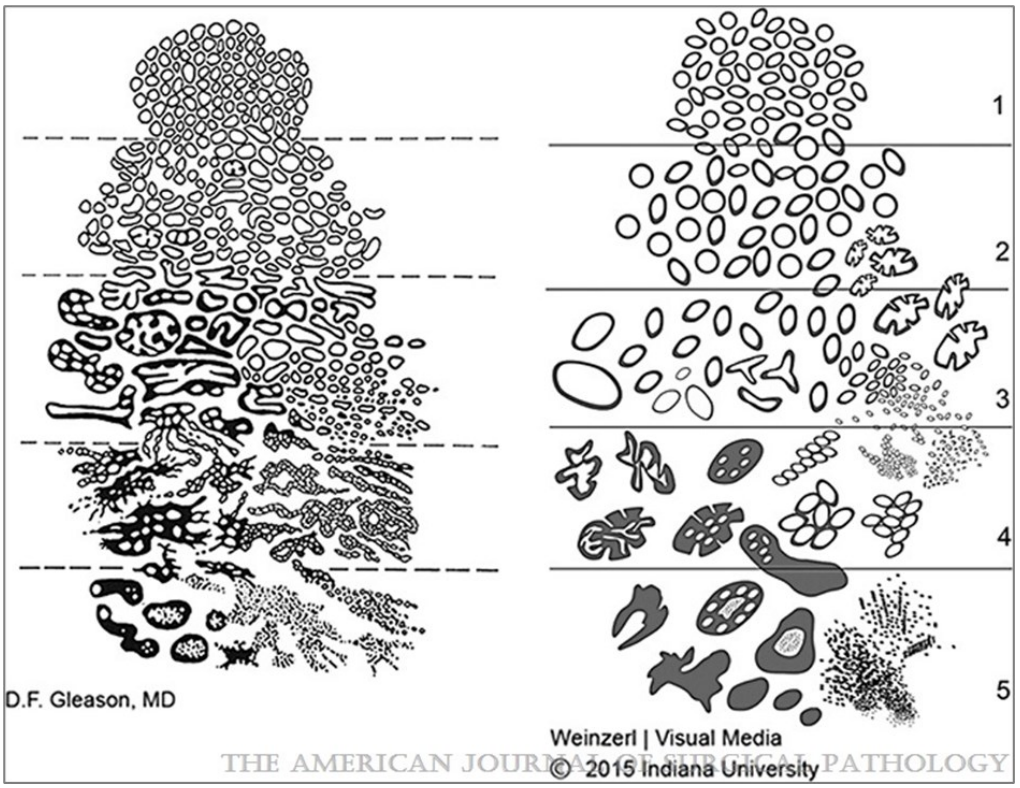

Figure 3. Prostatic adenocarcinoma (histologic patterns): original (left) and 2015 Modified ISUP Gleason schematic diagrams. Reprint with permission from Wolters Kluwer Health, Inc. [5].

Grade Group	Gleason score	Description
1	3 + 3 = 6 or less	Only individual discrete well-formed glands
2	3 + 4 = 7	Predominantly well-formed glands with lesser component of poorly-formed/fused/cribriform/glomeruloid glands
3	4 + 3 = 7	Predominantly poorly-formed/fused/cribriform/glomeruloid glands with lesser component of well-formed glands*
4	4 + 4 = 8	Only poorly-formed/fused/cribriform/glomeruloid glands
	3 + 5 = 8	Predominantly well-formed glands and lesser component lacking glands**
	5 + 3 = 8	Predominantly lacking glands and lesser component of well-formed glands**
5	4 + 5 = 9	Lacks gland formation (or with necrosis) with or w/o poorly formed/fused/cribriform/glomeruloid glands
	5 + 4 = 9	
	5 + 5 = 10	

*Table 2. Histological definition of the ISUP Grade Group system. * * For cores or RP specimens with poorly-formed, fused, or cribriform glands greater than 95% or lack of glands altogether, the component of well-formed glands less than 5% is not considered in the grading. ** Poorly-formed/fused/cribriform glands can be a minor component. Glomeruloid differentiation was added to Gleason Grade 4*[5,114,115]*. Reprint with permission from Springer Nature* [5]*.*

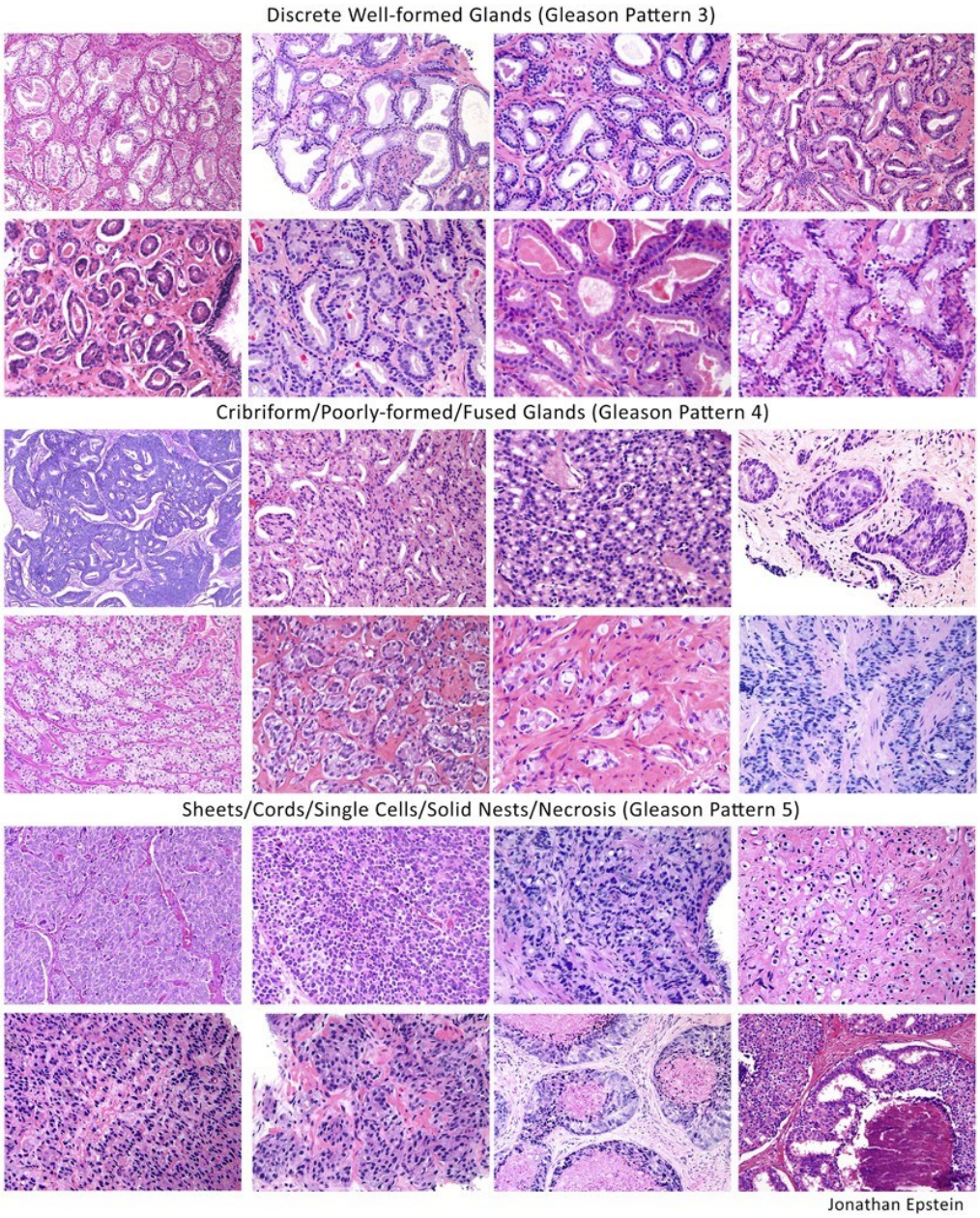

Figure 4. Prostate cancer grading system. Row 1: Large, uniformly-sized and -shaped glands. Variably sized and shaped glands, some with indentations. Medium-sized uniform glands. Varied gland size. Row 2: Small glands with occasional tangentially cut glands. Glands with open lumina, occasionally tangentially cut. Discrete, back-to-back glands. Branching glands. Row 3: Irregular, large cribriform glands with distinct lumina. Cribriform glands with narrow lumina, glomeruloid structures, and merged glands. Small, round, irregular cribriform glands. Small round cribriform glands. Row 4: Poorly formed glands with nuclei arranged on the periphery. Small, poorly formed glands. Small, poorly formed glands. Merged, poorly formed glands. Row 5: Cancerous tissue in sheets. Cancerous sheets with rosette formation. Small nests and cords of tumor with clear vacuoles. Individual cells. Row 6: Cancer nests and cords with vague lumina. Solid cancer nests. Solid nests with comedonecrosis. Cribriform glands with central necrosis. Reprint with permission from Springer Nature[116].

The term 'modified Gleason grading system' was accepted in clinical diagnostics at the ISUP consensus meeting in 2014. The modified Gleason grading system gave detailed support in the grading of the following: mucinous adenocarcinoma by defining it to its base differentiation, glomeruloid differentiation by grading it always as GG 4, and of intraductal carcinoma by rejecting its grading in the GS (Figure 3 and Figure 4) [5,117,118].

During the most recent ISUP consensus meeting in 2019, it was agreed that secondary GGs 4 and 5 were reported in biopsies in less than 5% of the volume. Most pathologists report GG 4 and 5 in the GS as the second grade for prostatectomies, when they constitute more than 5% of the volume. In less than 5% of the volume, the highest grades are reported as the tertiary grade for prostatectomies[119].

Despite its high prognostic value, GG still presents challenges as its reproducibility shows inter-and intraobserver variability, especially for non-specialized pathologists. Quantitative Gleason is seen as a continuum of differentiation grade patterns more than categorical classes and should be broken into relative scales of different grades. Quantitative Gleason grading is less susceptible to interobserver variability and offers more detailed reports. The presence of tertiary high GG correlates with a negative outcome[120,121]. According to a study by Wulzyn E et al., artificial intelligence (AI) can predict patient outcomes effectively based on GG with continuous and discrete GG on a par with or better than GG in the patient reports[122].

Developments in AI and computational technology have shown that AI-based algorithms perform at the level of experienced uropathologists[123–126]. Although there is a need for extensive validation of these algorithms in clinical settings, they offer future potential for improvement. Mainly, non-specialized pathologists can reduce inter- and intraobserver variability with algorithms[127,128].

2.3.6.2 The significance of low-grade prostate cancer

Overtreatment of low-grade prostate cancer (GS 6 or lower) is a well-known issue caused by systematic biopsies from PSA tests. It is suggested to rename GG 1 PCa as it exhibits slow progression and is more similar to non-cancerous precursor lesions based on histological evidence of neoplasia. This approach could help reduce overtreatment, minimize side effects from treatment, decrease patient anxiety, and lower the financial strain on the healthcare system[129,130].

A pathologist considers a GS of 6 to be cancer due to its similar appearance to higher-grade cancer, lack of basal cell layer, and potential for perineural and local invasion. GS 6 prostate cancer also has molecular changes seen in higher-grade cancers, such as the TMPRSS2:ERG gene fusion [131].

However, studies have shown that this type of cancer rarely has extracapsular extension and is unlikely to spread to the lymph nodes[132–134]. Based on clearly different gene expressions, GG1 can be separated from csPCa. A 49-gene expression signature from the Cancer Genome Atlas (TCGA) accurately separates GG1 from GG3 or higher[135]. Other assessments (Prolaris and Decipher) have confirmed the differences in gene expression between GG1 and csPCa[136,137]. To avoid unnecessary treatment, some argue that Gleason score 6 should not be referred to as cancer but as an indolent lesion of epithelial origin (IDLE) [138]. This practice has been adopted in other organ systems to prevent overtreatment[135,139,140]. A motivation for declassifying GG1 as cancer is the growing use of mpMRI. The improved accuracy of mpMRI with targeted biopsy has led to greater certainty that pure GG1 after the biopsy accurately reflects the GG1 present at prostatectomy[103,136]. However, some clinically significant PCas and their stages are still overlooked by mpMRI and mpMRI-guided biopsies[137,141].

From a clinical viewpoint, reclassifying a GS of 6 as an IDLE tumor on biopsy poses the danger of patients not adhering to long-term monitoring and being unaware of the possibility of developing a higher-grade adenocarcinoma. The chance of upgrading from a GS 6 biopsy to a GS 7 or higher during radical prostatectomy has been reported as 36%[111]. Thus, vigilant monitoring is essential. If GS 6 is not considered cancer, the risk of more advanced disease may go unnoticed, and compliance with AS may be jeopardized[142].

2.3.6.3 TNM

The Tumor Lymph Node Metastasis Classification of Malignant Tumors (TNM) by the Union for International Cancer Control (UICC) in collaboration with the American Joint Committee on Cancer (AJCC) is a globally accepted standard for staging the extent of cancer spread (Table 3)[143].

T	**Primary tumor**	
T0	No evidence of primary tumor	
T1	Clinically inapparent tumor that is not palpable	
	T1a	Tumor incidental histological finding in 5% or less of tissue resected
	T1b	Tumor incidental histological finding in more than 5% of tissue resected
	T1c	Tumor identified by needle biopsy (inter alia because of elevated prostate-specific antigen [PSA])
T2	Tumor that is palpable and confined within the prostate	
	T2a	Tumor involves one-half of one lobe or less
	T2b	Tumor involves more than half of one lobe, but not both lobes
	T2c	Tumor involves both lobes
T3	Tumor extends through the prostatic capsule	
	T3a	Extracapsular extension (unilateral or bilateral)
	T3b	Tumor invades seminal vesicle(s)
T4	Tumor is fixed or invades adjacent structures other than seminal vesicles: external sphincter, rectum, levator muscles, and/or pelvic wall	
N	**Regional (pelvic) Lymph Nodes**	
NX	Regional lymph nodes cannot be assessed	
N0	No regional lymph node metastasis	
N1	Regional lymph node metastasis	
M	**Distant Metastasis**	
M0	No distant metastasis	
M1	Distant metastasis M1a Non-regional lymph node(s) M1b Bone(s) M1c Other site(s)	

Table 3. Definitions of American Joint Committee on Cancer TNM Criteria for prostate cancer. Clinical Tumour Node Metastasis (TNM) classification of prostate cancer, 8th edition, 2017, John Wiley and Sons. Reproduced with permission, as

The correct classification of prostate cancer stage is crucial for grouping patients for optimum treatment. The EAU guidelines state that local staging examinations are only indicated for intermediate and high-risk patient groups[93]. The high accuracy of mpMRI for detecting index lesions with outstanding soft tissue differentiation is the most precise modality for local T-staging of PCa[144]. mpMRI is beneficial for the determination of the T stage, either organ-confined (<T2 disease) or locally advanced (>T3 disease)[10]. mpMRI has shown a specificity of 67% and a sensitivity of 79% for detecting extraprostatic extension (EPE) in PCa[145]. Higher field strengths using functional imaging techniques can somewhat improve sensitivity. Local staging is not included in PI-RADS v2, though the incorporation of staging will be considered in future PI-RADS versions as relevant data and experience become available[146].

Pathological stages pT1a, pT1b, and pT1c do not exist. Prostate cancer that is histopathologically confirmed to be confined to the organ after RP is considered pathological stage pT2. The current TNM classification no longer uses pT2 substages as clinical evidence is lacking for their use[143,147].

2.4 Artificial Intelligence algorithms

Recent advances in deep learning (DL) have directly extracted previously unexplored information from cancer images, which supports a future with simplification and enrichment in clinical decision-making[148]. Current AI operates within a broad range of modalities, from radiology, pathology, and molecular diagnostics to health records. AI-driven exploration of multiple modalities could be reachable using emerging technologies[149]. Despite encouraging results, few algorithms have reached clinical implementation[25]. Therefore, an approach is required to reach actual patient value by focusing on clinical value and technological development. Current challenges include the generalizability and robustness of algorithms in clinical practice.

The generalizability and robustness of clinical algorithms describe the ability of an AI model to perform well on unseen data and in different settings. Generalizability means that the AI model can be applied to new patients or diseases and still provides accurate results. Robustness defines the AI model's ability to handle variations in the input data and still provide accurate results. These properties are essential for clinical pathology AI solutions because medical imaging data can be highly variable. A model that is not robust or generalizable may not be helpful in a clinical setting.

The most crucial obstacle to the clinical implementation of algorithms is limited generalizability, which occurs when a lack of all essential clinical features is observed in the limited training sets[25,150]. Clinical settings have many more source variations, such as scanners, stainings, and procedures that influence datasets. Consequently, the number of laboratories for assessing algorithms and training has typically been too small[151]. The influence of different patient populations between centers and countries has not been studied, even in other disciplines, such as radiology[152]. The primary observation with limited generalizability is the drop in performance when optimally functioning algorithms of their data are implemented on other data sources. Performance drops were observed in PCa classification when other scanners were used on the same slides[153]. Similar observations appeared for renal histopathology and nodal breast cancer metastases [154,155].

Creating a robust algorithm requires a dataset rich in variation from different staining batches, laboratories, and scanners. Additional variation could be added by different augmentation techniques, such as distribution shifting of the training data to match the test data distribution better. The goal is to make the AI model more resilient to variations in the input data by simulating color augmentation, especially, to mimic variation between laboratories[156,157]. Data augmentation

techniques are used to produce the variations that the model will encounter in real-world scenarios. A different and possibly additional technique to adapt an algorithm to variation is normalizing the images to a well-defined common standard by removing the variation from the images, mainly for color specification differences[154,158–161].

2.4.1 Validation of Artificial Intelligence algorithms

Algorithm validation is central to understanding the suitability of algorithms for clinical applications and collecting evidence on the safety and accuracy of the algorithms for regulatory approval. Validating AI algorithms in pathology involves evaluating their performance on a set of test data separate from the data that are used to train the model. The goal is to test a model on unseen data in a presumed real-world scenario. In pathology, several metrics exist to assess AI algorithm performance, including accuracy, sensitivity, specificity, and the area under the receiver operating characteristic (ROC) curve. Additionally, cross-validation allows for the model assessment by dividing the data into several subsets, training the model on some of these subsets, and testing the model on the remaining subsets. This assessment strategy can allow estimates of the model's performance on unseen data.

Usually, validation methods are applied during the early stages of algorithm development. Aberrations between the results of training data and the validation set can point to overtraining and indicate improvements by using additional techniques such as data augmentation or model regularization or reducing the complexity of the deep learning architecture. Even clinical evaluation of the data set and annotations can be required. Most studies use an independent data set from the same source to verify the model's performance. This level of the performance test is called internal validation and is the first practical step toward clinical implementation[162].

The next step towards regulatory approval should be external validation, which uses a set of previously unseen cases from a source not included in the training data, as shown in several studies[125,153,163,164]. This approach can reveal generalizability problems[165]. Collaborations to create generally accessible datasets for validation have been observed in projects such as the ‘Big Picture’ for Pathology and VAI-B within mammography[166,167]. These datasets can support regulatory approval. However, good performance on an external dataset does not directly imply the clinical usefulness of an algorithm and should not be regarded as such[168]. Even trials with clinical outcomes as endpoints to demonstrate long-term effects are also necessary to emphasize the clinical usefulness of AI algorithms[151].

Finally, validation of AI algorithms in pathology should be performed in a clinical setting with the involvement of pathologists to ensure the clinical validity and utility of the algorithm. Rather than focusing on algorithm performance, the clinical practice of the pathologist along with an array of immunohistochemistry and consultations should be included in the evaluation of the depiction. Campanella and colleagues state that a 100% sensitivity with a modest false positive rate should be the aim for algorithms in clinical settings[153].

2.4.2 Clinical digital pathology

The use of AI algorithms in a clinical workflow requires the implementation of digital pathology in the laboratory (Figure 5). The digitalization of the glass slides data signifies a safer and more efficient workflow. The digital pathology process represents a significant advancement in realizing the full potential of whole slide images (WSI)[169].

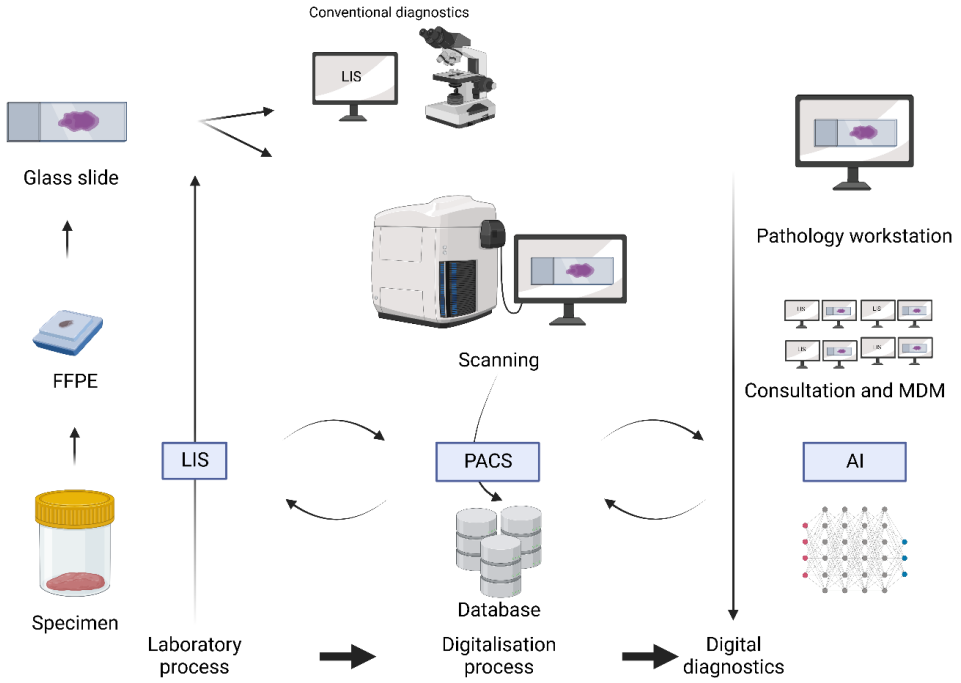

Figure 5. Digitalization facilitates digital diagnostics, consultation, and multidisciplinary meetings (MDM). Integration of Laboratory Information System (LIS), Picture Archiving And Communication System (PACS), and AI algorithms in digital diagnostics. FFPE (Formalin-fixed paraffine-embedded).

Validation of digital pathology involves ensuring that the digital images and associated data are accurate, reliable, and consistent with the original pathology specimens. There are several steps involved in validating digital pathology systems, including the following:

1. Image quality assessment: This involves evaluating the quality of the digital images captured by the system to ensure sufficient resolution and clarity for diagnostic purposes. After digitization, the created WSI should be checked to guarantee adequate image quality and avoid technical flaws in the final diagnosis. Correctly processed routine slides should not cause any problems during scanning. Typically, around 90% should result in diagnostic-quality images. Slides with unique microscopic requirements, such as high magnification or multiple focus points, may benefit from specialized scanning protocols as these types of slides may be more susceptible to digitization issues[169]. Local experience in a multicenter pathology laboratory with a yearly turnover of approximately 900 000 scanned slides for clinical diagnostics in the Region of Scania in southern Sweden showed less than one per thousand rescanned slides.

2. Clinical validation: This involves evaluating the diagnostic performance of the digital pathology system in a clinical setting and comparing the results obtained from the digital system to those obtained from traditional pathology methods. Clinical validation is necessary to demonstrate the diagnostic performance of digital pathology systems, mainly when these systems are intended for primary diagnosis or to replace traditional pathology methods. For this purpose, recommendations from multiple expert organizations are available[169–173]. Several validation studies for whole-slide imaging (WSI) have been conducted, with the majority demonstrating a high degree of agreement between traditional microscopic and digital diagnoses [174,175].

3. Regulatory validation: This involves demonstrating to regulatory authorities that the digital pathology system is accurate, reliable, and consistent with traditional pathology methods. General guidelines for the validation process are published by the United States Food and Drug Administration (FDA). Generally, digital pathology devices intended for primary diagnosis or as a substitute for a pathologist's microscopic examination of glass slides must demonstrate through suitable validation studies that the device's output is equivalent to that of a trained pathologist who analyzes biopsy specimens on glass slides under a microscope[176].

In cases where the image quality of the digital pathology system is directly comparable to that of the microscopic slides, the clinical validation process can be less extensive, as the digital pathology system is less likely to introduce diagnostic errors. It should be noted that the validation and requirements for a digital pathology system can vary based on the intended use, country regulations, and the level of innovation of the system.

2.5 Management of prostate cancer

2.5.1 Overview

Clinical choices for the management of PCa are based on personalized, risk-adapted treatments. Key factors to consider are the TNM stage of PCa (local (T1-2), locally advanced (T3-4), locoregional (N1) or metastatic (M1); castration-resistant status), histological and molecular features (neuroendocrine, cribriform, intraductal patterns, DNA repair mismatch), patient's life expectancy, overall health, family history, and personal preferences[177]. The risk of biochemically recurrent disease is determined by baseline PSA level, biopsy grade, and clinical T stage and ultimately guides treatment decisions[178]. In addition to evidence-based guidelines, the Advanced Prostate Cancer Consensus Conference (APCCC) in 2022 conducted a survey to guide clinical decisions in areas lacking high-level evidence. The survey especially focused on novel advanced imaging and molecular characterization, coupled with emerging therapies that seem to improve outcomes in advanced PCa[177].

Generally, patients are categorized into low-, intermediate-, or high-risk groups based on their 5-year BCR rates of <25%, 25-50%, and >50%, respectively[179]. The intermediate-risk group is split into two sub-groups: low-intermediate (ISUP grade 2) and high-intermediate (ISUP grade 3), which improves the accuracy of risk classification[180,181].

Localized PCa is primarily managed using AS or radical local treatment. The physician decides on the treatment options, including AS, radiotherapy with potential ADT, or surgery with/without pelvic lymph node dissection (PLND). It is important to note that no specific active treatment method provides superior overall or prostate cancer-specific survival compared with other active management options for localized disease[93]. However, combining radical local treatment (surgery or external beam radiotherapy (EBRT)) with ADT offers the best outcomes[93,182]. Low-risk to low-

intermediate risk can undergo any of the above options; high-intermediate or high-risk patients are recommended one of the interventional therapies.

Adopting a watchful waiting (WW) or active surveillance (AS) strategy with treatment initiated upon progression is recommended for patients with a life expectancy of fewer than ten years. Regular monitoring through PSA tests and digital rectal examinations can determine whether a change in management is needed. Patients treated with definitive local therapies are consequently monitored for disease relapse and may not require further management.

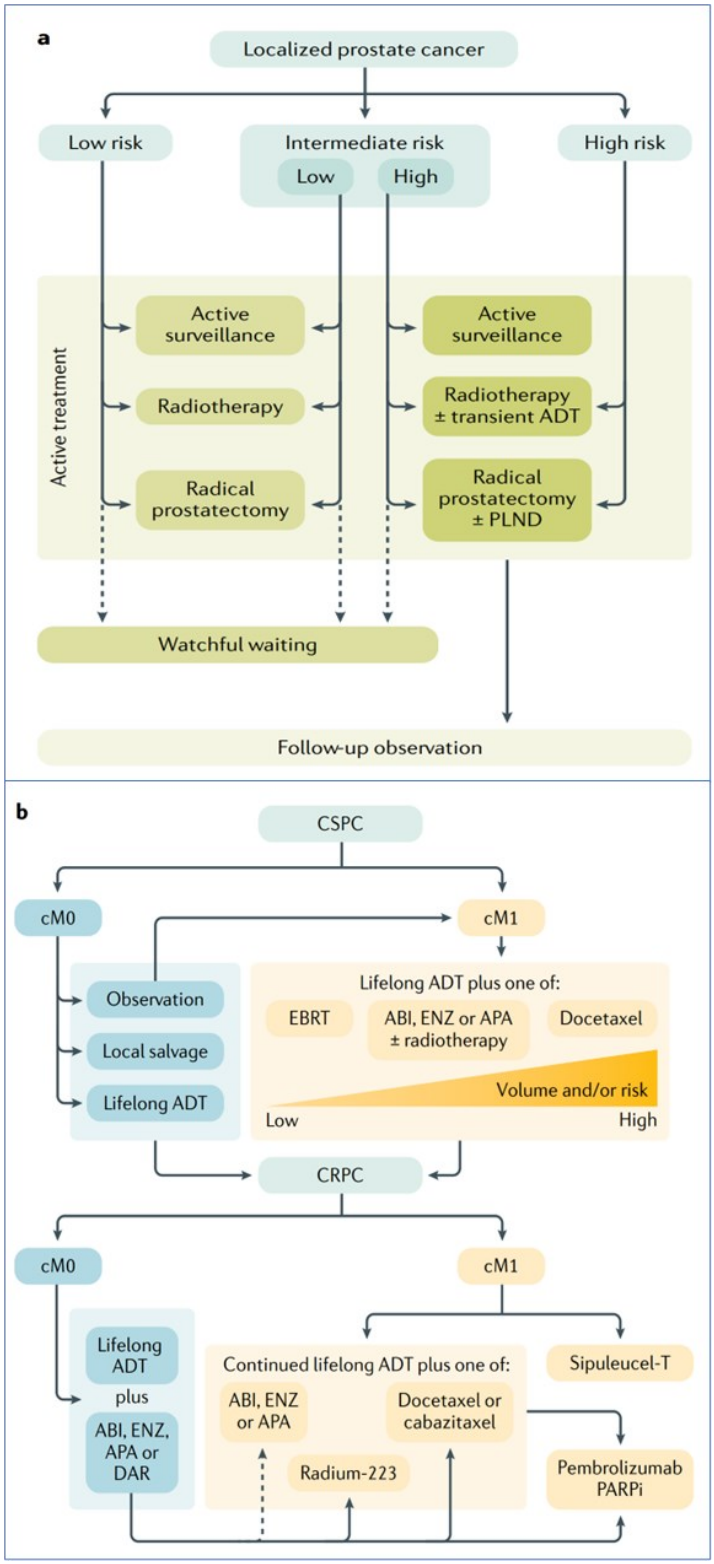
a
Localized prostate cancer
Low risk
Intermediate risk
Low
High
High risk
Active treatment
Active surveillance
Radiotherapy
Radical prostatectomy
Active surveillance
Radiotherapy ± transient ADT
Radical prostatectomy ± PLND
Watchful waiting
Follow-up observation
b
CSPC
cM0
cM1
Observation
Local salvage
Lifelong ADT
Lifelong ADT plus one of:
EBRT
ABI, ENZ or APA ± radiotherapy
Docetaxel
Volume and/or risk
Low
High
CRPC
cM0
cM1
Lifelong ADT
plus
ABI, ENZ, APA or DAR
Continued lifelong ADT plus one of:
ABI, ENZ or APA
Docetaxel or cabazitaxel
Radium-223
Sipuleucel-T
Pembrolizumab
PARPi

Figure 6. Overview of prostate cancer management.

***A**. Low- or intermediate-risk disease receives active surveillance (AS), radiation therapy (RT) with or without androgen deprivation therapy (ADT), or radical prostatectomy. Treatments such as AS, RT plus short-term ADT, or RP with or without pelvic lymph node dissection (PLND) are recommended for high intermediate- or high-risk disease. Patients with a limited life expectancy (< 10 years) can opt for watchful waiting and receive treatment when necessary, as indicated by follow-up tests, such as PSA and digital rectal examinations. After definitive local treatment, subsequent observation for recurrence is offered without the need for further interventional management.*

***B.** BCR stands for disease recurrence and is classified into cM0 and cM1. cM0, considered to have micrometastatic disease, may receive local salvage treatment, lifelong ADT, or observation. cM1, explicitly metastatic, is treated with lifelong ADT and a choice between docetaxel or androgen receptor signaling inhibitor (ARSI; abiraterone (ABI), enzalutamide (ENZ), or apalutamide (APA)). Radiotherapy or external beam radiotherapy (EBRT) may also be administered based on metastatic spread. Castration-resistant prostate cancer (CRPC), a further progression of PCa, is treated with ongoing ADT and an ARSI for cM0 CRPC, and ARSI, radium-223 (if only bone metastases are present), or chemotherapy (docetaxel before cabazitaxel) for cM1 CRPC. Some patients may benefit from new drugs like pembrolizumab or poly ADP-ribose polymerase inhibition (PARPi). Reprint with permission from Springer Nature*[178].

2.5.2 Active surveillance and watchful waiting

To reduce overtreatment, organ-confined PCa is managed using two practical strategies: AS and WW. AS is the preferred option for treating low-volume, low-grade PCa, which is otherwise eligible for curative treatment. The goal is to manage patients cautiously and only provide definitive treatment to those who may experience adverse outcomes over time[183]. This approach helps reduce excessive treatment and minimize treatment-related complications and side effects. However, the challenge is identifying patients who require definitive treatment and to demarcate the appropriate time for such treatment. AS is a safe treatment strategy for low- and intermediate-risk PCa compared to curative treatment with radiotherapy (RT) or radical prostatectomy (RP), as confirmed by several studies with long-term outcomes of ten years follow-up. There was no overall or cancer-specific survival differences between treatment modalities[184–186].

Aggressive treatment may be necessary, if there is evidence of disease progression during AS. Spontaneous grade progression from GS 3 to GS 4 or higher occurs in 1-2% of AS patients annually, particularly in high-volume GS 6 PCa[187]. However, grade progression is more commonly diagnosed during AS for simultaneous higher-grade cancer. Therefore, a considerable proportion of patients are reassigned to definitive treatment during AS. Treatment changes appear in 40 to 59% of AS patients within 10 years[184]. Men with long life expectancy are primarily considered to benefit from AS.

WW is also known as deferred treatment for PCa. The idea behind WW is to avoid the side effects and risks associated with unnecessary treatments and only start treatment when necessary. Monitoring during deferred treatment may be less frequent than for AS but still involves regular check-ups to assess the progression of PCa. However, passive monitoring does not involve any monitoring and leaves it up to the patient to visit the doctor. Passive monitoring is suitable for patients who are unable to endure the physical strain of treatment due to age, frailty or other illnesses and do not have significant symptoms of PCa[188].

The Scandinavian Prostate Cancer Group Study 4 study supported surgery for men younger than 65 years and for those with intermediate-risk cancer concerning PCa-associated death. Surgery only reduced the risk of PCa metastasis in older men[189]. A recent study showed improved survival outcomes for older men with high-grade PCa who were receiving local therapy, especially surgery, when they were compared to their hormone-therapy or observation only counterparts[190]. Consequently, ideal patient selection for therapy should not be solely based on age.

2.5.3 Radiotherapy

Ablative radiotherapy was found to be a curative and effective approach for localized therapy of 60% of men with localized PCa[191]. RT treatment options for clinically localized disease include EBRT using intensity-modulated or volumetric arc methods and/or interstitial brachytherapy. The cellular response to radiotherapy is complex, and the main goal is to deliver enough DNA damage to cancer cells to disrupt their ability to proliferate and survive while minimizing damage to normal cells[192].

Low-risk to intermediate-risk disease can be treated with low-dose permanent radioactive seed insertion, whereas high-risk localized diseases can be treated with a high short-term radioactive dose during EBRT of the ROI. The ESMO recommendations for the management of local and locoregional PCa add abiraterone-prednisone treatment to RT and ADT for high-risk PCa. High-risk PCa is defined by either N1 disease or at least two risk factors including T3-T4, PSA levels greater than 40 ng/ml and a GS of 8-10. Treatment for two years resulted in improvements in both metastases-free survival (MFS) (hazard ratio (HR): 0.54, 95% confidence interval (CI) 0.43-0.68, p = 3.2 x 10-7) and overall survival (HR: 0.63, 95% CI 0.48-0.82, p = 0.0005) among men with a very high-risk M0 PCa[193,194].

Intermediate-risk disease patients with a life expectancy of over ten years should be presented with active intervention options, such as prostatectomy or primary ablative radiotherapy, which can be administered as EBRT combined with 4-6 months of transient ADT or low-dose brachytherapy. Both prostatectomy and primary ablative RT options have similar efficacy but may have different adverse effects[195]. The patient's quality of life, after ablative-RT can be reduced by urinary side effects such as retention, hematuria, and dysuria, as well as bowel side effects such as diarrhea, rectal bleeding, and proctitis due to the proximity of the organs[196].

After primary treatment, salvage radiotherapy (SRT) is administered to patients with prostate cancer who experience BCR. BCR can be identified by increased PSA levels, which occurs in 27-53% of patients following radical local treatment[197]. SRT reduces the risk of systemic progression by 75% and increases the likelihood of progression-free after five years in patients with BCR or constantly elevated PSA levels after RP[198–200]. The most significant advantage of SRT is observed in patients with a rapid PSA doubling time and a PSA level of 0.2 ng/ml or less before undergoing SRT[198]. Additionally, combining ADT with luteinizing hormone-releasing hormone (LHRH) antagonists or inhibiting the AR with bicalutamide may enhance survival[201].

However, treatment decisions for patients with BCR after primary RT are limited by a lack of high-quality evidence. RP may be a local therapy option for certain patients with prostate cancer relapse[93,177].

2.5.4 Radical prostatectomy

RP is a surgical intervention that removes the entire prostate gland. Prostatectomy can be performed using various surgical techniques, such as open surgery, with a relatively large incision. Laparoscopic surgery is where small incisions are made, and the surgery is done with specialized instruments and a camera, and robotic surgery uses a robotic system controlled by the surgeon to perform the surgery.

PLND can extend RP as an addition to treating high-grade disease or suspected lymph node involvement. Nomograms can preoperatively support the risk assessment of lymph node involvement[202–204]. PLND does not improve outcome and can lead to an enhanced risk of complications[205]. However, PLND is essential for information on staging and prognosis in specific clinical cases. Patients' quality of life are decreased mainly by postoperative complications such as

erectile dysfunction (ED) and urinary incontinence (UI). The rates of ED and UI are approximately 70% and 20%[206] one year after surgery. A Cochrane review did not confirm any differences in survival, UI, or ED outcomes between open surgical prostatectomy and laparoscopic techniques[207].

2.5.5 Hormonal therapy

The aim of hormonal therapy is to lower the levels of androgen hormones or block their effects on cancer cells. The main hormones in PCa growth are testosterone and dihydrotestosterone (DHT). Hormonal therapy for PCa involves manipulating the hormone levels or blocking the action of hormones that promote the growth of PCa. Hormonal therapy is often combined with other treatments, such as RT or surgery in advanced local disease or metastatic cases.

Several types of hormonal therapies can be used to treat prostate cancer, including:

1. ADT involves reducing the levels of testosterone and DHT using drugs that block the production or action of these hormones. Common ADT drugs include gonadotropin-releasing hormone (GnRH) agonists, antagonists, and antiandrogens.

2. Orchiectomy is a surgical procedure that removes the testicles that are the primary source of testosterone in men.

3. Estrogen therapy involves using drugs that convert testosterone to estrogen, which slows cancer cell growth.

Another important category of hormonal therapy used in the treatment of prostate cancer is the androgen receptor signaling inhibitors (ARSI). ARSI medication, such as abiraterone, enzalutamide, apalutamide, darolutamide, bicalutamide, nilutamide, and flutamide, work by inhibiting androgen synthesis, blocking androgen receptor signaling or by competitive binding to ARs.

RT combined with transient ADT is superior to RT alone in terms of survival. Recommendations for transient use vary between intermediate-risk and high-risk local disease, from short periods of three months to extended treatment of three years[208].

Lifelong ADT is indicated in metastatic PCa (cM1) or BCR following curative treatment (cM0). Combination treatments are now the standard for mCSPC. Decisions should consider disease traits, patient health status, other medical conditions, personal preferences, and possible increased complications and treatment availability. It has been noted that AR antagonists or docetaxel combined with ADT in initial treatment is reliable and extends life[209]. Ongoing studies such as PEACE1 and ARASENS have combined ADT with docetaxel and local RT/abiraterone or darolutamide, which will determine, if triple combinations bring further improvements[210,211]. Other questions include how to identify and treat patients with limited metastases (oligometastatic disease) and if metastasis-directed therapy has added benefits for such a group[178]. The addition of abiraterone-prednisone to ADT and docetaxel in the PEACE-1 phase III trial led to improvements in both radiographic progression-free survival (rPFS) (HR 0.50, 99.9% CI 0.34-0.71, $p < 0.0001$) and OS (HR 0.75, 95.1% CI 0.59-0.95, $p = 0.017$). The study found that in the "high-volume" population, which consisted of men with at least four bone metastases, including at least one in the peripheral skeleton, or visceral metastases, the median survival time was 5.14 years with abiraterone-ADT-docetaxel, as compared to 3.47 years with ADT-docetaxel alone (HR 0.72, 95.1% CI 0.55-0.95, $p = 0.019$)[210]. Adding darolutamide to ADT plus docetaxel improved OS in the ARASENS phase III trial (HR 0.68, 95% CI 0.57-0.80, $p < 0.0001$). However, no data on rPFS or the disease burden are available[211].

In cases where AR therapy resistance appears, multiple alternatives have appeared. In mCRPC, taxane-based chemotherapy, ARSIs, and radium-223 chloride have improved OS[211].

Taxanes bind to tubulin, thereby they explicitly target and stabilize microtubules, which prevents the normal disassembly of tubules. This, in turn, disrupts the dynamic equilibrium of the cell's microtubule network, resulting in mitotic arrest, a disruption of mitotic spindle formation, and activates apoptosis. Microtubules are essential structures involved in cell division and the maintenance of cell shape[212]. A study on taxane-based therapy found the median OS in cabazitaxel was 15.1 months compared to 12.7 months in the mitoxantrone group (HR for death in the cabazitaxel group 0.70, 95% CI 0.59-0.83, $p < 0.0001$)[213]. The Cabazitaxel Resistance in the Castration-Resistant Prostate Cancer (CARD) trial found that cabazitaxel resulted in improvements in both rPFS (HR 0.54, 95% CI 0.40-0.73, $p < 0.001$; medians: 8.0 versus 3.7 months) and OS (HR 0.64, 95% CI 0.46-0.89, $p = 0.008$; medians: 13.6 versus 11.0 months) in men with mCRPC. These men had previously been treated with docetaxel and had experienced progression within 12 months while receiving a new ARSI. Compared to either abiraterone or enzalutamide, cabazitaxel showed a median rPFS of 8.0 months versus 3.7 months (HR 0.54, 95% CI 0.40-0.73, $p < 0.001$). The median OS of 13.6 months versus 11.0 months (HR 0.64, 95% CI 0.46-0.89, $p = 0.008$) [214]. In the enzalutamide group, an ARSI, the median OS was 18.4 months compared to 13.6 months in the placebo group (HR for death in the enzalutamide group 0.63; 95% CI 0.53-0.75; $p < 0.001$)[215]. Radium-223 treatment showed a significant improvement in mean OS compared to placebo (14.9 months vs. 11.3 months, HR 0.70; 95% CI 0.58-0.83; $p < 0.001$)[216]. The mechanism of radium-223 treatment is based on its similarity to calcium and it is taken up by areas of increased bone turnover, such as areas of bone metastases. Once inside the bone, radium-223 emits alpha particles with a short penetration range, which exclusively targets the surrounding cancer cells, thereby causing DNA double-strand breaks that might be irreparable and lead to cell death[217]. All studies were conducted during ADT alone; the benefits for patients receiving these mCSPC treatments are unknown. Abiraterone and enzalutamide extended progression-free lifetime and improved response rates in clinical trials and are now standard treatments before or after docetaxel[215,218–220]. The optimal sequence of treatments for mCRPC, especially with previous mCSPC treatments, is still debated. Docetaxel is less effective when previously administered for mCSPC, but enzalutamide and abiraterone remain beneficial. Cabazitaxel stays active after docetaxel and enzalutamide treatment.

Unfortunately, biomarkers that could aid in personalized treatment choices and sequences are mainly lacking. It is important to note that the presence of AR-V7 only indicates the effectiveness of taxane therapy compared to ARSI rather than providing comprehensive treatment management[51]. In the PROfound trial, olaparib was tested against a second ARSI in men with mCRPC, BRCA1 and BRCA2 alterations and whose disease had progressed prior ARSI (and docetaxel in some patients). An updated analysis of the trail revealed a significant improvement in OS for patients treated with olaparib (HR 0.69, 95% CI 0.50-0.97, $p = 0.0175$; medians: 19.1 months versus 14.7 months), with the benefit primarily seen in men with BRCA alterations[221].

2.5.6 Immunotherapies

The field of immunotherapies is developing fast and holds great promise for certain techniques. mCRPC is the main indication for immunotherapy.

The primary mechanisms for the techniques under clinical evaluation are:

- Immunogenic:

- The patient's dendritic cells that target the prostate epitope PAP to induce a T cell attack on the tumor cells are injected into the patient's bloodstream (Sipuleucel-T).
- A viral vector-based vaccine that targets PSA molecules is injected. The immune system recognizes these antigens as foreign and triggers an immune response, explicitly targeting cells expressing the PSA and other PCa antigens. This response includes activating specialized immune cells, such as T cells and natural killer cells, which directly attack the cancer cells (Prostvac).
- Immune checkpoint inhibitors: Medication that disrupts cancer cells' mechanisms to evade immune detection by blocking PD1/PDL1, enhancing the immune system's response.
- Radioligand therapy: In lutetium-177 prostate-specific membrane antigen (177Lu-PSMA-617), a PSMA antibody is combined with lutetium-177 that delivers beta-particle radiation precisely and specifically to PSMA-positive cells and the surrounding microenvironment.

Sipuleucel-T is a vaccine made from a patient's dendritic cells that target the prostate epitope PAP to boost T cell recognition and clear PCa cells[222]. According to the IMPACT study, sipuleucel-T extends OS by four months from 25.9 to 21.4 months in mCRPC but does not affect disease progression[223]. The first FDA-approved immunotherapy treatment against PCa sparked attention and interest in developing specific immune detection for PCa.

Later trials with PROSTVAC, a viral vector–based immunotherapy against PSA-positive PCa, disappointed in phase 3 trials as there was no improvement in survival[224,225].

Pembrolizumab is an immune checkpoint inhibitor and a monoclonal antibody that blocks immune evasion of tumors by binding to PD1 on T cells, which showed limited efficacy as a single drug against mCRPC in the KEYNOTE-199 trial[226]. Nevertheless, it showed promising results in cases with high skeletal tumor load regardless of PDL1 positivity. The effectiveness of drugs such as pembrolizumab or durvalumab that target PD1/PDL1, may be enhanced by either using it with enzalutamide or in patients with numerous DNA repair alterations who are being treated with PARPi[228,229]. The FDA approved pembrolizumab for cancers with a loss of function of the MMR genes that ultimately lead to high microsatellite instability (MSI-H) or high tumoural mutation burden. Despite the current lack of solid evidence for PCa immunotherapy treatment, evaluating these factors in mCRPC patients may provide individualized treatment options in the future. According to the Consultation Conference on Molecular Pathology of Urogenital Cancers, patients with known metastatic disease should undergo somatic tumor DNA testing when medically necessary. The testing should include evaluating defective MMR genes (MutS Homolog 2 (MSH2), MutS Homolog 6 (MSH6), MutL Homolog 1 (MLH1), Postmeiotic Segregation Increased 2 (PMS2)) through MMR immunohistochemistry (IHC) with or without MSI testing. The testing should include sequencing for at least BRCA1 and BRCA2 to detect any HR pathway defects and copy number alterations[229]. Stopsack et al. recommended BRCA1 IHC as a predictive biomarker for generally applied therapies for metastatic disease[230].

The combination of 177Lu-PSMA-617 showed significant improvements in both rPFS and OS compared to the best standard of care alone in men with mCRPC who had undergone at least one taxane and at least one novel ARSI. Results from the VISION trial indicated a reduction for rPFS (HR 0.40, 99.2% CI 0.29-0.57, $p < 0.001$; medians: 8.7 versus 3.4 months) and OS (HR 0.62, 95% CI 0.52-0.74, $p < 0.001$; medians: 15.3 versus 11.3 months)[231]. Patients were selected for PSMA positivity based on PSMA PET imaging[232].

2.6 Disease prediction

2.6.1 Nomograms

PCa nomograms are graphical tools that are used to predict the likelihood of PCa recurrence after surgery or other treatments. These nomograms blend an assortment of clinical and pathological variables including the patient's age, GS, and cancer stage, to calculate the likelihood of cancer recurrence. Nomograms can help guide treatment decisions, thus allowing the physician to consider the specific characteristics of an individual patient's cancer and be able to predict the likelihood of recurrence for that patient.

Several prostate cancer nomograms have been developed and used, including the CAPRA risk score, the D'Amico risk classification system, and the MSKCC nomogram. These nomograms are typically used in conjunction with other diagnostic tests to determine the best treatment options for individual patients.

Assessment tool	Primary outcome	Variables	Low risk	Intermediate risk	High risk
Partin table	Extent of disease probability	PSA, GS, T-stage	OC 88% EPE 11% SVI 1% LNM 0%	OC 38–58% EPE 36–48% SVI 4–7% LNM 2–6%	OC 5–12% EPE 23–33% SVI 22–23% LNM 32–48%
MSKCC	Extent of disease probability Progression-free probability after radical prostatectomy	Age, PSA, GS, T-stage, percent positive biopsies	Dynamic Prostate Cancer Nomogram Coefficients are available at: https://www.mskcc.org/nomograms/prostate/pre_op/coefficients		
D'Amico risk group	Progression-free probability after radical prostatectomy	PSA, GS, T-stage	PSA<10ng/ml and; GS ≤6 and; T1–T2a	PSA 10–20ng/ml or; GS 7 or; T2b	PSA >20ng/ml or GS 8–10 or; T2c–T3
CAPRA score	Progression-free probability after radical prostatectomy	Age, PSA, GS, T-stage, percent positive biopsies	0–2	3–5	6–10

Table 4. Nomograms for prostate cancer risk classification at diagnosis. PSA: Prostate-Specific Antigen; GS: Gleason Score; T-stage: Tumor Stage; BCR: Biochemical Recurrence; OC: Organ-Confined; EPE: Extracapsular Extension; SVI: Seminal Vesicle Involvement; LNM: Lymph Node Involvement; MSKCC: Memorial Sloan Kettering Cancer Center.

2.6.1.1 Partin tables

Partin tables are a tabular tool that is used to predict the likelihood of PCa spreading beyond the prostate gland in men diagnosed with the disease. By inputting the values of cancer grade, stage, and

serum PSA level into the tables, a score that reflects the likelihood of cancer spread can be generated. The original study introduced the Partin tables in 1993[233]. The tables have been revised to incorporate the most recent trends in the presentation and clinical stages of newly discovered prostate cancer cases[7,235].

2.6.1.2 The Memorial Sloan Kettering Cancer Center nomogram

The MSKCC nomogram considers the patient's age, cancer stage, tumor grade, the relationship between cancer-positive and cancer-negative biopsies, and the serum PSA level. By inputting these values into the nomogram, a score that reflects the recurrence likelihood can be generated. The different nomograms are available online (https://www.mskcc.org/nomograms/prostate). Several studies have validated the MSKCC nomogram as a valuable tool for predicting prostate cancer outcomes[235–239].

2.6.1.3 D'Amico risk stratification

The d'Amico risk stratification system is based on PSA, GS and T-stage. The initial goal of the retrospective cohort study 1998 was to compare treatments (RP, EBRT and radioactive seed implants with or without ADT) for 1872 patients with clinically localized PCa treated between January 1989 and October 1997. The results showed that low-risk patients had similar 5-year PSA outcomes regardless of treatment, whereas intermediate- and high-risk patients treated with RP or RT had better outcomes than those treated with an implant. Adding ADT did not improve PSA outcomes in high-risk patients in this study[240].

2.6.1.4 Cancer of the Prostate Risk Assessment

The CAPRA nomogram considers the stage of PCa, tumor grade, patient's age, percentage of biopsy cores positive for cancer, and presence or absence of specific PSA levels. By inputting these values into the nomogram, a score that reflects the likelihood of recurrence is generated. The study that introduced the CAPRA system was published in 2005. It featured a group of more than 1400 men diagnosed with prostate cancer between 1992 and 2001 and underwent a radical prostatectomy

without additional radiation or hormonal therapy (Figure 7)[8].

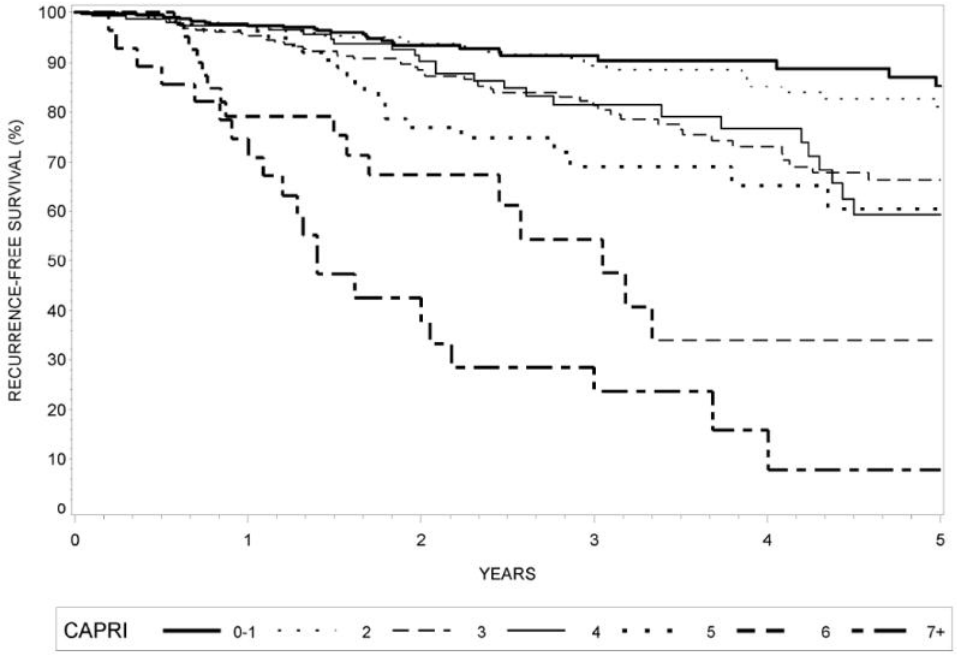

Figure 7. 5-year Kaplan-Meier survival curves. Survival curves for 5-year recurrence-free survival among patients with each CAPRA score. Permission for reprint from Wolters Kluwer Health, Inc[8].

The CAPRA system was externally validated in 22 studies with good performance in academic and community settings[241].

2.6.2 Biomarkers in prostate cancer

Biomarkers are molecules or characteristics that are measured in a person's biological samples (such as urine, blood, or tissue) and are utilized to indicate the presence or progression of a disease. Biomarkers are essential for PCa assessment and are usually categorized into diagnostic, prognostic, and predictive groups. The classification of biomarkers is not static as new biomarkers are constantly being discovered and studied.

The Prostate Health Index (PHI) is a blood test used to detect PCa by combining three types of prostate-specific antigens. A meta-analysis of over 2900 men showed that PHI had better accuracy in detecting PCa than fPSA[242]. Another test, the PCA3 score, is obtained from urine samples and is specific to PCa. The PCA3 score can predict malignancy in men with elevated PSA and negative biopsy results[243]. PCA3 is a long non-coding RNA (lncRNA) that is overexpressed in prostate cancer cells compared to PCA3 in normal prostate cells. The presence and levels of PCA3 RNA can indicate the presence of prostate cancer[244,245]. The Stockholm-3 model measures the levels of five plasma markers (PSA, free PSA, hK2, MSMB, and MIC1) in a blood sample and analyzes 101 genetic variants. These results, combined with the patient's age, family history, and previous biopsy, resulted in a risk score for PCa that performs better than PSA alone in detecting csPCa[246].

Other commercially available tests for PCa detection, prediction and prognosis are shown in Table 5.

Test	Definition
Mi-Prostate Score	A urine-based test that combines measurements of three genes (PCA3, T2:ERG, and serum PSA) to assess the risk of aggressive PCa and aid in determining the need for a prostate biopsy[248].
Oncotype DX	A genomic test that analyzes the activity of 17 genes in a PCa tumor to predict the likelihood of disease recurrence after surgery and help guide decisions about the need for additional treatment, such as radiation[248].
Confirm MDx	A tissue-based test that assesses the methylation status of three genes (GSTP1, APC, and RASSF1) in negative prostate biopsy samples to identify the presence of undetected cancer and determine the need for a repeat biopsy[249].
Prolaris	A genetic test that measures the expression of 31 cell cycle progression genes in prostate cancer tissue to predict the risk of disease progression and inform treatment decisions[250].
Prostate Core Mitomic	A test that analyzes mitochondrial DNA mutations in prostate biopsy tissue to identify PCa aggressiveness and aid in treatment decision-making[251].
4K Score	A blood test that combines four prostate-specific biomarkers (Total PSA, Free PSA, Intact PSA, and Human Kallikrein 2) with clinical information to predict the risk of aggressive PCa and the need for a biopsy[252].
Prostarix	A urine-based test that measures the levels of four metabolites (sarcosine, alanine, glycine, and glutamate) to predict the likelihood of a positive prostate biopsy result and aid in biopsy decision-making[253].
Decipher	A genomic test that analyzes the activity of 22 genes in PCa tissue to predict the likelihood of metastasis after surgery and help guide decisions about the need for additional treatment, such as radiation[254].

Table 5. Tests for commercially available decision-making support in PCa.

An upcoming area for diagnostics and predictive testing is circulating tumor DNA (ctDNA), which refers to small fragments of DNA that circulates throughout the bloodstream after being shed by PCa cells. These fragments contain genetic alterations specific to the tumor, making ctDNA a valuable biomarker for PCa that can be detected through a simple blood test. Mutations in genes such as TP53, PTEN, BRCA1, and BRCA2 have been detected through ctDNA analysis in mCRPC. Although ctDNA analysis seems promising, further research and validation are needed to establish its utility, sensitivity, and specificity in different stages and subtypes of prostate cancer[255].

3 Aims of the study

This thesis aimed to compare mpMRI and histological findings and determine their impact on survival over time.

The specific goals of the studies presented are as follows:

1. To determine whether mpMRI combined with general prostate cancer risk assessment tools (CAPRA, Partin tables, MSKCC nomograms) can predict overall adverse findings and BCR in an RP cohort.

2. To determine if the mpMRI-visibility of PCa lesions is reflected in the protein expression status of PTEN and ERG and could be used to identify patients at risk of specific adverse findings (BCR, EPE, SVI, LNM) in an RP cohort.

3. To determine the histopathological composition of mpMRI-visible and invisible PCa lesions and assess whether the stromal signature could be used to stratify patients for BCR in an RP cohort.

4. To determine whether a neural network trained to classify GG can perform as well as a pathologist in a clinical setting for preoperative Bx series and be able to stratify patients based on BCR in an RP cohort.

4 Materials and methods

4.1 Data sources and ethics statement

The data for the studies were obtained from the Department of Urology and Pathology, HUS Helsinki University Hospitals, Finland. All data were retrospective, and utilized the patient's unique Finnish social security number (Henkilötunnus) to collate data from different databases. The clinical data for the studies included laboratory data as PSA, pathological data as diagnosis, stage, and grade on RP and Bx, and radiologic data as PI-RADS. The locations of the ROI were compared and collected between radiology and pathology. The studies were carried out in compliance with the Declaration of Helsinki and received approval from the Institutional Ethics Committee of Helsinki University Hospital (diary number 386/13/03/02/2014). Specific patient consent is redundant for retrospective studies I-IV, therefore no consents were obtained.

4.2 Study settings

4.2.1 Study I-III

In studies I, II, and III, we utilized the same cohort of 598 consecutive patients who underwent RALP as their primary treatment at the discretion of the treating clinician at HUS Helsinki University Hospitals from January 2014 to September 2015 (Figure 8). Lymphadenectomy (LA) was performed on 188 patients. The threshold for an extended lymphadenectomy, according to the MSKCC nomogram, was a GG score of 3 or higher or a greater than 5% risk of lymph node-positive disease. 387 patients in the cohort received preoperative mpMRI, whereas 211 RALP patients who did not receive mpMRI were monitored during follow-up to eliminate any referral bias towards preoperative mpMRI.

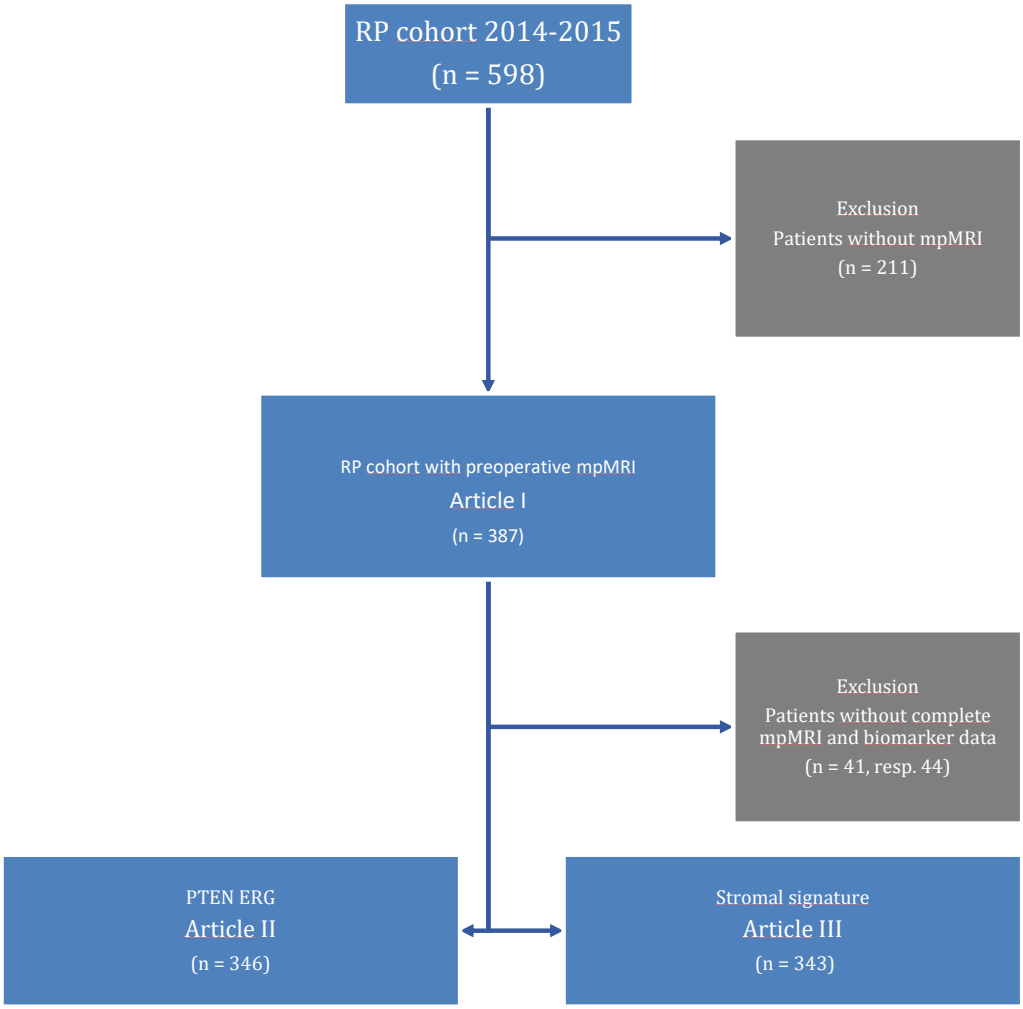

Figure 8. Flowchart for studies I-III with the number of patients. Forty-one patients were excluded from Article II, whereas 44 were excluded from Article III.

Preoperative prostate mpMRI scans were performed using a Philips Achieva 3.0T device, which produced three-millimeter-thick image slices. The modalities included T2WI and DWI that comprises ADC mapping and dynamic contrast-enhanced (DCE) sequence in compliance with the Society of Urogenital Radiology Guidelines. The imaging protocol followed the PI-RADS recommendations. The mpMRIs were reported using the PI-RADSv1 standard, and a structured form was used that included information such as the number of lesions (up to 4), location, size (volume and maximum diameter), capsule contact length, EPE, seminal vesicle invasion (SVI), and lymph node metastasis (LNM). On average, each of the four radiologists reviewed 200 prostate mpMRI cases per year.

After a transperitoneal radical prostatectomy, the prostate and lymph nodes were fixed in formalin and embedded in paraffin at Helsinki University Hospital Laboratory Services (HUSLAB). The central sections of the prostate were sliced horizontally and vertically at the apex and base, respectively. The seminal vesicles were sliced separately. Obturator and inguinal lymph nodes were sliced separately on both sides. Diagnostic slides were prepared and stained with H&E. The entire prostate tissue was

included in the slides. The pathological anatomical diagnosis (PAD) included the following information: primary and secondary GS, tumor volume, margin status, EPE, SVI, node status (NS), and pT. Adverse findings were identified as EPE, SVI, or LNM.

The tissue microarray (TMA) construction was created using 1.0 mm punches according to the annotations of the pathologist. Three punches were taken from the ROI 1 on the mpMRI, two from ROI 2 and 3, and two from the clinically critical mpMRI-invisible lesion. One neighboring benign core per RP specimen was taken as a staining control. Visibility was defined according to clinical relevance. PI-RADS scores of 3-5 were categorized as detected and visible cancers, whereas PI-RADS scores of 0-2 were regarded as missed or invisible cancers.

The TMA blocks were sliced at four µm thickness and stained in first-round staining for HE, PTEN, and ERG. Three uropathologists (KS, SN, and TM) scrutinized for quality control for GG and tissue representativeness. The expression of PTEN and ERG in the TMAs was assessed by three separate observers (JE, KoS, and TM). Staining quality was verified using an internal control. PTEN cytoplasmatic positivity was required in the benign prostatic epithelium and cytoplasm, whereas ERG nuclear positivity was required in the endothelium. PTEN expression was classified as low, intermediate, and high to be grouped into negative (negative or low) and positive (intermediate or high).

In Study II, we divided the cohort into three groups based on mpMRI visibility: Group A (n=90) with only visible lesions, Group B (n=221) with both visible and invisible lesions, and Group C (n=35) with only invisible lesions (Figure 9).

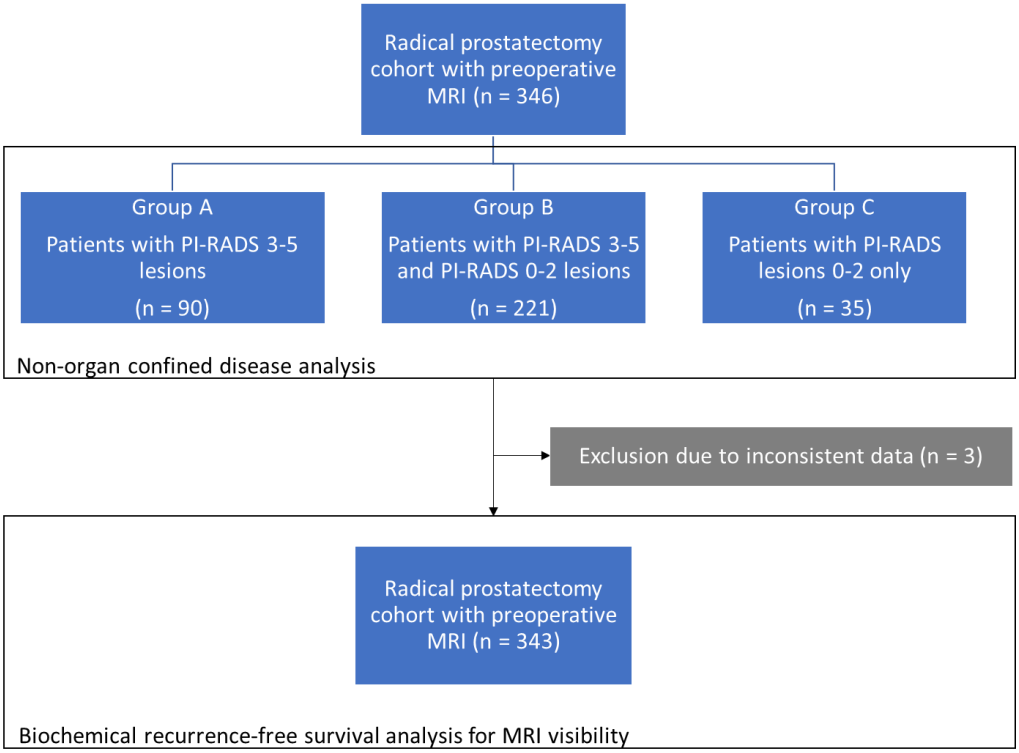

Figure 9. Flowchart of article II with cases and their distribution into groups A (mpMRI visible only, n = 35), B (mpMRI visible and invisible, n = 221), and C (mpMRI invisible, n = 35). Modified from Eineluoto et al., Eur Urol Focus 2020.

For study III, TMA slices were stained with a first-round of fluorescence staining for CD8, FAP, CD163, and PanEpi (consisting of PanCK, PanCK AE1/3, and E-Cadherin), and costained with DAPI before scanning into five-channel fluorescence images. After scanning and removing the first-round staining and antibodies, a second-round of fluorescence staining was performed with alpha-smooth muscle actin (SMA), and the slides were scanned again. The images of the second round were projected on the first-round image using the DAPI signal as a spatial reference. Image analysis defined the total stroma area determined by all marker-defined cells. Then, the epithelial area was detected by thresholding the PanEpi channel and converting the image mask into objects. Finally, these objects were subtracted from the total tissue to create the stroma area. The glandular lumen was defined by filling and subtracting the epithelial mask (Figure 19A-B). The fractions of the tissue compartments were plotted for benign tissue, visible and invisible lesions for mpMRI.

TMA slides were co-stained with FAP and SMA. After scanning, the FAP- and SMA-positive pixels were counted, normalized to the total tissue pixel counts, and plotted on the total stromal area as benign tissue and visible and invisible lesions for mpMRI. Survival analysis was performed for BCR-free time for this group after eliminating 25 cases due to incomplete data (n = 318).

In study III, the Helsinki RP cohort was introduced as a continuous, population-based collection of RP specimens from 1983 to 1998 in the Department of Pathology of Helsinki University Hospital. This cohort was used as an independent validation set for the prognostic value of FAP, thereby implementing a technique more accessible in a clinical setting. TMA samples included two cores from the primary GG, one core from the secondary, and the other from adjacent benign tissue. Double-antibody tissue staining was utilized for FAP (brown) and SMA (red). Then, the slides were analyzed with image analysis using a machine-learning technique (Figure 22A-B). Cancer cores were meaned for the same patient. The endpoint was disease-specific survival (DSS), with a median duration of follow-up being 16.5 years. All patients with neoadjuvant chemotherapy and non-representative FAP stainings were excluded from the cohort, resulting in an independent data set of 311 patients.

4.2.2 Study IV

A total of 750 patients (n = 750) who underwent prostate biopsies at HUS between 2016 and 2017 formed the cohort. Clinical and pathological information was gathered from all patients to create a training group of 331 individuals, an independent test set of 391, a comparative group of 710, and an RP group of 126 (Figure 10).

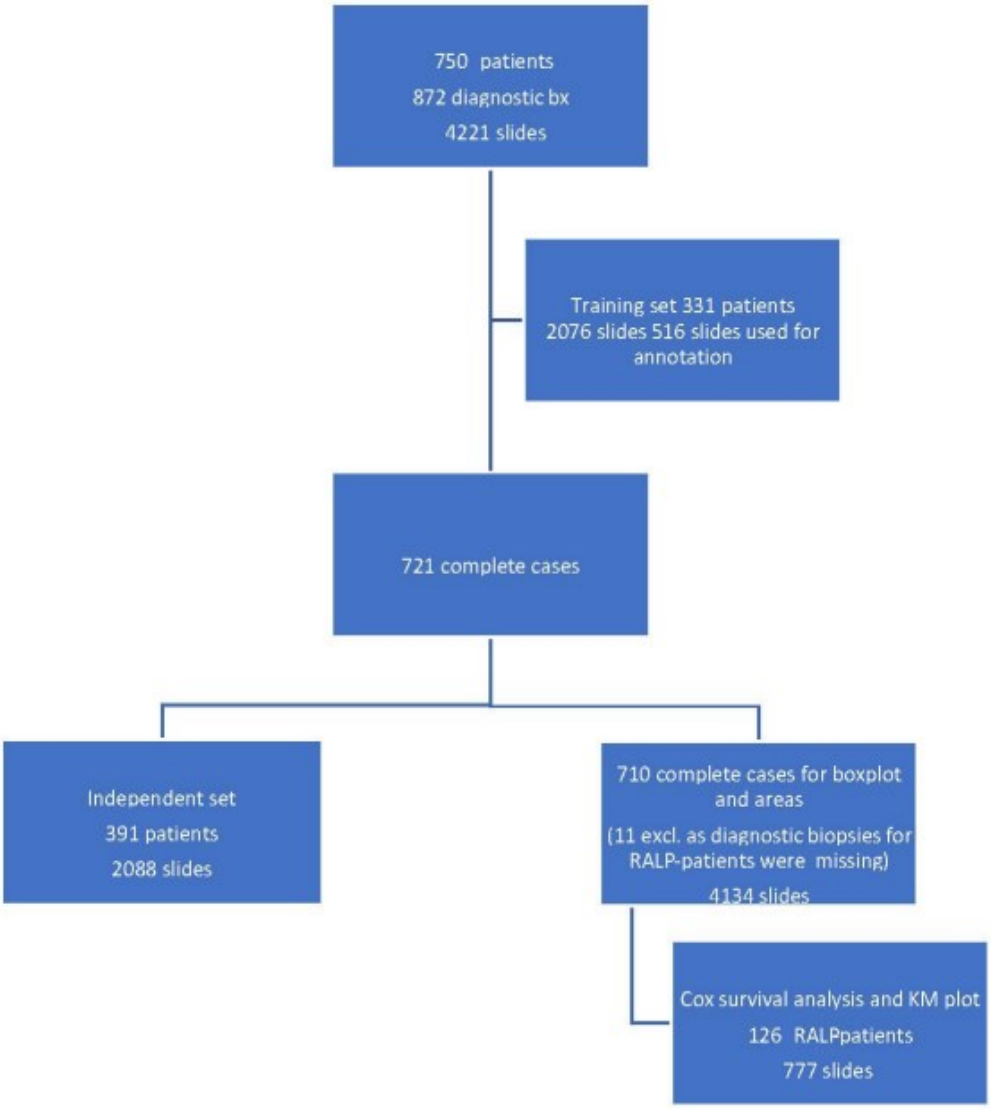

Figure 10. Workflow of the study cohort data selection depicting a training set, independent set, and radical prostatectomy (RALP) patient cohort from 872 prostate core biopsy series. From Sandeman et al. Diagnostics (2022).

For RALP patients, the information about EPE, SVI, NS, and pT were compiled from electronic pathology reports. Adverse findings in the RALP group were defined as EPE, SVI, or positive NS. All postoperative follow-up PSA values were collected for survival analysis. Detection of two consecutive PSA values equal to or higher than 0.2 ng/ml was classified as a BCR, with the date of the first elevated value as the start of the event. All biopsies were scanned at 0.26 µm/pixel, which resulted in an optical magnification of 41x.

In the AI algorithm, two convolutional neural networks (CNN), CNN-T and CNN-GG, were trained for the multi-class semantic segmentation of tissue and GGs. The training was conducted under full supervision using annotated data in the Aiforia software by two expert uropathologists who reached a consensus on strong pixel-level multi-class segments for both tissue and GGs.

After AI analysis of the slides, a proportional GGs were adapted to generate a GS according to the ISUP Consensus Conference 2014 guidelines for addressing the most common and most aggressive Gleason patterns as defined by pathologists. The GS was converted to an ISUP grade group for cross-tabulation and evaluation between AI and pathologists for GG in a 6-tier grouping (benign and GGs 1-5) for the biopsy series. The cross-tabulation results were used for iterative training by the pathologists. Finally, a filter curve was used to determine the correct filter size for a fluent clinical workflow. A visualization of the project is shown in Figure 11.

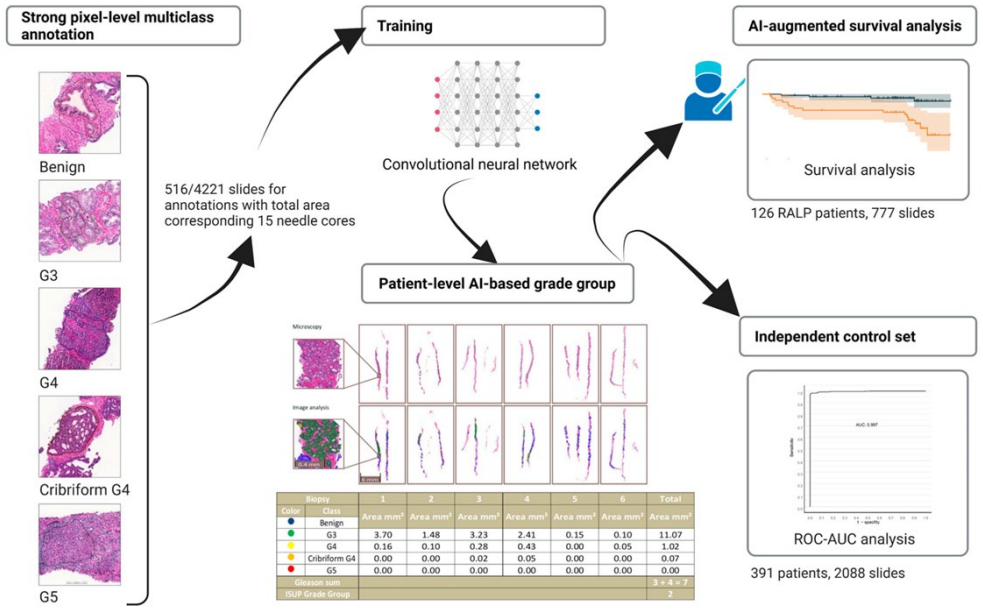

Figure 11. Graphical abstract. From Sandeman et al. Diagnostics (2022).

4.3 Statistics

In Study I, logistic regression models were used to examine the association between adverse findings (EPE, SVI, LNM), Partin Table estimates, MSKCC preoperative nomogram, and clinical variables. Cox proportional hazards models and Kaplan-Meier survival curves were created to predict BCR. The impact of mpMRI was assessed by comparing all models with and without mpMRI, using decision curve analysis, ROC AUC curves, and the multiparametric Wald test. For 81 patients with missing values for positive and total biopsy cores, the missing values were imputed using chained equations[256].

Study II evaluated the relationship between mpMRI visible and invisible groups using Pearson's chi-squared test and Fisher's exact test. Logistic regression with the ROC area under the curve (AUC) was used to examine non-OC findings such as EPE, SVI, LNM, and BCR after RP. Kaplan-Meier survival analysis was utilized to analyze BCR (two consecutive PSA values greater than 0.2 ng/ml after RALP), and Cox proportional hazard models were applied.

In both study I and study II, a p-value of less than 0.05 was considered statistically significant. Study III utilized R Statistical Software v. 3.6.1 and the packages ‘survival’ and ‘mice’ for the statistical analysis. Study IV also used R Statistical Software v. 3.6.1 and utilized packages precrec and mfp for the analysis[257].

For Study III, the normality of data was tested using the Kolmogorov-Smirnov test. The differences between two continuous variables were analyzed using either the Student's t-test (paired) for normally distributed data or the Mann-Whitney U test for non-normal data. Pearson and Spearman correlation coefficients were calculated for the correlations between continuous variables and continuous and categorical variables. Survival analysis was conducted using the Cox proportional hazard regression model and Kaplan-Meier plots, and the proportional hazard assumption was tested using the Schoenfeld test. The area under the receiver operating characteristic AU ROC curve was used to assess the prognostic value of a single-cell subtype compared to clinical variables. Bonferroni correction was applied for multiple testing, and results with $p < 0.05$ were considered significant. All analyses were performed using IBM SPSS 26 or R Statistical Software, and data were plotted in R, SPSS 26, or Microsoft Excel.

In Study IV, statistical analyses were performed using a filter size of 15,000 square microns, which was determined to perform best in the Bloom filter analysis for class stratification. The predictive accuracy of the algorithm was determined by ROC AUC analysis. Interrater agreement between the AI model and the original classifications was measured using Cohen's weighted kappa coefficient. Generalized linear models were employed to assess the connection between the clinical GG and the AI-determined tumor area. Multivariable logistic regression models were utilized to investigate the relationship between biopsy AI results and adverse outcomes on the RALP specimen (EPE, SVI, or positive NS). The predictive value of the AI-based GG and the original GG on BCR during postoperative follow-up were evaluated using Cox proportional hazard regression models and Kaplan-Meier survival curves. A significance level of 0.05 was used for all statistical analyses using R Statistical Software version 4.1.0[258] and the 'caret' and 'survival' package[259,260].

5 Results

5.1 Study I

In study I, all multivariate regression models were significantly correlated with adverse findings (EPE, SVI, LNM) at RP. Adding mpMRI parameters to the models also resulted in significant correlations with adverse findings, which differed significantly from the results obtained without mpMRI (Wald test, $p < 0.001$) (Table 6).

Model without mpMRI parameters				Model with mpMRI parameters			
	Estimate	OR (95% CI)	*p* value		Estimate	OR (95% CI)	*p* value
				MRI			
-	-	-	-	MRI ANY	1.420	4.14 (2.641–6.481)	**<0.001**
-	-	-	-	PI-RADS ≥ 3	1.218	3.40 (1.249–9.149)	**0.017**
-	-	-	-	MRI prostate volume	-0.013	0.99 (0.972–1.003)	0.095
PARTIN				**PARTIN + MRI**			
Partin ANY	0.026	1.03 (1.012–1.041)	**<0.001**	Partin ANY	0.025	1.03 (1.011–1.039)	**<0.001**
-	-	-	-	MRI ANY	1.277	3.59 (2.116–6.075)	**<0.001**
-	-	-	-	PI-RADS ≥ 3	0.837	2.31 (0.83–6.425)	0.110
-	-	-	-	MRI prostate volume	-0.010	0.99 (0.973–1.008)	0.235
MSKCC				**MSKCC + MRI**			
MSKCC ANY	0.053	1.05 (1.04–1.069)	**<0.001**	MSKCC ANY	0.045	1.05 (1.03–1.063)	**<0.001**
-	-	-	-	MRI ANY	1.139	3.12 (1.944–5.019)	**<0.001**
-	-	-	-	PI-RADS ≥ 3	1.090	2.97 (1.071–8.258)	**0.037**
-	-	-	-	MRI prostate volume	-0.017	0.98 (0.968–0.999)	**0.042**
CLINICAL				**CLINICAL + MRI**			
PSAPre	0.041	1.04 (1.012–1.073)	**0.008**	PSAPre	0.052	1.05 (1.017–1.091)	**0.003**
Age	0.036	1.04 (0.999–1.076)	0.059	Age	0.144	1.16 (1.033–1.291)	**0.011**
GGG ≥ 3	0.508	1.67 (1.028–2.686)	**0.039**	GGG ≥ 3	0.521	1.68 (1.006–2.819)	**0.048**
Positive Bx(%)	0.024	1.02 (1.012–1.036)	**<0.001**	% positive biopsies	0.022	1.02 (1.01–1.034)	**<0.001**
cT ≥ 3	1.382	3.98 (2.029–7.817)	**<0.001**	cT ≥ 3 given MRI ANY	2.047	7.74 (1.868–32.093)	**0.005**
-	-	-	-	cT ≥ 3 given MRI OC	0.426	1.53 (0.659–3.56)	0.323
-	-	-	-	MRI ANY given cT ≥ 3	1.218	3.38 (1.939–5.893)	**<0.001**
-	-	-	-	MRI ANY given cT < 3	-0.403	0.67 (0.14–3.187)	0.614
-	-	-	-	PI-RADS ≥ 3	1.104	3.02 (0.985–9.236)	0.054
-	-	-	-	MRI prostate volume	0.184	1.20 (1.002–1.442)	**0.049**
-	-	-	-	Age x MRI prostate vol.	-0.003		**0.033**
-	-	-	-	cT ≥ 3 x MRI ANY	-1.621		0.056

MRI: magnetic resonance imaging; ANY: suggestion of extraprostatic extension, seminal vesicle invasion or lymph node involvement; OC: organ-confined (≤pT2); cT: clinical stage

Table 6. Regression model summaries: prediction of any adverse findings at prostatectomy. Sandeman et al., Prostate MRI combined with CAPRA, MSKCC, and Partin cancer nomograms significantly enhances the prediction of adverse findings. From Sandeman et al. PLOS ONE, 2020.

The ROC AUC analyses revealed that risk nomograms combined with mpMRI outperformed the models without mpMRI, resulting in a net benefit in the decision curve analyses (Figure 12).

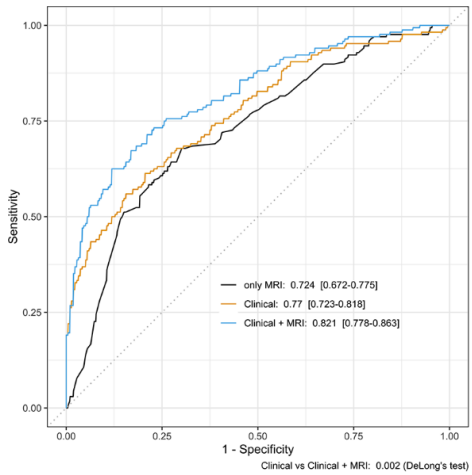
Sensitivity
1 - Specificity
only MRI: 0.724 [0.672-0.775]
Clinical: 0.77 [0.723-0.818]
Clinical + MRI: 0.821 [0.778-0.863]
Clinical vs Clinical + MRI: 0.002 (DeLong's test)

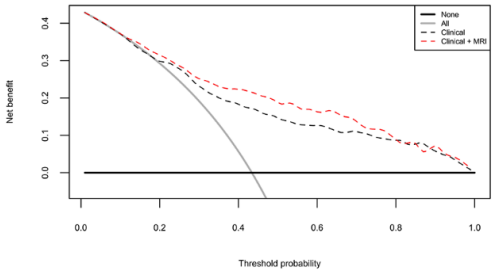
None
All
Clinical
Clinical + MRI
Net benefit
Threshold probability

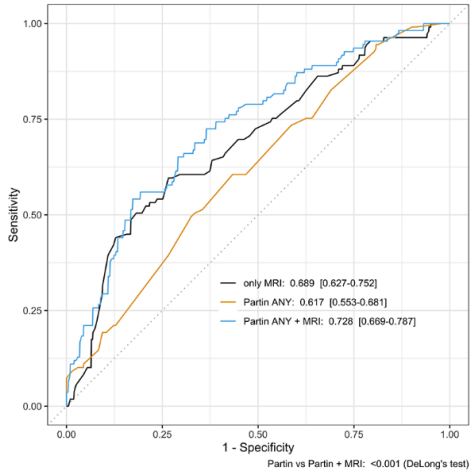
Sensitivity
1 - Specificity
only MRI: 0.689 [0.627-0.752]
Partin ANY: 0.617 [0.553-0.681]
Partin ANY + MRI: 0.728 [0.669-0.787]
Partin vs Partin + MRI: <0.001 (DeLong's test)

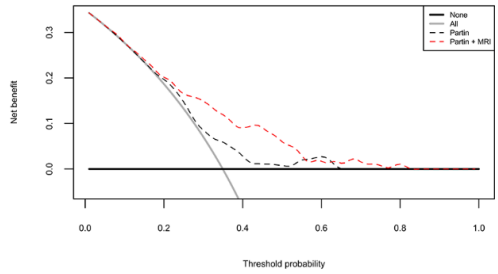
None
All
Partin
Partin + MRI
Net benefit
Threshold probability

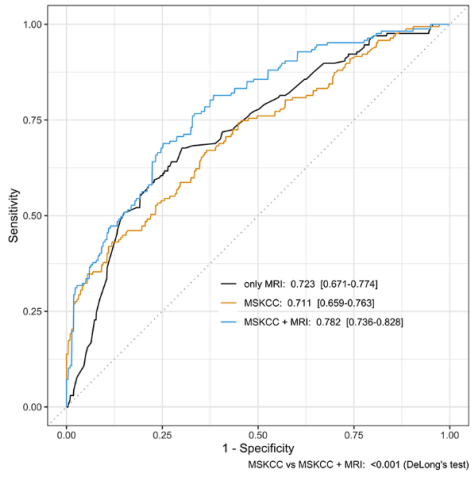
Sensitivity
1 - Specificity
only MRI: 0.723 [0.671-0.774]
MSKCC: 0.711 [0.659-0.763]
MSKCC + MRI: 0.782 [0.736-0.828]
MSKCC vs MSKCC + MRI: <0.001 (DeLong's test)

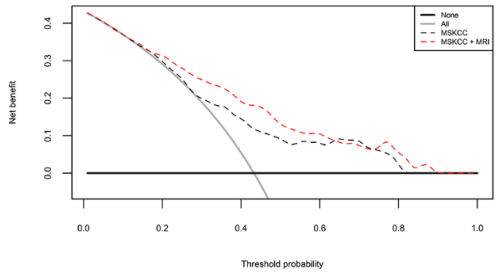
None
All
MSKCC
MSKCC + MRI
Net benefit
Threshold probability

Figure 12. Additive predictive value of any adverse findings by mpMRI in ROC AUC and decision curve analysis for a) clinical characteristics; b) Partin table estimates; c) MSKCC nomogram parameters. Modified from Sandeman et al., Prostate MRI added to CAPRA, MSKCC and Partin cancer nomograms significantly enhanced the prediction of adverse findings and biochemical recurrence after radical prostatectomy. From Sandeman et al. PLOS ONE, 2020.

Kaplan-Meier analysis of BCR-free survival indicated a statistically significant difference between the high and intermediate/low CAPRA risk groups. The 3-year MSKCC survival percentage was 80%. Additionally, mpMRI indication of non-OC PCa had a significantly lower BCR-free survival time than OC PCa across the separated datasets (Figure 13).

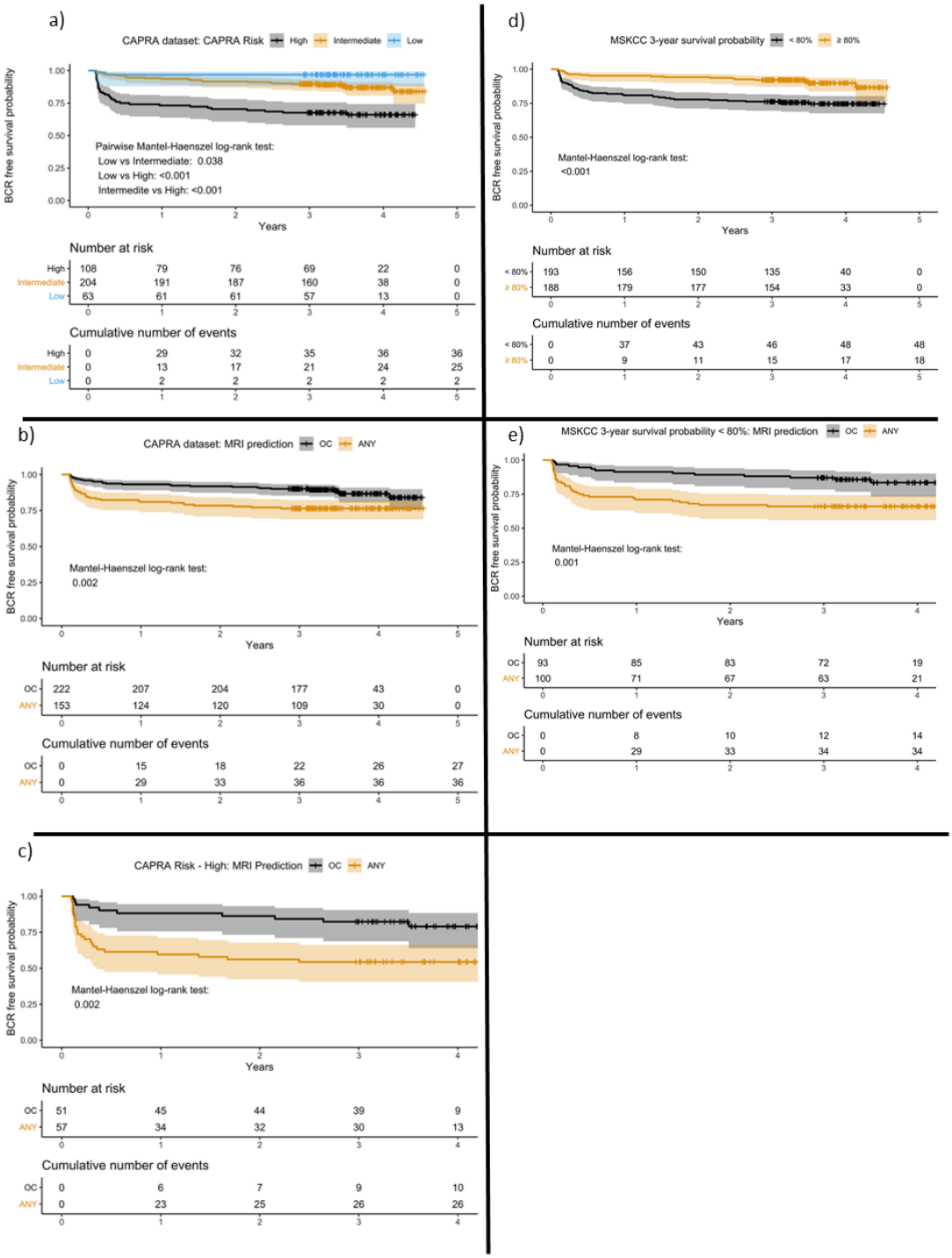

Figure 13. Biochemical recurrence-free survival. a) CAPRA nomogram results for high-, intermediate-, and low-risk groups; b) CAPRA results with mpMRI indicating non-organ confined findings; c) Survival plot for mpMRI with any adverse finding (ANY) versus organ-confined (OC) in the CAPRA high-risk group; d) MSKCC 3-year survival probability with a cut-off 80%; e) MSKCC with mpMRI indicating non-organ confined findings. ANY=suggestion of extraprostatic extension, seminal vesicle

invasion, or lymph node involvement in mpMRI; MRI=magnetic resonance imaging; OC=organ confined. Modified from Sandeman et al., Prostate MRI added to CAPRA, MSKCC and Partin cancer nomograms significantly enhanced the prediction of adverse findings and biochemical recurrence after radical prostatectomy. From Sandeman et al. PLOS ONE, 2020.

Except for age, all preoperative clinical variables demonstrated statistically significant separation between the nomogram and nomogram + mpMRI groups in the Kaplan-Meier survival curve analysis. (Figure 14).

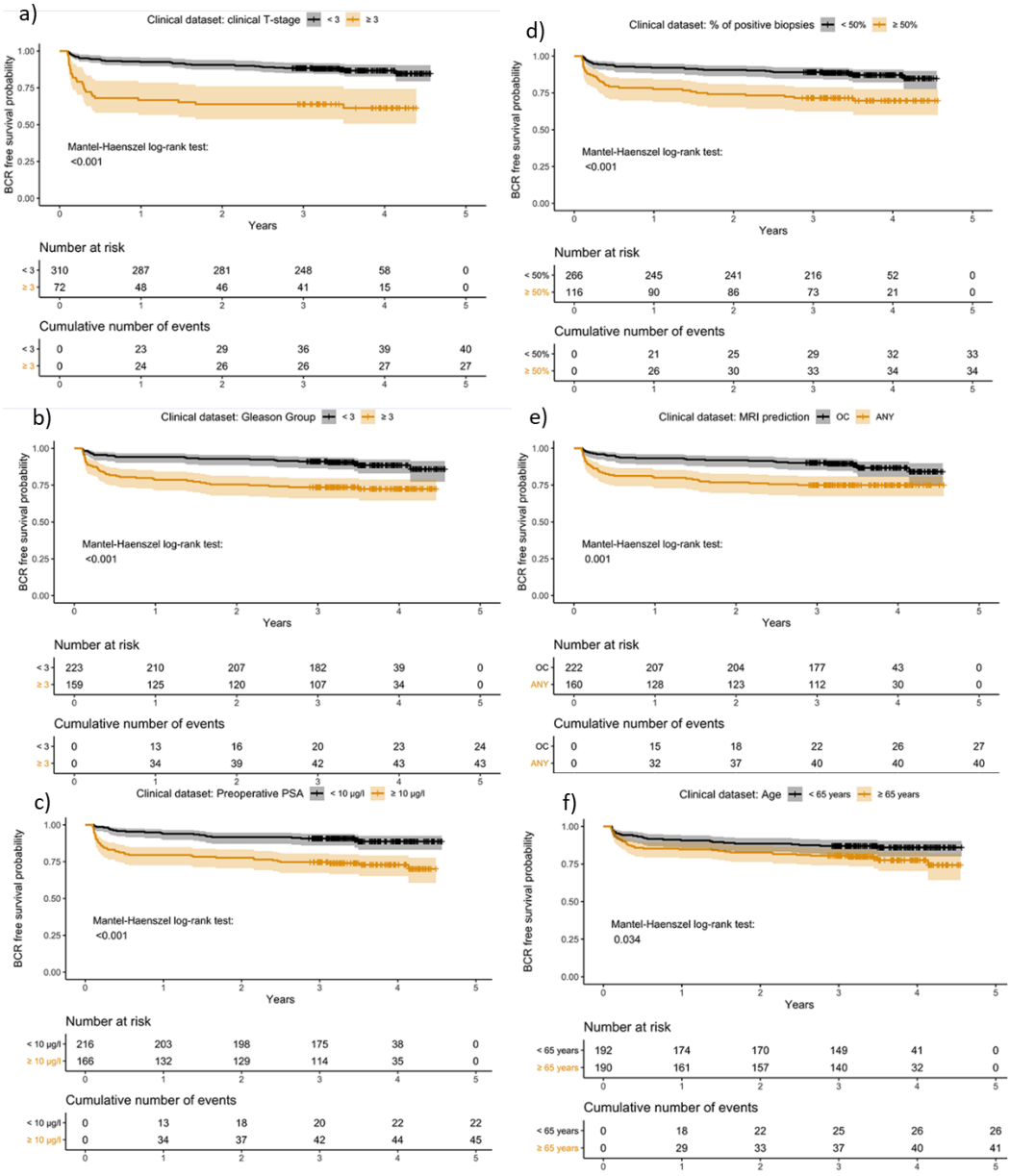

Figure 14. BCR-free survival probability–Kaplan-Meier survival analysis for clinical parameters: a) clinical T-stage equal or higher than 3 (follow-up data for clinical T-stage missing for one patient); b) Gleason Grade Group equal to or higher than 3; c) preoperative PSA equal to or higher than 10 µg/l; d) the percentage of positive biopsies equal or higher than 50%; e)

mpMRI prediction for any adverse finding; f) age at operation ≥65 years. Modified from Sandeman et al., Prostate MRI added to CAPRA, MSKCC and Partin cancer nomograms significantly enhances the prediction of adverse findings and biochemical recurrence after radical prostatectomy. From Sandeman et al. PLOS ONE, 2020.

5.2 Study II

Patients with visible lesions on mpMRI showed a significantly higher GG, more EPE (>pT2: 44.6% vs. 11.4%; p < 0.001), SVI (21.1% vs. 0%; p = 0.003) and LNM (pN1: 12.2% vs. 0%; p = 0.033) in comparison to invisible mpMRI lesions. Patients with visible lesions on mpMRI developed significantly more BCR than those without (21.1% vs. 5.7%; p = 0.039).

Visible lesions were significantly more frequent than invisible lesions and PTEN loss (17.2% vs. 43.3%; p = 0.006), whereas they appeared with less ERG expression than invisible lesions on mpMRI, although this comparison was not statistically significant (Table 7).

	A: visible lesions only (n = 90)		**B: visible and invisible lesions (n = 221)**		**C: invisible lesions only (n = 35)**		**p value**		
	Result	**IQR/% of total**	**Result**	**IQR/% of total**	**Result**	**IQR/% of total**	**A vs B**	**B vs C**	**A vs C**
Median age (yr)	65	60–69	65	60–69	61	55–65	0.8 a	**0.001 a**	**0.003 a**
Median preoperative PSA (ng/m	10.0	6.5–16	8.4	6.3–12	7.1	5.2–11	0.08 a	0.1 a	0.037 a
Biochemical recurrence	19	21	31	14	2	5.7	0.1 b	0.3 c	0.039 b
Gleason grade group at RP									
1	1	1.1	5	2.3	8	23	0.7 c	**<0.001 c**	**<0.001 c**
2	30	33	90	41	18	51	0.2 b	0.2 b	0.06 b
3	38	42	107	48	8	23	0.3 b	**0.005 b**	**0.044 b**
4	4	4.4	6	2.7	0	0	0.5 b	1 c	0.6 c
5	17	19	13	5.9	1	2.8	**0.001 b**	0.7 c	**0.022 b**
Pathological stage at RP									
≤pT2	49	55	127	58	31	89	0.6 b	**<0.001 b**	**<0.001 b**
Extraprostatic extension	41	46	92	42	4	11	0.5 b	**0.001 b**	**<0.001 b**
Seminal vesicle infiltration	19	21	22	10	0	0	**0.008 b**	0.052 c	**0.003 b**
Lymph node metastasis	11	12	10	4.5	0	0	**0.014 b**	0.4 c	**0.033 c**
PTEN, visible lesions (n = 311)									
Intact	50	56	129	58	–	–	0.6 b	NA	NA
Loss	39	43	74	34	–	–	0.1 b	NA	
NA or data missing	1	1.1	18	8.1	–	–	NA	NA	
PTEN, invisible lesions (n = 256)									***A visible vs C invisible***
Intact	–	–	139	63	25	71	NA	0.3 b	0.1 b
Loss	–	–	22	10	6	17	NA	0.2 b	**0.006 b**
NA or data missing	–	–	60	27	4	11	NA	NA	NA
ERG, visible lesions (n = 311)									
Negative	72	80	147	67	–	–	0.018 b	NA	NA
Positive	18	20	62	28	–	–	0.1 b	NA	
NA or data missing	–	–	12	5.4	–	–	NA	NA	
ERG, invisible lesions (n = 256)									***A visible vs C invisible***
Negative	–	–	148	67	29	83	NA	0.059 b	0.7 b
Positive	–	–	25	11	3	8.6	NA	0.6 b	0.1 b
NA or data missing	–	–	48	22	3	8.6	NA	NA	NA

IQR = interquartile range; MRI = magnetic resonance imaging; NA = not applicable; PSA = prostate-specific antigen; RP = radical prostatectomy. a Mann-Whitney U; b Pearson's χ^2; c Fisher's exact.

Table 7. Characteristics of radical prostatectomy patients in mpMRI visible and invisible groups, and characteristics of tumor lesions between groups, cross-tabulation. Modified from Eineluoto et al. Eur Urol Focus, 2020.

In the ROC AUC analysis, mpMRI significantly predicted postoperative non-organ confined (non-OC) findings (p = 0.006, Figure 15). Biomarkers did not add any significant benefit to this model. In the multivariate logistic regression analysis, age, cT≥3, and preoperative PSA (clinical variables), prostate volume and the presence of any non-OC findings (mpMRI variables), significantly predicted non-OC disease. However, PI-RADS scores ≥3, ERG expression, and PTEN expression did not have statistically significant predictive value for non-OC PCa.

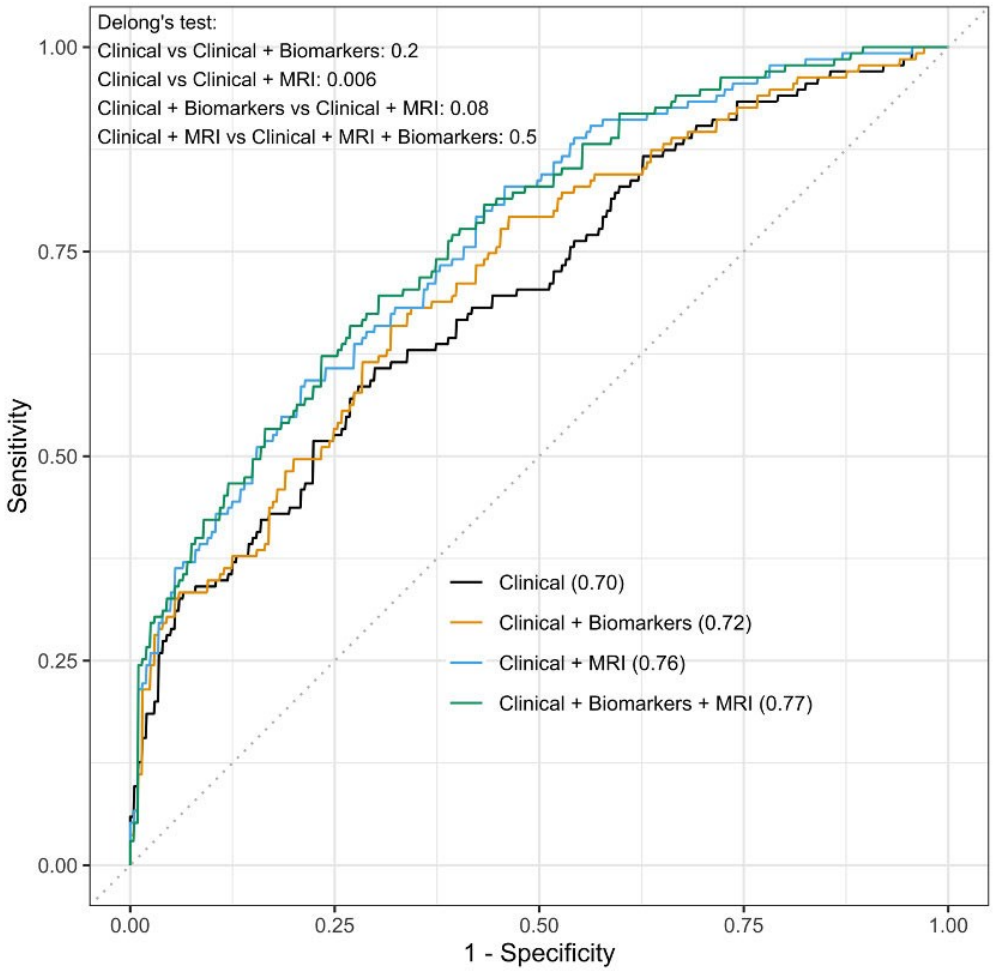

Figure 15. Prediction of non-organ-confined disease at radical prostatectomy histopathological analysis. ROC AUC analysis using DeLong's test for significance between different groups of variables. Modified from Eineluoto et al. Eur Urol Focus, 2020.

Kaplan-Meier BCR-free survival curve analysis was performed for groups A, B, and C. Group C had the best BCR-free survival without statistical significance (p = 0.09; Figure 16a). The same analysis was performed on group A (mpMRI visible) vs. groups B + C (mpMRI invisible and with at least one visible lesion) and then groups A + B vs. group C, but neither of these produced significant results (p = 0.055; Figure 16b and p = 0.1; Figure 16c).

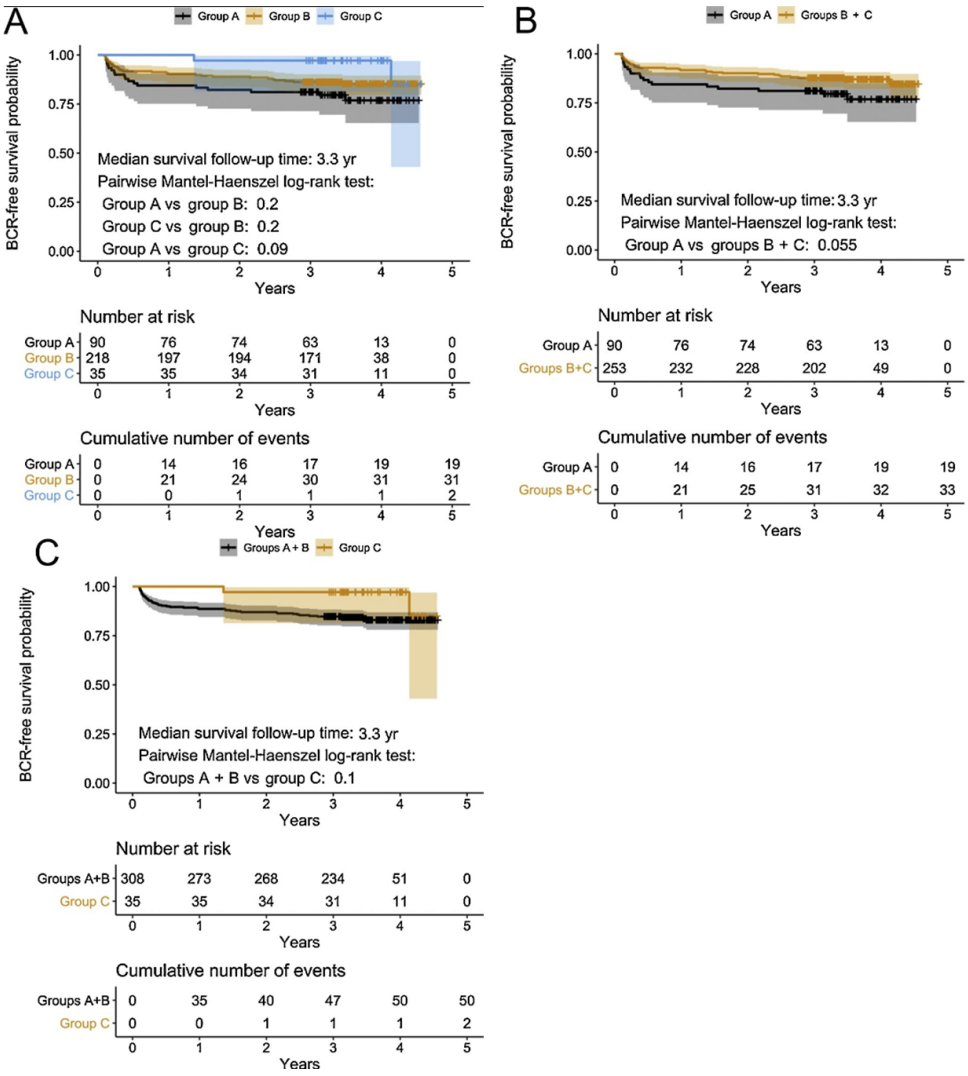

Figure 16. Biochemical recurrence-free survival curves between the groups with different mpMRI visibility of prostate cancer lesions. a) Group A vs. B vs. C; b) Group A vs. B + C; c) Group A + B vs. C. Group A = multiparametric MRI visible lesions only, n = 90; Group B = mpMRI visible and invisible lesions, n = 221; Group C = mpMRI invisible lesions only, n = 35. Modified from Eineluoto et al. Eur Urol Focus 2020.

The BCR-free survival ROC AUC analysis revealed a significant difference between the clinical and clinical + MRI groups (p = 0.001) (Figure 17).

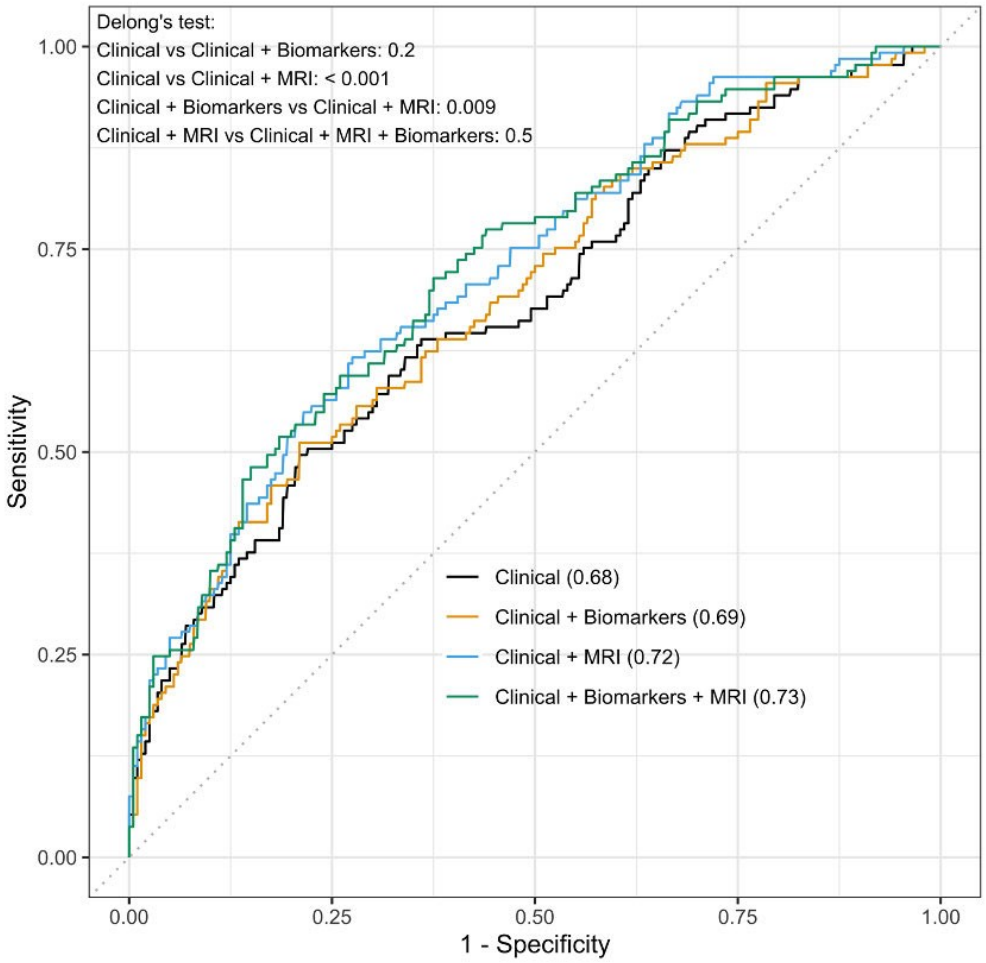

Figure 17. Prediction of biochemical recurrence after radical prostatectomy histopathological analysis. ROC AUC analysis with DeLong's test for significance between different groups of variables. Modified from Eineluoto et al. Eur Urol Focus, 2020.

PTEN and ERG expression did not significantly predict BCR-free survival (p = 0.5 and p = 0.2, respectively; Figure 18).

Furthermore, the results of Cox proportional hazards models did not show any significant difference in the biomarker status or mpMRI visibility groupings (A vs. B vs. C; A vs. B + C) from a model without

these variables (data not shown).

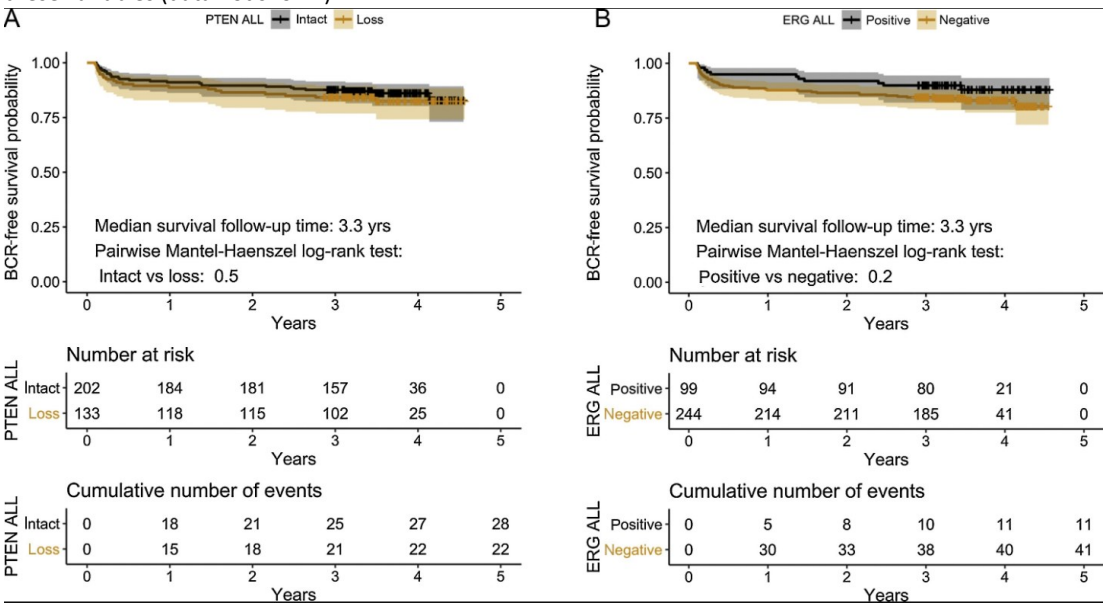

Figure 18. Biochemical recurrence-free survival between the groups with different biomarker status. a) PTEN intact/loss; b) ERG-positive/negative. Modified from Eineluoto et al. Eur Urol Focus, 2020.

5.3 Study III

In their tissue architecture, MRI false-negative lesions resemble benign tissue more than MRI true-positive lesions.

The tissue characteristics of the false-negative MRI lesions and benign tissue areas were similar. In contrast, MRI true-positive lesions had a higher epithelial and nuclear frequency and lower stromal content than MRI false-negative lesions and benign tissue areas ($p < 0.001$; Figure 19C–E).

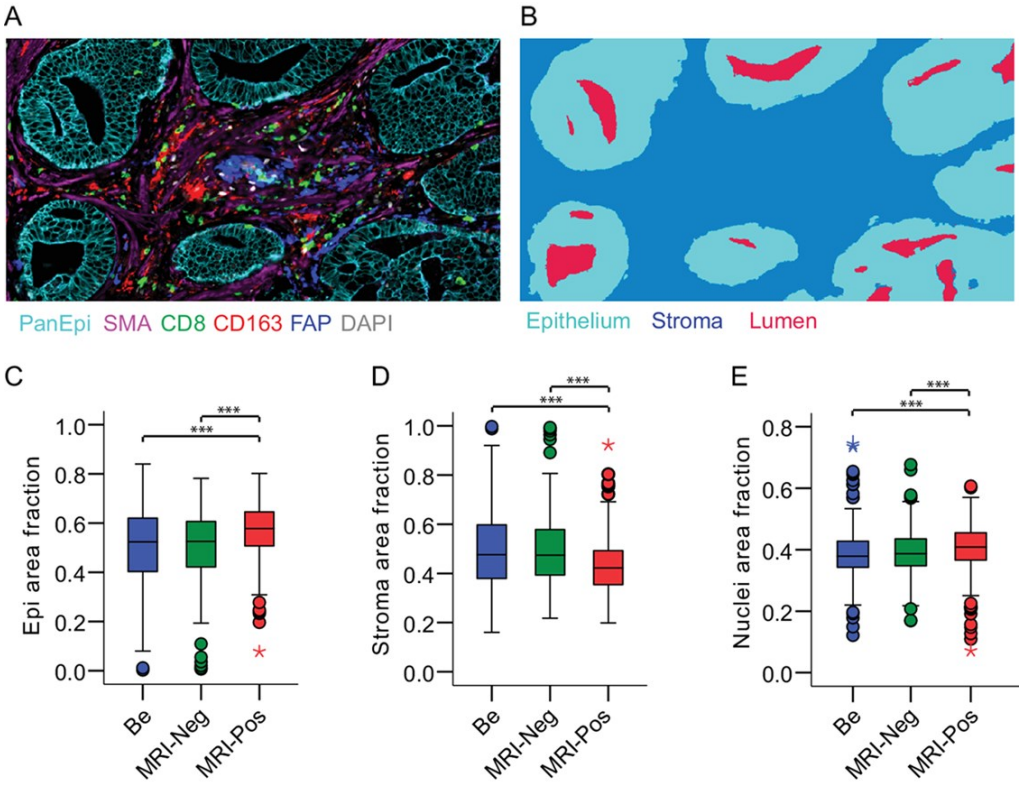

*Figure 19. Differences in tissue compartments in benign areas, mpMRI false-negative cancer lesions, and mpMRI true-positive cancer lesions (343 patients, 1606 TMA cores). A, Images of tissue stained with markers (PanEpi, SMA, CD8, CD163, FAP, DAPI). B, Image of tissue segmentation for epithelium, stroma, lumen. C-E, Quantification of mpMRI annotated tissue samples for epithelium, stroma, and nuclei areas as fractions of total tissue area. Results: benign vs. mpMRI false-negative vs. mpMRI true-positive, shown as boxplots with interquartile range, error lines within 1.5-fold IQR, circles within 3-fold IQR, and stars for extreme data points. Significance determined by Mann-Whitney U test (***, p < 0.001). From Pellinen et al. Cancer Research Communications, 2022.*

The composition of stromal cells differs in benign tissue, mpMRI false-negative cancer lesions, and mpMRI true-positive cancer lesions.

We analyzed stromal markers that reflect different cell populations (CD8, CD163, FAP, and SMA) in benign tissue, MRI false-negative lesions, and mpMRI true-positive lesions. The SMA-positive fraction was higher in the benign areas (59.7%) than in false-negative (55.9%) or true-positive (41.3%) lesions on mpMRI (Figure 20A). FAP positivity was lowest in benign tissue (0.3%), increased in false-negative lesions (1.4%), and highest in true-positive lesions (3.1%) (Figure 20B). CD163 positivity was higher in true-positive lesions (3.1%) than in false-negative (2.5%) or benign tissue (1.4%) (Figure 20C). CD8 positivity was similar between true-positive (1.5%) and false-negative lesions (1.4%) but lower in benign areas (0.8%) (Figure 20D). These results suggest differences in tumor stroma between benign tissue and cancer lesions and between true-positive and false-negative lesions.

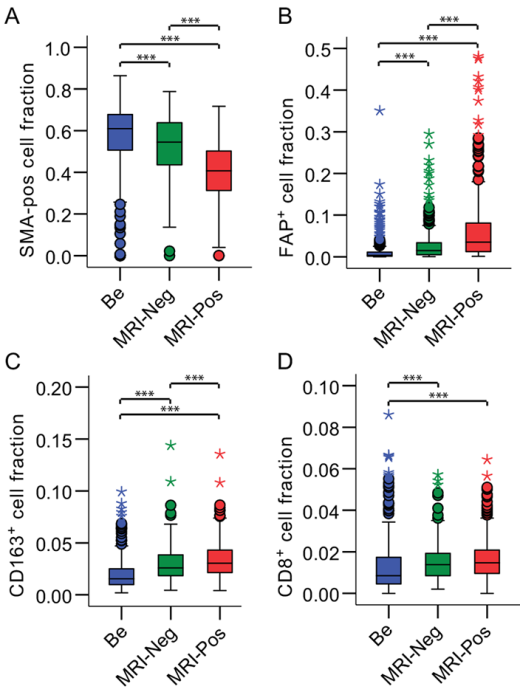

*Figure 20. Differences in stromal cell composition were analyzed in RALP tissue samples from benign and mpMRI-annotated areas. Cell areas were normalized to the total stromal area. The fraction of SMA-positive cells was higher in benign areas (Figure A), whereas the fraction of FAP-positive cells was lower in benign areas (Figure B). CD163 positivity was higher in mpMRI-positive lesions (Figure C), and CD8 positivity was lower in benign areas (Figure D). N(Benign) = 309 patients, N(mpMRI-negative) = 197 patients, N(mpMRI-positive) = 302 patients. Significance was determined using paired sample t-test or Mann–Whitney U test (***, p < 0.01). From Pellinen et al. Cancer Research Communications, 2022.*

FAP correlates with CD8 and CD163 and is linked to PTEN status and BCR.

Higher FAP and lower SMA cell fractions were linked to recurrent disease in true-positive mpMRI lesions ($p < 0.01$). FAP and SMA had an inverse correlation (corr=-0.30, $p < 0.01$). FAP positively correlated with CD8 (corr=0.44, $p < 0.01$) and CD163 (corr=0.43, $p < 0.01$), but SMA had a weak inverse correlation with CD8 (corr=-0.17, $p < 0.01$) and CD163 (corr=-0.21, $p < 0.01$). In subgroups defined by PTEN, ERG, Gleason grade grouping (GGG), and BCR status, the highest inverse correlation was found between FAP and PTEN status (corr=-0.31, $p < 0.01$) in mpMRI true-positive lesions. This association was also significant in mpMRI false-negative lesions (corr=-0.15, $p < 0.05$) (data not shown). A higher SMA cell fraction was associated with positive PTEN ($p = 0.025$) and ERG ($p = 0.001$) status and with lower GGG ($p < 0.001$). These results were also seen in mpMRI true-positive but not in mpMRI false-negative lesions (Table 8).

Variables	FAP			SMA		
	Low ($n = 151$)	High ($n = 151$)	P^a	Low ($n = 151$)	High ($n = 151$)	P
PTEN			**<0.001**			**0.025**
Neg ($n = 47$)	11(23%)	36(77%)		31 (66%)	16 (34%)	
Pos ($n = 255$)	140(55%)	115(45%)		120 (47%)	135 (53%)	
ERG			0.708			**0.001**
Neg ($n = 210$)	107 (51%)	103 (49%)		119 (57%)	91 (43%)	
Pos ($n = 92$)	44 (48%)	48 (52%)		32 (35%)	60 (65%)	
GGG			0.239			**<0.001**
1 ($n = 6$)	3 (50%)	3 (50%)		2 (33%)	4 (67%)	
2 ($n = 112$)	62 (55%)	50 (45%)		41 (37%)	71 (63%)	
3 ($n = 143$)	72 (50%)	71 (50%)		78 (55%)	65 (45%)	
4 ($n = 10$)	3 (30%)	7 (70%)		6 (60%)	4 (40%)	
5 ($n = 31$)	11 (34%)	20 (66%)		24 (77%)	7 (23%)	
BCR			**0.008**			**0.001**
No ($n = 248$)	133 (54%)	115 (46%)		113 (45%)	135 (55%)	
Yes ($n = 32$)	9 (28%)	23 (72%)		25 (78%)	7 (22%)	
NA ($n = 42$)						

[a]*P* value (Fisher exact when applicable, χ^2 when not). Significant *P* values are shown in bold.

Table 8. Association analysis of FAP and SMA with PTEN, ERG, GGG, and BCR in cohort I. TMA cores represent visible regions. From Pellinen et al. Cancer Research Communications, 2022.

Stromal FAP and SMA in true-positive mpMRI lesions predict BCR.

The Cox regression analysis of continuous image analysis values found that higher stromal fractions of FAP-positive cells and lower stromal fractions of SMA-positive cells in true-positive cancer lesions predicted earlier-onset BCR. However, none of the mfIHC method variables predicted BCR in false-negative lesions or benign tissue samples (Table 9). As anticipated, preoperative risk factors such as d'Amico and CAPRA scores predicted recurrence, but none of the mpMRI variables had a significant impact on BCR. Postoperative factors were significant predictors of earlier recurrence, including tumor surface percentage, GGG, capsular invasion length, seminal vesicle invasion, and pTNM stage.

Clinical variable	P	HR	P corr	mfIHC variable[a]	P	HR	P corr
Age	0.02	1.06	1.00	MRI-pos_Area_Nuclei	0.40	1.02	1.00
cT	0.01	1.60	0.50	MRI-pos_Area_Lumen	0.68	1.01	1.00
PSA	0.09	1.02	1.00	MRI-pos_Area_Epithelium	0.21	0.98	1.00
dAmico_risk	**0.00**	**2.73**	**0.01**	MRI-pos_Area_Stroma	0.21	1.02	1.00
CAPRA_risk	**0.00**	**2.93**	**0.00**	MRI-pos_Count_Lumen	0.46	1.00	1.00
MRIPROSTVOL	0.81	1.00	1.00	MRI-pos_CD163-pos cells	0.72	0.96	1.00
MRIFOCI	0.86	0.96	1.00	MRI-pos_CD8-pos cells	0.41	0.86	1.00
MRI1VOLUME	0.11	1.07	1.00	MRI-pos_FAP-pos cells	**0.00**	**1.04**	**0.01**
MRI1PIRADS	0.14	1.21	1.00	MRI-pos_SMA-pos cells	**0.00**	**0.96**	**0.01**
MRI1CAPSCONT	0.04	1.52	1.00	MRI-neg_Area_Nuclei	0.75	1.01	1.00
MRI1CAPSCONTMM	0.00	1.03	0.21	MRI-neg_Area_Lumen	0.61	0.98	1.00
MRIEPE	0.23	1.45	1.00	MRI-neg_Area_Epithelium	0.46	1.01	1.00
MRIEPE PI-RADS	0.13	1.12	1.00	MRI-neg_Area_Stroma	0.46	0.99	1.00
MRICLAS	0.20	0.12	1.00	MRI-neg_Count_Lumen	0.50	1.01	1.00
MRINCLAS	0.61	0.64	1.00	MRI-neg_CD163-pos cells	0.79	1.04	1.00
PROSTWEIGHT	0.95	1.00	1.00	MRI-neg_CD8-pos cells	0.81	1.06	1.00
FOCUSES	0.15	0.81	1.00	MRI-neg_FAP-pos cells	0.47	1.03	1.00
PERCSURFACE	**0.00**	**1.03**	**0.01**	MRI-neg_Sma-pos cells	0.39	0.99	1.00
GGG	**0.00**	**2.03**	**0.00**	Be_Area_Nuclei	0.08	1.04	1.00
POSMARG	0.00	1.05	0.26	Be_Area_Lumen	0.81	1.00	1.00
EPE	**0.00**	**1.08**	**0.00**	Be_Area_Epithelium	0.50	1.01	1.00
PN INV	0.11	2.70	1.00	Be_Area_Stroma	0.50	0.99	1.00
SVI	**0.00**	**3.37**	**0.03**	Be_Count_Lumen	0.26	1.03	1.00
pTNM	**0.00**	**1.25**	**0.00**	Be_CD163-pos cells	0.53	1.08	1.00
PTEN status	0.03	0.42	1.00	Be_CD8-pos cells	0.09	1.21	1.00
ERG status	0.17	0.54	1.00	Be_FAP-pos cells	0.94	1.00	1.00
				Be_Sma-pos cells	0.00	0.97	0.21

Table 9. Univariable Cox regression analysis for clinicopathological and mfIHC variables in cohort I. NOTE: Bolded values are significant with Bonferroni correction. Abbreviations: Be, benign; EPE, extraprostatic extension; MM, millimeters; mpMRI-pos, mpMRI-positive lesion; mpMRI-neg, mpMRI-negative lesion; MRIPROSTVOL, mpMRI prostate volume; MRI1CAPSCONT, mpMRI capsular contact; MRICLAS, mpMRI classification; MRINCLAS, mpMRI N classification; P corr, Bonferroni-corrected P-value; PN INV, perineural invasion; pTNM, pathologic stage; SVI, seminal vesicle invasion. amfIHC variables as continuous values. From Pellinen et al. Cancer Research Communications, 2022.

Survival analyses were performed using only mpMRI-detected true-positive lesions. Kaplan–Meier analysis based on patient histogram distributions showed that dividing patients based on a 20% FAP positivity cut-off or a conservative median cut-off led to worse BCR-free survival with higher stromal FAP cell fraction (20% cut-off: HR 4.48, 95% CI 2.1–9.7; median cut-off: HR 2.75, 95% CI 1.3–5.9; Figure 21B–D). However, patients with a higher stromal SMA-positive cell fraction had a better outcome (median cut-off: HR 0.25, 95% CI 0.1–0.6; Figure 21E–H).

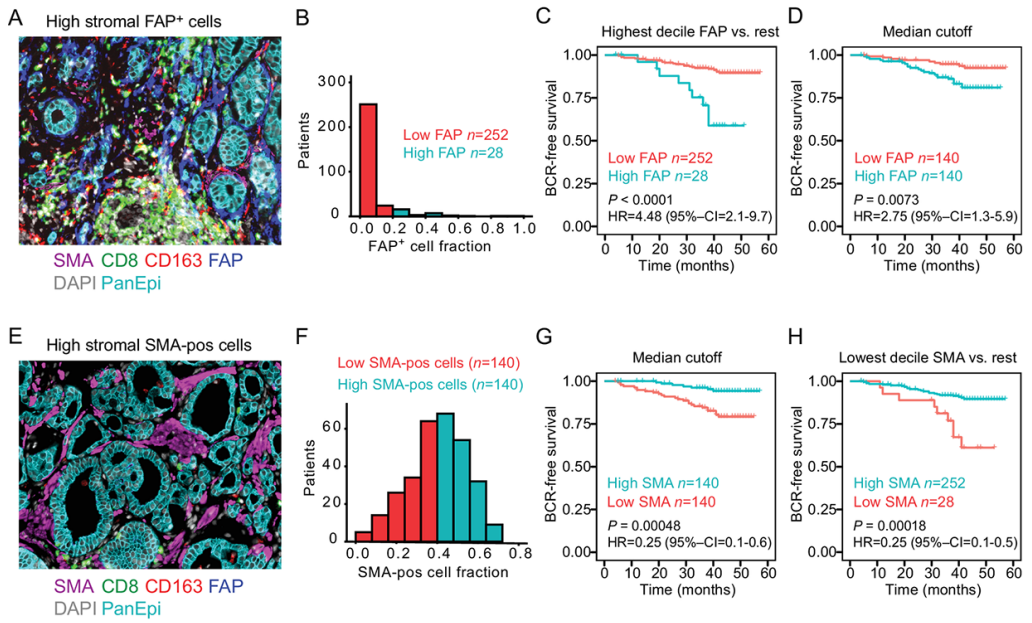

Figure 21. Kaplan-Meier plots demonstrate that stromal FAP and SMA in true-positive mpMRI lesions predict biochemical recurrence. The plots show the log-rank P values and hazard ratios (HRs) with 95% confidence intervals (95% CI) from univariable Cox regression survival analyses using dichotomized values. Figure A shows a case with a high fraction of FAP+ stromal cells. Figure B shows the distribution of stromal FAP positivity (fraction from total stroma) in 280 patients, with red columns representing patients with low FAP positivity (90% of patients with <20% fraction from stroma) and cyan columns represent patients with high FAP+ cell fraction (highest decile, 10% of patients). Figure C shows the Kaplan-Meier plot for patients with low and high FAP fractions. Figure D shows the Kaplan-Meier plot for patients with low and high FAP fractions using median cut-off dichotomization. Figure E shows a case with a high fraction of stromal SMA-positive cells, and Figure F shows the distribution of stromal SMA positivity (fraction from total stroma) in 280 patients. Figure G shows the Kaplan-Meier plot of SMA-positive cell fraction with median dichotomization. Figure H shows the Kaplan-Meier plot of SMA-positive cell fraction with dichotomization using the lowest decile versus the rest of the patients. From Pellinen et al. Cancer Research Communications, 2022.

FAP was validated as a prognostic marker using a different staining protocol and an independent patient cohort.

The association of high FAP and PTEN loss with recurrent disease was confirmed using Fisher's exact tests ($p < 0.001$ and $p = 0.004$, respectively). The validation was done using chromogenic IHC/machine-learning technology (data not shown). The Kaplan-Maier survival analysis (Figure 22C-D) and multivariable Cox regression analysis (Figure 22E) showed that high FAP tissue positivity predicted biochemical recurrence (BCR) in mpMRI true-positive lesions of RALP samples and is an independent factor. The high FAP-positive tissue fraction also predicted DSS and was independent of patient age, GS, and pTNM class when dichotomized using median or highest decile cut-offs (Figure 22F–H).

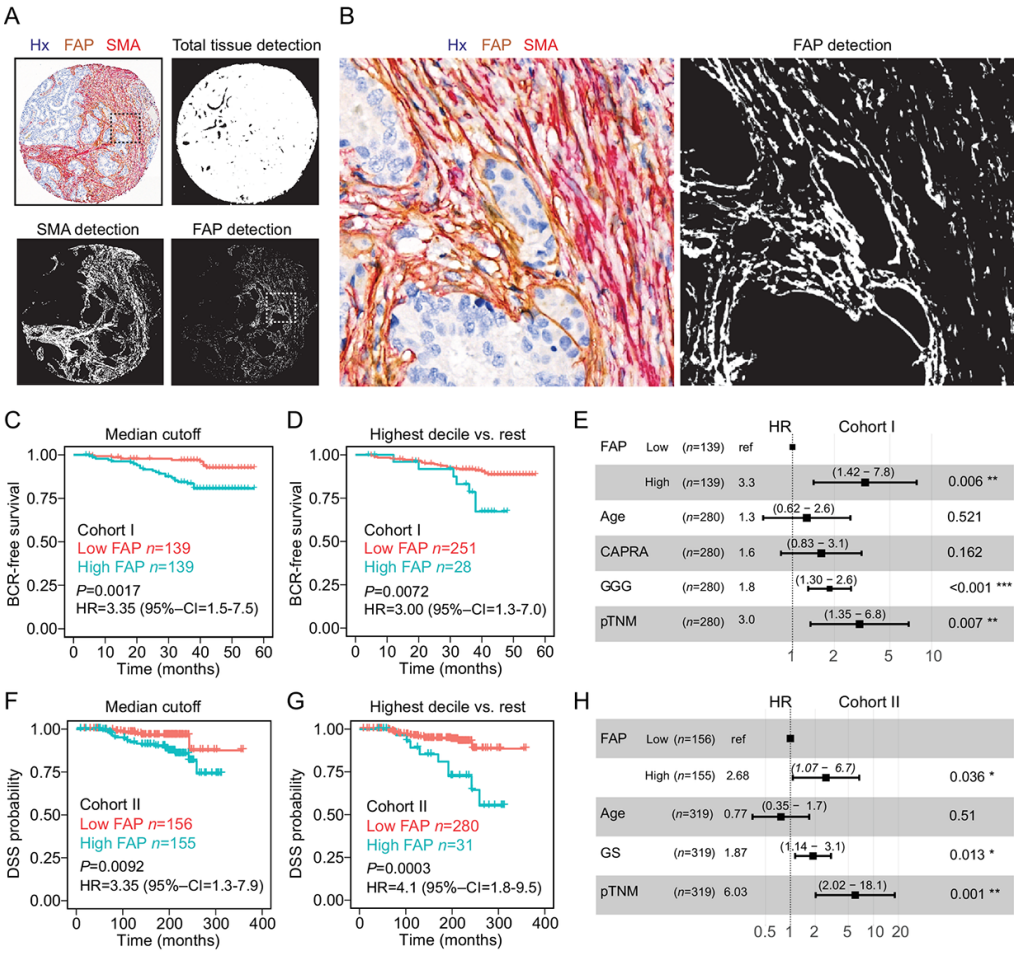

*Figure 22. Validation of FAP as a prognostic factor. A and B, Total tissue, FAP+ pixels, and SMA-positive pixels were detected using machine-learning and double-antibody chromogenic staining for FAP and SMA (stained with hematoxylin, Hx). C and D Kaplan–Meier survival plots show BCR outcomes for patients with low and high FAP in mpMRI true-positive lesions, determined by chromogenic IHC and machine learning in Cohort I (mpMRI-RALP cohort). E, Cox regression analysis for median dichotomized FAP in mpMRI true-positive lesions (BCR outcome) in cohort I (chromogenic IHC) shows significance (**, p <0.01; ***, p < 0.001). F and G, Kaplan–Meier survival plots show disease-specific survival (DSS outcome) for patients with low and high FAP in cancer lesions determined by chromogenic IHC and machine learning, using the same algorithm as in cohort I (Cohort II). H, Multivariable Cox regression analysis for median dichotomized chromogenic FAP in cancer lesions (DSS outcome) in cohort II (chromogenic IHC) shows significance *, p < 0.05; **, p < 0.01. 95% CI. From Pellinen et al. Cancer Research Communications, 2022.*

5.4 Study IV

AI algorithm performance and accuracy

The optimal filter size for benign vs. malignant classification (a) and GG classification (b) was determined using the Bloom filter curve method by comparing sensitivity and specificity of the AI

model to the pathological report. (Figure 23).

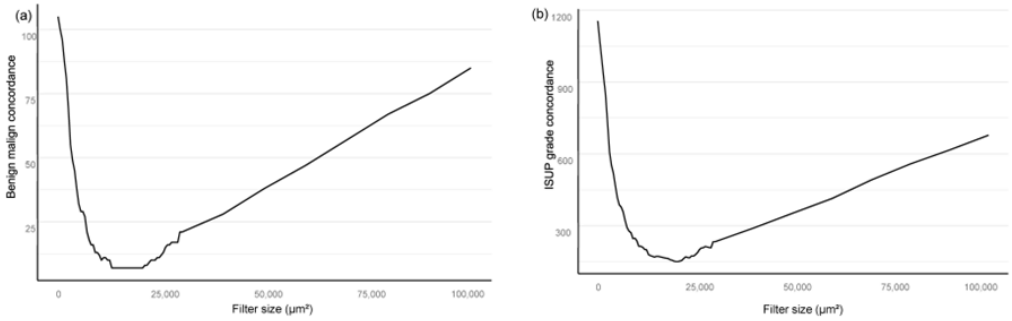

Figure 23. Determining the minimal filter size for distinguishing benign and malignant tissues (a) and different grade groups (b) using a Bloom filter algorithm based on its comparison with clinical diagnosis in terms of performance. From Sandeman et al. Diagnostics (2022).

The evaluation was conducted without reference to validation results. The smallest unit of measurement for the filter area was square micrometers. A filter area of 15,000 square micrometers (Figure 23) was identified as the best size for the algorithm, which lead to a high accuracy of 0.997 in detecting malignant and benign cells (Figure 24).

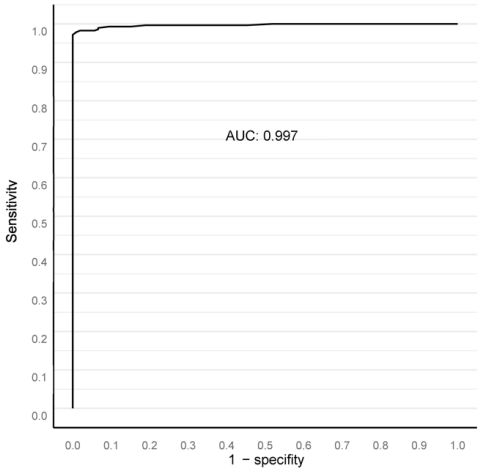

Figure 24. ROC AUC analysis comparing benign and malignant cases based on clinical diagnosis at the biopsy session level, with a 15,000 square micron filter applied. From Sandeman et al. Diagnostics (2022).

The performance of the algorithm was evaluated by determining the sensitivity, specificity, negative predictive value (NPV), and positive predictive value (PPV) for the benign class and for each GG (Table 10). The overall weighted kappa value achieved by the algorithm was 0.76 ($p < 0.0001$). Predictive values for the algorithm's performance were determined for clinically relevant groups ISUP GG1-2 versus ISUP GG3 to 5 (Table 11).

	Class					
	Benign	GG1	GG2	GG3	GG4	GG5
Cases, n (%)	112 (28%)	85 (21%)	83 (21%)	68 (17%)	18 (5%)	31 (8%)
Sensitivity	0.98	0.72	0.70	0.15	0.11	0.81
Specificity	0.98	0.93	0.87	0.98	0.95	0.90
PPV	0.96	0.73	0.59	0.63	0.09	0.41
NPV	0.99	0.92	0.92	0.85	0.96	0.98

Accuracy = 0.67. Cohen's weighted kappa = 0.77. $p < 0.0001$.

Table 10. Accuracy of the AI algorithm: Predictive values for all classes. From Sandeman et al. Diagnostics (2022).

	Class				
	Benign versus Malign	Benign to Grade 1 versus 2–5	Benign to Grade 2 versus 3–5	Only Malignant Cases Grade 1 versus 2–5	Only Malignant Cases Grade 1–2 versus 3–5
Number of Cases	112/285	197/200	280/117	85/200	168/117
Sensitivity	0.98	0.89	0.98	0.75	0.96
Specificity	0.98	0.89	0.79	0.89	0.79
PPV	0.96	0.88	0.92	0.74	0.87
NPV	0.99	0.89	0.93	0.89	0.93
Accuracy	0.98	0.89	0.92	0.85	0.89
Cohen's Kappa ($p < 0.0001$)	0.96	0.78	0.80	0.63	0.76

Table 11. Accuracy of the AI algorithm: Predictive values for dichotomized groups. From Sandeman et al. Diagnostics (2022).

Determinants of cancer extent by image analysis correlated with the clinical diagnosis.

Logistic regression models were used to confirm statistically significant associations between the tumor area graded for all classes by AI and the clinical diagnosis based on the pathologist's findings (Table 12).

Tumor Area in mm^2	Odds Ratio	95% CI	*p*
G3	1.14	(1.08–1.19)	<0.0001 *
G4	1.14	(1.1–1.18)	<0.0001 *
Cribriform G4	1.22	(1.16–1.28)	<0.0001 *
G5	1.08	(1.05–1.12)	<0.0001 *

n = 397; *: *p*-values < 0.05 were considered significant.

Table 12. Generalized linear modeling demonstrated a statistically significant relationship between the clinical GG and the AI-determined tumor area for each class for the independent set, indicating that every AI-determined-class-dependent tumor area similarly attributed to the AI-assessed GG as the pathologist. From Sandeman et al. Diagnostics (2022).

AI predicted biopsy-adverse pathological findings after RP

The usefulness of AI in predicting extensive cancer following surgery was analyzed for the total area. Additionally, the percentage of cancer detected by AI per biopsy session was plotted against the

negative pathological findings at prostatectomy (Figure 25).

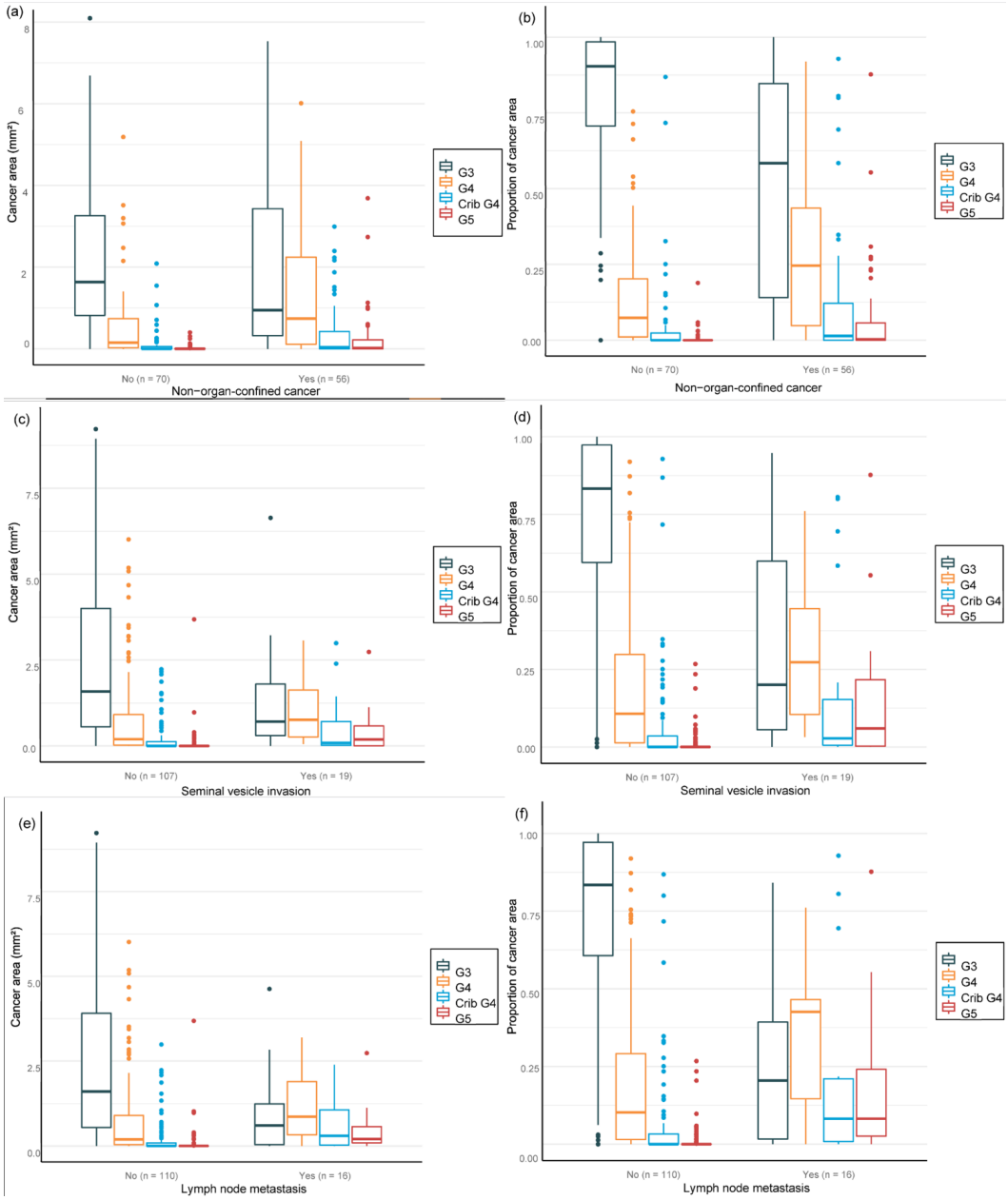

Figure 25. Distribution of Gleason grade in areas (a,c,e) and percentage of cancer areas (b,d,f) by AI in biopsy session compared to non-organ confined adverse findings (a,b), seminal vesicle invasion (c,d), and lymph node involvement (e,f) at prostatectomy. Modified from Sandeman et al. Diagnostics (2022).

Logistic regression analysis of grade pattern 5 areas was significantly correlated with negative pathological results. The AI-designated areas of cribriform grades 4 and 5 in biopsy samples showed a significant association with SVI and LN metastasis during RP (Table 13).

Clinical Outcome	Tumor Area in mm^2	Odds Ratio	95% CI	*p*
Non-organ-confined disease	G3	0.93	(0.78–1.07)	0.35
	G4	1.39	(0.99–2.04)	0.07
	Cribriform G4	1.89	(0.89–4.70)	0.12
	G5	48.52	(3.03–4125)	0.03 *
Seminal vesicle invasion	G3	0.82	(0.56–1.07)	0.22
	G4	0.72	(0.41–1.10)	0.17
	Cribriform G4	2.46	(1.16–5.45)	0.02 *
	G5	5.58	(1.57–30.56)	0.02 *
Lymph node metastasis	G3	0.73	(0.44–1.03)	0.13
	G4	0.8	(0.48–1.20)	0.32
	Cribriform G4	2.66	(1.23–6.06)	0.01 *
	G5	4.09	(1.25–20.12)	0.04 *

*: *p*-values < 0.05 were considered significant.

Table 13. Multi-regression models for adverse pathological findings at prostatectomy show a statistically significant correlation between the area of cribriform G4 and G5 for seminal vesicle invasion and lymph node metastasis, as G5 shows high OR for non-organ-confined disease. From Sandeman et al. Diagnostics (2022).

Neural-network-based GG was non-inferior to the human observer in predicting disease recurrence.

The Kaplan-Meier survival analysis showed that using either pathologists or AI to evaluate the GG effectively divided patients into groups with different probabilities of BCR after RALP. This finding held even when patients were divided into GG1-2 and GG3-5 groups, with a more distinct separation of survival curves observed for the GG assessment using a neural network (Figure 26).

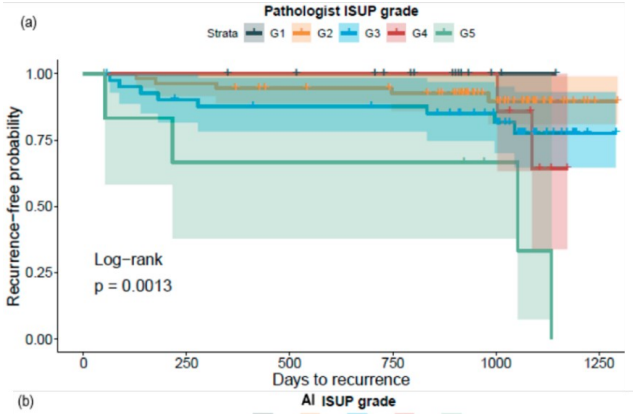
(a)
Pathologist ISUP grade
Strata G1 G2 G3 G4 G5
Recurrence−free probability
1.00
0.75
0.50
0.25
0.00
Log−rank
p = 0.0013
0
250
500
750
1000
1250
Days to recurrence

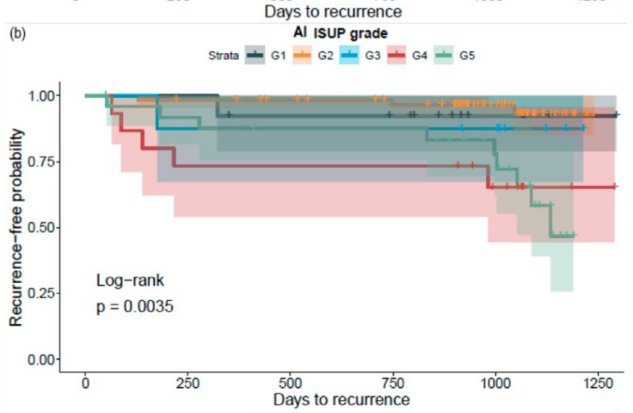
(b)
AI ISUP grade
Strata G1 G2 G3 G4 G5
Recurrence−free probability
1.00
0.75
0.50
0.25
0.00
Log−rank
p = 0.0035
0
250
500
750
1000
1250
Days to recurrence

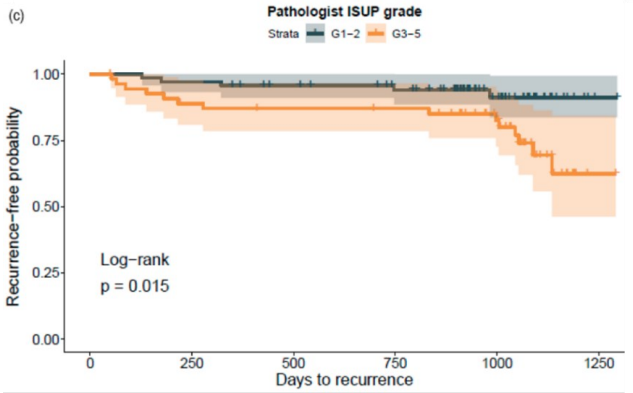
(c)
Pathologist ISUP grade
Strata G1−2 G3−5
Recurrence−free probability
1.00
0.75
0.50
0.25
0.00
Log−rank
p = 0.015
0
250
500
750
1000
1250
Days to recurrence

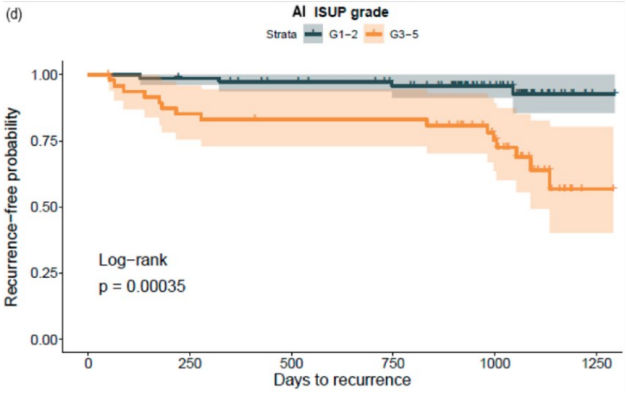
(d)
AI ISUP grade
Strata G1−2 G3−5
Recurrence−free probability
1.00
0.75
0.50
0.25
0.00
Log−rank
p = 0.00035
0
250
500
750
1000
1250
Days to recurrence

Figure 26. Kaplan–Meier survival analysis for biochemical recurrence on non-stratified (a,b) and stratified (1–2 versus 3–5) (c,d) cancer-positive biopsies for the prostatectomy cohort. The graph shows 95% confidence intervals. Modified from Sandeman et al. Diagnostics (2022).

A Cox proportional HR analysis revealed a correlation between an increase in the GG and a heightened risk of BCR, regardless of whether a pathologist or AI made the assessment (Table 14). This relationship remained consistent even when the groups were divided into GG1-2 and GG3-5. However, an increase in the proportion of patients with grade pattern 3 was associated with a reduced risk of BCR. Conversely, a significant increase in the risk of BCR was observed with an increase in the proportion of grade pattern 5 (Table 14).

Parameter	Hazard Ratio	95% CI	*p*
Pathologist ISUP GG	2.09	(1.38–3.16)	<0.001 *
AI ISUP GG	1.80	(1.27–2.53)	<0.001 *
AI Gleason	2.15	(1.34–3.44)	<0.01 *
G3 area (mm^2)	0.94	(0.77–1.14)	0.51
G4 area (mm^2)	1.03	(0.99–1.06)	0.19
Crib G4 area (mm^2)	1.13	(0.57–2.24)	0.72
Total G4 area (mm^2)	1.03	(0.99–1.07)	0.18
G5 area (mm^2)	1.10	(0.99–1.23)	0.07
Total cancer area (mm^2)	1.02	(0.99–1.05)	0.22
G3 proportion of cancer (%)	0.13	(0.04–0.47)	<0.01 *
G4 proportion of cancer (%)	3.59	(0.65–19.72)	0.14
Crib G4 proportion of cancer (%)	2.94	(0.52–16.59)	0.22
Total G4 proportion of cancer (%)	3.97	(0.99–15.9)	0.05
G5 proportion of cancer (%)	243.7	(28.8–2062)	<0.001 *
Strata			
Pathologist ISUP GG1–2 versus 3–5	3.31	(1.19–9.23)	0.02 *
AI ISUP GG1–2 versus 3–5	5.91	(1.96–17.83)	<0.01 *

n = 126; *: *p*-values < 0.05 were considered significant.

Table 14. Cox proportional-hazard regression analysis. From Sandeman et al. Diagnostics (2022).

6 Discussion

6.1 Study I

Adding mpMRI to clinical parameters or MSKCC or Partin nomograms improves the accuracy of predicting adverse events (EPE, SVI, or NS) in RP. Adding mpMRI to existing predictive tools, such as CAPRA and MSKCC nomograms, significantly ($p < 0.001$) enhances the prediction of BCR.

These results are generally in line with those reported in the recent literature. A large meta-analysis with pooled data from more than 9700 patients showed a sensitivity of 0.57, 0.58, and 0.61, and a specificity of 0.91, 0.91, and 0.88 for EPE, SVI, and overall stage T3 detection, respectively, by mpMRI with RP as reference[261]. Using a 3T field for mpMRI increases the ability to detect EPE and SVI. However, the heterogeneous nature of the studies cited made it difficult to apply the results of the meta-analysis in a general sense, and the technique alone lacks sufficient accuracy to stage local PCa reliably. However, by integrating mpMRI findings with clinical data, the prediction of the correct T stage can be significantly enhanced.

Several studies have shown a clear benefit for using mpMRI and risk nomograms. Morlacco et al. evaluated 914 patients and found that mpMRI facilitated the determination of the extent of the disease[262]. The risk factors in that groups cohort and ours were similar (≥pT3 49% vs. 44%), though they used non-structured reports and 1.5T mpMRI with a subgroup of 501 patients with an

endorectal coil in comparison to our structured reporting and 3T pelvic coil. Their findings may not accurately reflect the impact of mpMRI as their study population consisted of high-risk patients from the pre-PI-RADS era. Furthermore, Morlacco et al. did not mention the characteristics of their non-mpMRI group, which could have resulted in a bias in favor of the mpMRI cohort.

Grivas et al. evaluated 527 patients and concluded that 3T mpMRI with non-structured reporting had high diagnostic accuracy for SVI using RP as a reference[263]. They reported higher AUC values for the Partin nomogram combined with mpMRI (0.93) than for the non-mpMRI cohort (0.84). Our results showed 0.73 for the model with mpMRI and 0.69 without mpMRI, and this discrepancy suggested a difference in background risk for biopsy GSs within the cohorts between the two studies.

Gupta et al. found that mpMRI has a higher predictive accuracy for EPE than the Partin table when using RP as a reference in two studies with only 60 and 158 subjects, respectively. In the first study, mpMRI achieved an AUC of 0.82, whereas Partin tables had an AUC of 0.62, which was also higher than ours for mpMRI (AUC of 0.62)[264]. In their second study, mpMRI had an AUC of 0.88 for predicting OC disease, whereas Partin tables had an AUC of 0.70[265]. Feng et al. also found that mpMRI improved the AUC for EPE prediction, with AUCs of 0.92 and 0.94 for Partin tables and MSKCC, respectively[266]. However, it is worth noting that these studies relied upon the reporting of only one radiologist, which may have introduced bias and affected the results[264–266], in contrast to the group of four radiologists used in our study.

Our data suggest that combining mpMRI with established prediction tools can increase their effectiveness in predicting BCR after RP. This was demonstrated by the high-risk CAPRA and MSKCC groups, especially for BCR during the first year. The use of mpMRI alone was able to distinguish BCR survival between the two groups. Our findings align with a pre-PI-RADS study that found mpMRI helpful in predicting BCR after RP in localized PCa[267]. Using a structured imaging reporting system, such as PI-RADS 1.0, could further enhance the predictive value of mpMRI. We used PI-RADS 1.0 in our study, which allowed for a longer follow-up time and evaluation of BCR as an endpoint. The newer PI-RADS 2.0/2.1 versions have been shown to improve diagnostic performance and inter-reader reliability[268].

The literature summary and our results support the use of preoperative mpMRI for staging, particularly EPE and SVI. Radiologists can assess tumor size, location, and stage, and mpMRI patients were less prone to get nerve-sparing surgery and to have positive margins[269]. Our study did not address the benefit of mpMRI for LNM detection, though Valentin et al. showed a sensitivity of 81% and a specificity of 99% for LNM greater than 4 mm with LA as the reference[270]. A novel nomogram was developed for clinical use for nodal status evaluation by the addition of several mpMRI variables before RP[271]. This finding could inspire an enhanced use of preoperative mpMRI even though some uncertainties with current mpMRI diagnostics remain.

The limitations of this study are its single-center and retrospective nature. Not all patients with RP underwent a preoperative mpMRI at our center, as the choice for preoperative mpMRI was partly at the surgeon's discretion. However, demographics were similar between patients with and without preoperative mpMRI. Improved translational quality assurance and research could be achieved by encouraging pathologists to adopt regional reporting systems such as PI-RADS.

The strength of this study was a complete consecutive RALP cohort at our hospitals without mpMRI selection bias. Four radiologists reported mpMRIs with a structured PI-RADS system, and RP was the reference for the radiologic findings.

mpMRI of the prostate before surgery improves the accuracy in predicting adverse outcomes after RP and BCR. It should be used in conjunction with risk stratification nomograms.

6.2 Study II

We conclude that lesions visible on mpMRI had a higher incidence of PTEN loss. Moreover, we obtained specific adverse findings EPE, SVI and LNM in addition to increased BCR after RP. The lesions also had a higher degree of GG. mpMRI visibility of lesions impacted BCR-free survival, as demonstrated by the Kaplan-Meier curves, with a median follow-up of 3.3 years, although this difference was not statistically significant.

Missed PCa lesions on mpMRI seemed less aggressive, multifocal, and small (< 5 mm in diameter)[14]. A recent study showed that a biopsy-naïve patient cohort with ≥ 2 negative mpMRIs did not differ from a cohort with negative biopsies in the detection rate of csPCa[273]. Finally, a study with 320 cases of only PI-RADS ≤2 lesions reported a csPCa disease-free survival of 99.6% with a median follow-up time of 57 months[273].

Only a few studies have reported a combination of biomarkers and mpMRI as a method to enable the detection of csPCa. A comparison of the molecular characteristics between mpMRI visible and invisible lesions was performed by Lee et al., who showed only CHD1-deletions with SPINK1-biomarker absence in mpMRI invisible cancers[274].

A study reported that when gene expression analysis was performed on prostate lesions, mpMRI visibility was associated with genetic features linked to a poor prognosis, independent of tumor size and GG. The authors concluded that tumor size and GG did not wholly determine MRI visibility[276]. Another study found, higher panel scores and genetic risks associated with metastases using the Decipher® test in mpMRI visible lesions[276]. Further, mpMRI visible lesions with intraductal carcinoma or cribriform differentiation were associated with genetic enrichment[277]. These studies had small cohort sizes with relatively short follow-up times.

We found mpMRI visible and invisible lesions differed in ERG rearrangement (27% vs. 14%) and PTEN loss (29% vs. 15%), in line with contemporary literature, which shows ERG rearrangement between 36-78% and PTEN loss between 18-42% in csPCa[20–22]. Kaplan-Meier analysis did not show statistically significant differences in BCR outcome between visible and invisible lesions. The study found no added benefit for using ERG and PTEN expression using logistic when subjected to regression or survival analysis. This apparent lack of benefit could be a factual finding, though an experimental shortcoming due to a short follow-up period or a limited number of cases with only visible or invisible lesions could not be ruled out. Another limitation of the study was the absence of a validation set.

The strength of this study was the use of whole-mount RP pathology specimens as a reference for mpMRI findings. Furthermore, the selection of patients for mpMRI was not biased, as the cohort consisted of all patients who underwent RALP at our hospitals.

The impact of mpMRI visibility on PCa progression requires long-term clinical studies that combine imaging and follow-up data. The use of mpMRI is increasing, which has led to a growing data pool. Biomarkers hold potential for prognosis, especially in early biopsy stages. DCE-MRI that reflects the microcirculation of PCa, is a promising biomarker[95]. However, the use of biomarkers in a clinical setting requires further validation. The role of both mpMRI data and biomarkers as an aid to clinical decision-making remains to be seen.

6.3 Study III

This study investigated the relationship between mpMRI and prostate tumor biology. We focused on identifying a specific stromal signature for visibility that correlated with a clinically relevant survival endpoint. The study demonstrated that visible and invisible lesions differed clearly in the constitution of their stroma, especially for fibroblasts and CD163-positive immune cells. Stromal cells, especially those with FAP positivity, in mpMRI visible lesions (PI-RADS) influenced patient outcomes. Our results suggested an association between preoperative clinical imaging (mpMRI) and tissue biomarker status.

The results showed that MRI-positive tumors had higher cellularity and glandularity and lower lumen area compared to benign tissue and MRI-negative tumors, which were confirmed by histological characteristics reported by other studies[16,278,279]. This finding supports the idea that MRI-negative tumors resemble benign tissue more[280]. The study also found that high stromal fibroblast FAP levels, as in desmoplastic stroma, were associated with PTEN loss, linked to cancer initiation and progression[282–286]. The study found that FAP was an independent predictor of prostate cancer progression to metastatic disease and could be used as a prognostic biomarker in combination with mpMRI results. These findings could impact clinical decision-making for prostate biopsy and treatment. Patients with high stromal FAP content in MRI-positive tumors may require more intensive follow-up and radical treatment. Further studies are needed to confirm the potential value of FAP as a predictive biomarker.

6.4 Study IV

This study is the first to demonstrate the prognostic value of a CNN-model-based GG used for evaluating diagnostic biopsies. The model adequately classified the diagnostic biopsies and showed predictive accuracy in differentiating patients into risk groups for BCR after RALP, ad minimum, equal to that obtained by multiple pathologists. Our results suggest a substantial predictive accuracy that needs confirmation on a more extended follow-up period.

The identification of PCa is not usually an issue. Likewise, Campanella et al. demonstrated that this could be performed using an AI-based approach, using only weakly supervised training for cancer detection[153]. Nevertheless, their solution was a binary cancer detection algorithm that lacked the ability to predict disease recurrence. The main clinical challenge within PCa diagnostics on a biopsy series is consistently accurate grading to support clinical decision-making.

Our clinically-focused study is unique in that the neural network algorithm achieved the accuracy of multiple pathologists at the patient level for the entire biopsy set. In contrast, other studies are limited to single-slide diagnostics[123–125]. The clinical environment did not affect our results, as 15 independent pathologists with varying expertise in prostate diagnostics evaluated the biopsies. The algorithm was created by two uropathologists who supplied strong image labeling and employed a smaller training set than the separate testing group. The strong image labels seemed to enhance the accuracy in differentiating between GG1-2 and GG3-5 over that of an earlier report that used pure Gleason 3 + 3, 4 + 4, and 5 + 5 slides for training its algorithm[125]. Pure differentiation of one GG in tumors is rare in clinical practice as it is a rare biological phenomenon.

Since its implementation, the GG that is based on glandular architecture has been the most significant prognostic and predictive factor, with some adjustments to minimize inter-observer variability. [4,5,120]. In our study, the GG determined by general pathologists was likely to underrate the presence of Gleason 4 or 5, as the AI algorithm trained by expert pathologists detected small but clinically significant foci of high-grade cancer.

AI models offer correct stratification and personalized medicine opportunities by coherently identifying morphological features, proportions, and environments compared to rigid GG categories. Pathologists can reduce interobserver variation by consistent AI-based grading, as the algorithm does not differ in daily performance as a human observer does[286]. Despite the potential challenges due to differing interpretations of grading patterns at the institutional level, a new grading algorithm can be optimized by training it with locally selected cases. Our algorithm can assist pathologists, even those with limited prostate pathology experience, as shown in the studies of Bulten and Steiner[127,128].

This study confirmed a correlation between the area of cribriform G4 and G5 in prostate biopsies and adverse outcomes following RALP, such as seminal vesicle invasion and positive lymph node status. The higher the G5 area, the more likely the disease will not be confined to the prostate. Furthermore, the presence of G5 was a strong predictor of BCR, which is consistent with previous studies[121,287].

The algorithm identified all cancer areas. However, using a 15,000-micron filter in our study resulted in five false-negative findings, of which three were graded as GG1, one as GG2, and one as GG3. Only two patients with benign biopsies were incorrectly classified as malignant and graded as GG1. The filter was chosen to replicate a comprehensive workflow, thus highlighting the need to develop more advanced algorithms to detect small GG3 and GG4 areas accurately.

A vulnerability of our study is the absence of an external validation set. On the other hand, cohorts with completely structured data for preoperative biopsies, RALP specimens, and follow-up for BCR are uncommon. In addition, biopsy handling and tissue preparation methods differ between institutions. Algorithms do not perform as correctly in external validation sets as in the initial material. These restrictions emphasize the necessity for future clinical trials to demonstrate that cancer detection and grading by AI performs equal to that of the expert pathologist[25,168].

Finally, the human eye may have overlooked biological and clinical signals relevant to cancer prediction in histology[288]. AI can categorize patients into various life expectancies within a given GG and contribute to multidisciplinary prognostic models for clinical decision-making. For example, an AI algorithm combined with molecular characteristics improved prediction in a brain tumor model more than by simply morphological traits or mutational status alone[289]. DL models have been used to investigate the molecular features that can predict the response to therapy in prostate cancer[290]. Proof that risk factors for PCa progression and therapy resistance can be derived from histological data at a clinically appropriate level is still expected[148,291].

Recent technological advancements, such as high-throughput slide scanners, fast internet connections, high server capacity, and high-resolution monitors, have enabled large-scale implementation of digital pathology to cope with high clinical volumes without compromising diagnostics at multicenter pathology laboratories in Nordic countries. Nonetheless, the modification to digital pathology is not homogenous, as financial support and international guidelines for adapting, validating, and accepting digital pathology are under development.

7 Conclusions

I. By incorporating preoperative mpMRI data, existing prediction tools become more accurate in predicting the stage at RP and time to BCR. mpMRI is easily accessible before RP and should be considered a supplementary tool along with nomograms.

II. Tumors that are not visible on mpMRI appear less aggressive in terms of PTEN loss, EPE, SVI, LNM, GG score, and BCR after RP than tumors that are visible on mpMRI.

III. High stromal FAP is an independent predictive biomarker of prostate cancer progression to BCR and should be considered for clinical use in biopsy assessment to support treatment decisions.

IV. A deep learning model can accurately detect and grade prostate cancer in biopsies, comparable to those made by fully trained uropathologists, and can also predict the likelihood of adverse staging and recurrence after surgical treatment.

V. Digital pathology with the integrated clinical use of AI is expected to support individual treatment decisions. The growing data pools with structured clinical and visual data will support predictive and prognostic models.

8 Acknowledgments

I want to thank countless people for this part of our shared journey that started in the autumn of 2017 in Helsinki. This journey with this multidisciplinary specialist group made me appreciate the value of cooperation and sharing in research and life. Without each one of you, I would not have come this far.

Special thanks go to my excellent supervisors. Without them and their persistent support, I would not have made it to the end. **Tuomas Mirtti** supported me as a colleague and friend in my international career to become a pathology consultant and head of the Pathology Unit in Malmö. Meanwhile, he facilitated my research 'at a distance' and kept me on the academic trail with persistence and patience. During our conversations, I highly valued his accurate insights into the developments of uropathology, digital pathology, and artificial intelligence, which are the basis for the next steps in cooperation, research, and development. **Antti Rannikko** showed me the need for basic questions and multidisciplinary expertise in clinical research. I thank both for their explicit support while creating the hypotheses, analyses, and conclusions in every part of the thesis. I enjoyed our friendly chats as much as the space for individual development and learning during this process.

I am grateful to **Andrew Erickson** for his enthusiasm, innovative ideas, and optimistic perspective on Finnish clinical-academic resources. **Juho Eineluoto**'s support was invaluable during periods of intense workload. **Joona Pohjonen** provided a priceless, comprehensive analysis of the subjects. **Teijo Pelinen** used his unparalleled multiplexing skills to separate tissue components on a cellular level meticulously. **Sami Blom** broadened my perspective and deepened my understanding of AI-driven solutions in pathology. **Anu Kenttämies** offered an in-depth view from the standpoint of the radiologist. **Stig Nordling** consistently lent his extensive clinical experience as a pathologist to support the projects.

I thank **Adrian Malén**, **Annabrita Hemmes**, **Anniina Manninen**, **Anssi Petas**, **Carolin Stürenberg**, **Henrikki Santti**, **Juuso Juhila**, **Katja Välimäki**, **Konrad Sopyllo**, **Mika Matikainen**, **Olli Kallioniemi**, **Petrus Järvinen**, **Tuomas Kilpeläinen**, **Ville Koponen**, **Riku Turkki**, **Suvi Marjasuo**, and **Tuomas Ropponen** for their irreplaceable efforts in our projects.

Understanding that everyone's time is precious, I sincerely thank my reviewers, **Leena Latonen** and **Pirkko-Liisa Kellokumpu-Lehtinen**. I appreciate their prompt voluntary feedback, interest, and fresh perspectives on my thesis.

I sincerely thank my colleagues and mentors at the Pathology Department of HUSLAB, Helsinki. The resourcefulness and dedication of this community enriched my journey into the realms of pathology and academia. Each individual introduced me to distinctive and impactful clinical and academic decision-making strategies, emphasizing the importance of decisive action. Through your guidance, I have understood that no one truly succeeds alone.

My current workplace in Malmö, where I serve as the head of the unit and a pathologist, has played a fundamental role in finalizing the thesis. My head of department, **Gunilla Bodelsson**, my colleagues and co-heads of the unit, **Ivica Filinic** and **Adna Mehmedi**, as well as my fellow pathologist colleagues, have taken significant responsibility for our shared mission, thereby facilitating my ability to concentrate on writing and finalizing the thesis.

I express my deepest gratitude to those who influenced my journey. Juggling an international clinical career alongside this academic endeavor was made smoother thanks to the immense understanding from my wife, **Hisae**, and our children, **Miku** and **Yuma**. My father, **John**, always lent a keen ear,

demonstrating genuine interest in the insights I gained during my learning journey. I warmly thank my dearest Finnish friends: **Tapsa**, with whom I have shared countless swimrun training hours, and **Aaro**, whose unique insights during our discussions have been precious.

References

1. Sung H, Ferlay J, Siegel RL, et al. Global cancer statistics 2020: GLOBOCAN estimates of incidence and mortality worldwide for 36 cancers in 185 countries. *CA Cancer J Clin*. 2021;71(3):209-249.

2. Finnish Cancer Registry; 2019. https://syoparekisteri.fi.

3. Catalona WJ. Prostate Cancer Screening. *Med Clin North Am*. 2018;102(2):199-214.

4. Gleason DF. Classification of prostatic carcinomas. *Cancer Chemother Rep*. 1966;50(3):125-128.

5. Epstein JI, Egevad L, Amin MB, Delahunt B, Srigley JR, Humphrey PA. The 2014 international society of urological pathology (ISUP) consensus conference on gleason grading of prostatic carcinoma definition of grading patterns and proposal for a new grading system. *Am J Surg Pathol*. 2016;40(2):244-252.

6. Godoy G, Chong KT, Cronin A, et al. Extent of Pelvic Lymph Node Dissection and the Impact of Standard Template Dissection on Nomogram Prediction of Lymph Node Involvement. *Eur Urol*. 2011;60(2):195-201.

7. Eifler JB, Feng Z, Lin BM, et al. An updated prostate cancer staging nomogram (Partin tables) based on cases from 2006 to 2011. *BJU Int*. 2013;111(1):22-29.

8. Cooperberg MR, Pasta DJ, Elkin EP, et al. The University of California, San Francisco cancer of the prostate risk assessment score: a straightforward and reliable preoperative predictor of disease recurrence after radical prostatectomy. *J Urol*. 2005;173(6):1938-1942.

9. Fütterer JJ, Briganti A, De Visschere P, et al. Can Clinically Significant Prostate Cancer Be Detected with Multiparametric Magnetic Resonance Imaging? A Systematic Review of the Literature. *Eur Urol*. 2015;68(6):1045-1053.

10. Weinreb JC, Barentsz JO, Choyke PL, et al. PI-RADS Prostate Imaging - Reporting and Data System: 2015, Version 2. *Eur Urol*. 2016;69(1):16-40.

11. Khoo CC, Eldred-Evans D, Peters M, et al. Likert vs PI-RADS v2: a comparison of two radiological scoring systems for detection of clinically significant prostate cancer. *BJU Int*. 2020;125(1):49-55.

12. Kasivisvanathan V, Rannikko AS, Borghi M, et al. MRI-Targeted or Standard Biopsy for Prostate-Cancer Diagnosis. *The New England journal of medicine*. 2018;378(19). doi:10.1056/NEJMOA1801993

13. De Visschere PJL, Naesens L, Libbrecht L, et al. What kind of prostate cancers do we miss on multiparametric magnetic resonance imaging? *European radiology*. 2016;26(4):1098-1107.

14. Johnson DC, Raman SS, Mirak SA, et al. Detection of Individual Prostate Cancer Foci via Multiparametric Magnetic Resonance Imaging. *Eur Urol*. 2019;75(5):712-720.

15. Woo S, Suh CH, Kim SY, Cho JY, Kim SH. Diagnostic Performance of Prostate Imaging Reporting and Data System Version 2 for Detection of Prostate Cancer: A Systematic Review and Diagnostic Meta-analysis. *Eur Urol*. 2017;72(2):177-188.

16. Chatterjee A, Watson G, Myint E, Sved P, Mcentee M, Bourne R. Changes in ep-ithelium, stroma, and lumen space correlate more strongly with gleason patternand are stronger predictors of prostate ADC changes than cellularity metrics. *Radiology*. 2015;277:751-762.

17. Molecular hallmarks of multiparametric magnetic resonance imaging visibilityin prostate cancer. *Eur Urol*. 2019;76:18-23.

18. Gibbs P, Liney GP, Pickles MD, Zelhof B, Rodrigues G, Turnbull LW. Correlationof ADC and T2 measurements with cell density in prostate cancer at 3.0 Tesla. *Invest Radiol*. 2009;44:572-576.

19. Rosenkrantz AB, Mendrinos S, Babb JS, Taneja SS. Prostate cancer foci detectedon multiparametric magnetic resonance imaging are histologically distinct fromthose not detected. *J Urol*. 2012;187:2032-2038.

20. Lahdensuo K, Erickson A, Saarinen I, et al. Loss of PTEN expression in ERG-negative prostate cancer predicts secondary therapies and leads to shorter disease-specific survival time after radical prostatectomy. *Mod Pathol*. 2016;29(12):1565-1574.

21. Boström PJ, Bjartell AS, Catto JWF, et al. Genomic predictors of outcome in prostate cancer. *Eur Urol*. 2015;68(6):1033-1044.

22. Lokman U, Erickson AM, Vasarainen H, Rannikko AS, Mirtti T. PTEN Loss but Not ERG Expression in Diagnostic Biopsies Is Associated with Increased Risk of Progression and Adverse Surgical Findings in Men with Prostate Cancer on Active Surveillance. *European Urology Focus*. 2018;4(6):867-873.

23. Mithal P, Allott E, Gerber L, et al. PTEN loss in biopsy tissue predicts poor clinical outcomes in prostate cancer. *Int J Urol*. 2014;21(12):1209-1214.

24. Ullman D, Dorn D, Rais-Bahrami S, Gordetsky J. Clinical Utility and Biologic Implications of Phosphatase and Tensin Homolog (PTEN) and ETS-related Gene (ERG) in Prostate Cancer. *Urology*. 2018;113:59-70.

25. van der Laak J, Litjens G, Ciompi F. Deep learning in histopathology: the path to the clinic. *Nat Med*. 2021;27(5):775-784.

26. De Marzo AM, Platz EA, Sutcliffe S, et al. Inflammation in prostate carcinogenesis. *Nat Rev Cancer*. 2007;7(4):256-269.

27. Yang XJ, Lecksell K, Gaudin P, Epstein JI. Rare expression of high-molecular-weight cytokeratin in adenocarcinoma of the prostate gland: a study of 100 cases of metastatic and locally advanced prostate cancer. *Am J Surg Pathol*. 1999;23(2):147-152.

28. Bostwick DG, de la Roza G, Dundore P, Corica FA, Iczkowski KA. Intraepithelial and stromal lymphocytes in the normal human prostate. *Prostate*. 2003;55(3):187-193.

29. Kellokumpu-Lehtinen P, Santti R, Pelliniemi LJ. Early cytodifferentiation of human prostatic urethra and Leydig cells. *Anat Rec*. 1979;194(3):429-443.

30. Tapanainen J, Kellokumpu-Lehtinen P, Huhtaniemi PLJ. Age related changes in endogenous steroids of human fetal testis during early and midpregnancy. *J Clin En-docrinol Metab*. 1982;52:98-102.

31. Kellokumpu-Lehtinen P, Santti R, Pelliniemi LJ. Correlation of early cytodifferentiation of the human fetal prostate and Leydig cells. *Anat Rec*. 1980;196(3):263-273.

32. Corona G, Vignozzi L, Rastrelli G, Lotti F, Cipriani S, Maggi M. Benign prostatic hyperplasia: a new metabolic disease of the aging male and its correlation with sexual dysfunctions. *Int J*

Endocrinol. 2014;2014:329456.

33. Ahlgren G, Rannevik G, Lilja H. Impaired secretory function of the prostate in men with oligo-asthenozoospermia. *J Androl*. 1995;16(6):491-498.

34. Malm J, Hellman J, Hogg P, Lilja H. Enzymatic action of prostate-specific antigen (PSA or hK3): Substrate specificity and regulation by Zn2+, a tight-binding inhibitor. *Prostate*. 2000;45(2):132-139.

35. Bouchelouche K, Choyke PL, Capala J. Prostate specific membrane antigen- a target for imaging and therapy with radionuclides. *Discov Med*. 2010;9(44):55-61.

36. Grignon DJ. Unusual subtypes of prostate cancer. *Mod Pathol*. 2004;17(3):316-327.

37. George J. Netto, Mahul B. Amin, James G. Kench. Tumours of the prostate: Introduction. In: WHO Classification of Tumours Editorial Board. Urinary and male genital tumours [Internet]. Lyon (France): International Agency for Research on Cancer; 2022. (WHO classification of tumours series, 5th ed.; vol. 8). Accessed November 27, 2022. https://tumourclassification.iarc.who.int/chaptercontent/36/95

38. Seipel AH, Wiklund F, Wiklund NP, Egevad L. Histopathological features of ductal adenocarcinoma of the prostate in 1,051 radical prostatectomy specimens. *Virchows Arch*. 2013;462(4):429-436.

39. Mano R, Tamir S, Kedar I, et al. Malignant Abnormalities in Male BRCA Mutation Carriers: Results From a Prospectively Screened Cohort. *JAMA Oncol*. 2018;4(6):872-874.

40. Page EC, Bancroft EK, Brook MN, et al. Interim Results from the IMPACT Study: Evidence for Prostate-specific Antigen Screening in BRCA2 Mutation Carriers. *Eur Urol*. 2019;76(6):831-842.

41. Sedhom R, Antonarakis ES. Clinical implications of mismatch repair deficiency in prostate cancer. *Future Oncol*. 2019;15(20):2395-2411.

42. Tomlins SA, Rhodes DR, Perner S, et al. Recurrent fusion of TMPRSS2 and ETS transcription factor genes in prostate cancer. *Science*. 2005;310(5748):644-648.

43. Magi-Galluzzi C, Tsusuki T, Elson P, et al. TMPRSS2-ERG gene fusion prevalence and class are significantly different in prostate cancer of Caucasian, African-American and Japanese patients. *Prostate*. 2011;71(5):489-497.

44. Haney NM, Faisal FA, Lu J, et al. PTEN loss with ERG negative status is associated with lethal disease after radical prostatectomy. *J Urol*. 2020;203(2):344-350.

45. Ahearn TU, Pettersson A, Ebot EM, et al. A Prospective Investigation of PTEN Loss and ERG Expression in Lethal Prostate Cancer. *J Natl Cancer Inst*. 2016;108(2). doi:10.1093/jnci/djv346

46. Stopsack KH, Su XA, Vaselkiv JB, et al. Transcriptomes of Prostate Cancer with TMPRSS2:ERG and Other ETS Fusions. *Mol Cancer Res*. 2023;21(1):14-23.

47. Cancer Genome Atlas Research Network. The Molecular Taxonomy of Primary Prostate Cancer. *Cell*. 2015;163(4):1011-1025.

48. Robinson D, Van Allen EM, Wu YM, et al. Integrative Clinical Genomics of Advanced Prostate Cancer. *Cell*. 2015;162(2):454.

49. Gurel B, Iwata T, Koh CM, et al. Nuclear MYC protein overexpression is an early alteration in human prostate carcinogenesis. *Mod Pathol*. 2008;21(9):1156-1167.

50. Stopsack KH, Nandakumar S, Wibmer AG, et al. Oncogenic Genomic Alterations, Clinical Phenotypes, and Outcomes in Metastatic Castration-Sensitive Prostate Cancer. *Clin Cancer Res*. 2020;26(13):3230-3238.

51. Graf RP, Hullings M, Barnett ES, Carbone E, Dittamore R, Scher HI. Clinical Utility of the Nuclear-localized AR-V7 Biomarker in Circulating Tumor Cells in Improving Physician Treatment Choice in Castration-resistant Prostate Cancer. *Eur Urol*. 2020;77(2):170-177.

52. Bratt O, Drevin L, Akre O, Garmo H, Stattin P. Family History and Probability of Prostate Cancer, Differentiated by Risk Category: A Nationwide Population-Based Study. *J Natl Cancer Inst*. 2016;108(10). doi:10.1093/jnci/djw110

53. Hemminki K. Familial risk and familial survival in prostate cancer. *World J Urol*. 2012;30(2):143-148.

54. Randazzo M, Müller A, Carlsson S, et al. A positive family history as a risk factor for prostate cancer in a population-based study with organised prostate-specific antigen screening: results of the Swiss European Randomised Study of Screening for Prostate Cancer (ERSPC, Aarau). *BJU Int*. 2016;117(4):576-583.

55. Jahn JL, Giovannucci EL, Stampfer MJ. The high prevalence of undiagnosed prostate cancer at autopsy: implications for epidemiology and treatment of prostate cancer in the Prostate-specific Antigen-era. *Int J Cancer*. 2015;137(12):2795-2802.

56. Yamoah K, Lee KM, Awasthi S, et al. Racial and ethnic disparities in prostate cancer outcomes in the Veterans Affairs health care system. *JAMA Netw Open*. 2022;5(1):e2144027.

57. Mahal BA, Alshalalfa M, Kensler KH, et al. Racial Differences in Genomic Profiling of Prostate Cancer. *N Engl J Med*. 2020;383(11):1083-1085.

58. Leitzmann MF, Rohrmann S. Risk factors for the onset of prostatic cancer: age, location, and behavioral correlates. *Clin Epidemiol*. 2012;4:1-11.

59. Pitkäniemi J, Malila N, Tanskanen T, Degerlund H, Heikkinen S, Seppä K. Finnish cancer register. Syöpärekisteri. Published June 6, 2017. https://syoparekisteri.fi

60. Kench JG, Kristiansen G, Berney DM. Prostatic acinar adenocarcinoma. In: WHO Classification of Tumours Editorial Board. Urinary and male genital tumours [Internet]. Lyon (France): International Agency for Research on Cancer; 2022. (WHO classification of tumours series, 5th ed.; vol. 8). Accessed December 3, 2022. https://tumourclassification.iarc.who.int/chapters/36/100

61. Totten RS, Heinemann MW, Hudson PB, Sproul EE, Stout AP. Microscopic differential diagnosis of latent carcinoma of prostate. *AMA Arch Pathol*. 1953;55(2):131-141.

62. Mostofi FK, Sesterhenn IA, Davis CJ Jr. A pathologist's view of prostatic carcinoma. *Cancer*. 1993;71(3 Suppl):906-932.

63. Magi-Galluzzi C. Prostate cancer: diagnostic criteria and role of immunohistochemistry. *Mod Pathol*. 2018;31(S1):S12-21.

64. Magi-Galluzzi C, Luo J, Isaacs WB, Hicks JL, de Marzo AM, Epstein JI. Alpha-methylacyl-CoA racemase: a variably sensitive immunohistochemical marker for the diagnosis of small prostate cancer foci on needle biopsy. *Am J Surg Pathol*. 2003;27(8):1128-1133.

65. Zhou M, Aydin H, Kanane H, Epstein JI. How often does alpha-methylacyl-CoA-racemase contribute to resolving an atypical diagnosis on prostate needle biopsy beyond that provided by basal cell markers? *Am J Surg Pathol*. 2004;28(2):239-243.

66. Trpkov K, Bartczak-McKay J, Yilmaz A. Usefulness of cytokeratin 5/6 and AMACR applied as double sequential immunostains for diagnostic assessment of problematic prostate specimens. *Am J Clin Pathol*. 2009;132(2):211-220; quiz 307.

67. Hameed O, Humphrey PA. Immunohistochemistry in diagnostic surgical pathology of the prostate. *Semin Diagn Pathol*. 2005;22(1):88-104.

68. Wu CL, Yang XJ, Tretiakova M, et al. Analysis of alpha-methylacyl-CoA racemase (P504S) expression in high-grade prostatic intraepithelial neoplasia. *Hum Pathol*. 2004;35(8):1008-1013.

69. Armah HB, Parwani AV. Atypical adenomatous hyperplasia (adenosis) of the prostate: a case report with review of the literature. *Diagn Pathol*. 2008;3(1):34.

70. Worschech A, Meirelles L, Billis A. Expression of alpha-methylacyl coenzyme A racemase in partial and complete focal atrophy on prostate needle biopsies. *Anal Quant Cytol Histol*. 2009;31(6):424-431.

71. Etzioni R, Gulati R, Cooperberg MR, Penson DM, Weiss NS, Thompson IM. Limitations of basing screening policies on screening trials: The US Preventive Services Task Force and Prostate Cancer Screening. *Med Care*. 2013;51(4):295-300.

72. European Commission. Recommendation on prostate cancer screening (COM/2022/474 final). Published September 20, 2022. Accessed April 2, 2023. https://health.ec.europa.eu/system/files/2022-09/com_2022-474_act_en.pdf

73. Oesterling JE, Jacobsen SJ, Chute CG, et al. Serum prostate-specific antigen in a community-based population of healthy men. Establishment of age-specific reference ranges. *JAMA*. 1993;270(7):860-864.

74. Carter HB, Pearson JD, Metter EJ, et al. Longitudinal evaluation of prostate-specific antigen levels in men with and without prostate disease. *JAMA*. 1992;267(16):2215-2220.

75. Johansson JE, Andrén O, Andersson SO, et al. Natural history of early, localized prostate cancer. *JAMA*. 2004;291(22):2713-2719.

76. Albertsen PC, Hanley JA, Fine J. 20-Year Outcomes Following Conservative Management of Clinically Localized Prostate Cancer. *JAMA*. 2005;293(17):2095.

77. Rider JR, Sandin F, Andrén O, Wiklund P, Hugosson J, Stattin P. Long-term outcomes among noncuratively treated men according to prostate cancer risk category in a nationwide, population-based study. *Eur Urol*. 2013;63(1):88-96.

78. Fenton JJ, Weyrich MS, Durbin S, Liu Y, Bang H, Melnikow J. Prostate-Specific Antigen-Based Screening for Prostate Cancer: Evidence Report and Systematic Review for the US Preventive Services Task Force. *JAMA*. 2018;319(18):1914-1931.

79. Pinsky PF, Miller E, Prorok P, Grubb R, David Crawford E, Andriole G. Extended follow-up for prostate cancer incidence and mortality among participants in the Prostate, Lung, Colorectal and Ovarian randomized cancer screening trial. *BJU International*. 2019;123(5):854-860. doi:10.1111/bju.14580

80. Schröder FH, Hugosson J, Roobol MJ, et al. Screening and prostate cancer mortality: results of the European Randomised Study of Screening for Prostate Cancer (ERSPC) at 13 years of follow-up. *Lancet*. 2014;384(9959):2027-2035.

81. Ilic D, Djulbegovic M, Jung JH, et al. Prostate cancer screening with prostate-specific antigen (PSA) test: a systematic review and meta-analysis. *BMJ*. 2018;362. doi:10.1136/bmj.k3519

82. Djulbegovic M, Beyth RJ, Neuberger MM, Stoffs TL, Djulbegovic B, Dahm P. Screening for prostate cancer: systematic review and meta-analysis of randomised controlled trials. *BMJ*. 2010;341. doi:10.1136/bmj.c4543

83. Martin RM, Donovan JL, Turner EL, et al. Effect of a Low-Intensity PSA-Based Screening Intervention on Prostate Cancer Mortality: The CAP Randomized Clinical Trial. *JAMA*. 2018;319(9):883-895.

84. Heidenreich A, Bastian PJ, Bellmunt J, et al. EAU Guidelines on Prostate Cancer. Part 1: Screening, Diagnosis, and Local Treatment with Curative Intent—Update 2013. *Eur Urol*. 2014;65(1):124-137.

85. Mottet N, van den Bergh RCN, Briers E, et al. EAU-EANM-ESTRO-ESUR-SIOG Guidelines on Prostate Cancer-2020 Update. Part 1: Screening, Diagnosis, and Local Treatment with Curative Intent. *Eur Urol*. 2021;79(2):243-262.

86. Catalona WJ, Richie JP, Ahmann FR, et al. Comparison of Digital Rectal Examination and Serum Prostate Specific Antigen in the Early Detection of Prostate Cancer: Results of a Multicenter Clinical Trial of 6,630 Men. *J Urol*. 2017;197(2S):S200-S207.

87. Raja J, Ramachandran N, Munneke G, Patel U. Current status of transrectal ultrasound-guided prostate biopsy in the diagnosis of prostate cancer. *Clin Radiol*. 2006;61(2):142-153.

88. Purohit RS, Shinohara K, Meng MV, Carroll PR. Imaging clinically localized prostate cancer. *Urol Clin North Am*. 2003;30(2):279-293.

89. Barentsz JO, Richenberg J, Clements R, et al. ESUR prostate MR guidelines 2012. *Eur Radiol*. 2012;22(4):746-757.

90. Barkovich EJ, Shankar PR, Westphalen AC. A systematic review of the existing Prostate Imaging Reporting and Data System version 2 (PI-RADSv2) literature and subset meta-analysis of PI-RADSv2 categories stratified by Gleason scores. *AJR Am J Roentgenol*. 2019;212(4):847-854.

91. Stabile A, Giganti F, Kasivisvanathan V, et al. Factors influencing variability in the performance of multiparametric magnetic resonance imaging in detecting clinically significant prostate cancer: A systematic literature review. *Eur Urol Oncol*. 2020;3(2):145-167.

92. Eldred-Evans D, Burak P, Connor MJ, et al. Population-Based Prostate Cancer Screening With Magnetic Resonance Imaging or Ultrasonography: The IP1-PROSTAGRAM Study. *JAMA Oncol*. 2021;7(3):395-402.

93. Mottet N, Bellmunt J, Bolla M, et al. EAU-ESTRO-SIOG Guidelines on Prostate Cancer. Part 1:

Screening, Diagnosis, and Local Treatment with Curative Intent. *Eur Urol*. 2017;71(4):618-629.

94. Vickers A, Carlsson SV, Cooperberg M. Routine Use of Magnetic Resonance Imaging for Early Detection of Prostate Cancer Is Not Justified by the Clinical Trial Evidence. *Eur Urol*. 2020;78(3):304-306.

95. Wu X, Reinikainen P, Kapanen M, Vierikko T, Ryymin P, Kellokumpu-Lehtinen PL. Dynamic Contrast-Enhanced Imaging as a Prognostic Tool in Early Diagnosis of Prostate Cancer: Correlation with PSA and Clinical Stage. *Contrast Media Mol Imaging*. 2018;2018:3181258.

96. Greer MD, Brown AM, Shih JH, et al. Accuracy and agreement of PIRADSv2 for prostate cancer mpMRI: A multireader study. *J Magn Reson Imaging*. 2017;45(2):579-585.

97. Zhang L, Tang M, Chen S, Lei X, Zhang X, Huan Y. A meta-analysis of use of Prostate Imaging Reporting and Data System Version 2 (PI-RADS V2) with multiparametric MR imaging for the detection of prostate cancer. *Eur Radiol*. 2017;27(12):5204-5214.

98. Turkbey B, Rosenkrantz AB, Haider MA, et al. Prostate Imaging Reporting and Data System Version 2.1: 2019 Update of Prostate Imaging Reporting and Data System Version 2. *Eur Urol*. 2019;76(3):340-351.

99. Harada T, Abe T, Kato F, et al. Five-point Likert scaling on MRI predicts clinically significant prostate carcinoma. *BMC Urol*. 2015;15:91.

100. Moore CM, Giganti F, Albertsen P, et al. Reporting Magnetic Resonance Imaging in Men on Active Surveillance for Prostate Cancer: The PRECISE Recommendations-A Report of a European School of Oncology Task Force. *Eur Urol*. 2017;71(4):648-655.

101. Noureldin ME, Connor MJ, Boxall N, Miah S, Shah T, Walz J. Current techniques of prostate biopsy: an update from past to present. *Transl Androl Urol*. 2020;9(3):1510-1517.

102. Baco E, Rud E, Eri LM, et al. A randomized controlled trial to assess and compare the outcomes of two-core prostate biopsy guided by fused magnetic resonance and transrectal ultrasound images and traditional 12-core systematic biopsy. *Eur Urol*. 2016;69(1):149-156.

103. Drost FJH, Osses DF, Nieboer D, et al. Prostate MRI, with or without MRI-targeted biopsy, and systematic biopsy for detecting prostate cancer. *Cochrane Libr*. Published online April 25, 2019. doi:10.1002/14651858.cd012663.pub2

104. Haffner J, Lemaitre L, Puech P, Haber GP, Leroy X, Jones JS. Role of magnetic resonance imaging before initial biopsy: comparison of magnetic resonance imagingtargeted and systematic biopsy for significant prostate cancer detection. *BJU Int*. 2011;108(8):E171-178.

105. Wegelin O, Exterkate L, van der Leest M, et al. The FUTURE trial: A multicenter randomised controlled trial on target biopsy techniques based on magnetic resonance imaging in the diagnosis of prostate cancer in patients with prior negative biopsies. *Eur Urol*. 2019;75(4):582-590.

106. Watts KL, Frechette L, Muller B, et al. Systematic review and meta-analysis comparing cognitive vs. image-guided fusion prostate biopsy for the detection of prostate cancer. *Urol Oncol*. 2020;38(9):734.e19-734.e25.

107. Xiang J, Yan H, Li J, Wang X, Chen H, Zheng X. Transperineal versus transrectal prostate biopsy in the diagnosis of prostate cancer: a systematic review and metaanalysis. *World J Surg Oncol*.

2019;17(1):31-31.

108. Tu X, Liu Z, Chang T, et al. Transperineal magnetic resonance imaging-targeted biopsy may perform better than transrectal route in the detection of clinically significant prostate cancer: Systematic review and meta-analysis. *Clin Genitourin Cancer*. 2019;17(5):e860-e870.

109. Pradere B, Veeratterapillay R, Dimitropoulos K, et al. Nonantibiotic Strategies for the Prevention of Infectious Complications following Prostate Biopsy: A Systematic Review and Meta-Analysis. *J Urol*. 2021;205(3):653-663.

110. Eggener SE, Badani K, Barocas DA, et al. Gleason 6 Prostate Cancer: Translating Biology into Population Health. *J Urol*. 2015;194(3):626-634.

111. Epstein JI, Feng Z, Trock BJ, Pierorazio PM. Upgrading and Downgrading of Prostate Cancer from Biopsy to Radical Prostatectomy: Incidence and Predictive Factors Using the Modified Gleason Grading System and Factoring in Tertiary Grades. *Eur Urol*. 2012;61(5):1019-1024.

112. Amin M Lin D Gore J Srigley J Samaratunga H E al, Amin MB, Lin DW, et al. The critical role of the pathologist in determining eligibility for active surveillance as a management option in patients with prostate cancer: consensus statement with recommendations supported by the College of American Pathologists, International Soci. *Arch Pathol Lab Med*. 2014;138(10):1387-1406.

113. Epstein JI, Allsbrook WC, Amin MB, Egevad LL, ISUP Grading Committee. The 2005 International Society of Urological Pathology (ISUP) Consensus Conference on Gleason Grading of Prostatic Carcinoma. *Am J Surg Pathol*. 2005;29(9):1228-1242.

114. Kweldam CF, Nieboer D, Algaba F, et al. Gleason grade 4 prostate adenocarcinoma patterns: an interobserver agreement study among genitourinary pathologists. *Histopathology*. Published online 2016. doi:10.1111/his.12976

115. Kweldam CF, van Leenders GJ, van der Kwast T. Grading of prostate cancer: a work in progress. *Histopathology*. 2019;74(1):146-160.

116. Epstein JI. Prostate cancer grading: a decade after the 2005 modified system. *Mod Pathol*. 2018;31(S1):S47-63.

117. Epstein JI. An update of the Gleason grading system. *J Urol*. 2010;183(2):433-440.

118. Fine SW, Amin MB, Berney DM, et al. A contemporary update on pathology reporting for prostate cancer: Biopsy and radical prostatectomy specimens. *Eur Urol*. 2012;62(1):20-39.

119. van Leenders GJLH, van der Kwast TH, Grignon DJ, et al. The 2019 International Society of Urological Pathology (ISUP) consensus conference on grading of prostatic carcinoma. *Am J Surg Pathol*. 2020;44(8):e87-e99.

120. Sauter G, Steurer S, Clauditz TS, et al. Clinical utility of quantitative Gleason grading in prostate biopsies and prostatectomy specimens. *Eur Urol*. 2016;69(4):592-598.

121. Sauter G, Clauditz T, Steurer S, et al. Integrating tertiary Gleason 5 patterns into quantitative Gleason grading in prostate biopsies and prostatectomy specimens. *Eur Urol*. 2018;73(5):674-683.

122. Wulczyn E, Nagpal K, Symonds M, et al. Predicting prostate cancer specific-mortality with artificial intelligence-based Gleason grading. *Communications Medicine*. 2021;1(1):1-8.

123. Nagpal K, Foote D, Liu Y, et al. Development and validation of a deep learning algorithm for improving Gleason scoring of prostate cancer. *NPJ Digit Med*. 2019;2:48.

124. Ström P, Kartasalo K, Olsson H, et al. Artificial intelligence for diagnosis and grading of prostate cancer in biopsies: a population-based, diagnostic study. *Lancet Oncol*. 2020;21(2). doi:10.1016/S1470-2045(19)30738-7

125. Bulten W, Pinckaers H, van Boven H, et al. Automated deep-learning system for Gleason grading of prostate cancer using biopsies: a diagnostic study. *Lancet Oncol*. 2020;21(2):233-241.

126. Nagpal K, Foote D, Tan F, et al. Development and validation of a deep learning algorithm for Gleason grading of prostate cancer from biopsy specimens. *JAMA Oncol*. 2020;6(9):1372-1380.

127. Bulten W, Balkenhol M, Belinga JJA, et al. Artificial intelligence assistance significantly improves Gleason grading of prostate biopsies by pathologists. *Mod Pathol*. 2021;34(3):660-671.

128. Steiner DF, Nagpal K, Sayres R, et al. Evaluation of the Use of Combined Artificial Intelligence and Pathologist Assessment to Review and Grade Prostate Biopsies. *JAMA Netw Open*. 2020;3(11):e2023267.

129. Labbate CV, Paner GP, Eggener SE. Should Grade Group 1 (GG1) be called cancer? *World J Urol*. 2022;40(1):15-19.

130. Eggener SE, Berlin A, Vickers AJ, Paner GP, Wolinsky H, Cooperberg MR. Low-Grade Prostate Cancer: Time to Stop Calling It Cancer. *J Clin Oncol*. 2022;40(27):3110-3114.

131. Netto GJ, Cheng L. Emerging critical role of molecular testing in diagnostic genitourinary pathology. *Arch Pathol Lab Med*. 2012;136(4):372-390.

132. Kweldam CF, Wildhagen MF, Bangma CH, van Leenders GJLH. Disease-specific death and metastasis do not occur in patients with Gleason score ≤6 at radical prostatectomy. *BJU Int*. 2015;116(2):230-235.

133. JE Cowan Do adenocarcinomas of the prostate with Gleason score (GS) ≤6 have the potential to metastasize to lymph nodes? *Am J Surg Pathol*. 2012;36:1346-1352.

134. Anderson BB, Oberlin DT, Razmaria AA, et al. Extraprostatic Extension Is Extremely Rare for Contemporary Gleason Score 6 Prostate Cancer. *Eur Urol*. 2017;72(3):455-460.

135. Nikiforov YE, Seethala RR, Tallini G, et al. Nomenclature Revision for Encapsulated Follicular Variant of Papillary Thyroid Carcinoma: A Paradigm Shift to Reduce Overtreatment of Indolent Tumors. *JAMA Oncol*. 2016;2(8):1023-1029.

136. Russo F, Regge D, Armando E, et al. Detection of prostate cancer index lesions with multiparametric magnetic resonance imaging (mp-MRI) using whole-mount histological sections as the reference standard. *BJU Int*. 2016;118(1):84-94.

137. Soeterik TFW, van Melick HHE, Dijksman LM, Biesma DH, Witjes JA, van Basten JPA. Multiparametric Magnetic Resonance Imaging Should Be Preferred Over Digital Rectal Examination for Prostate Cancer Local Staging and Disease Risk Classification. *Urology*. 2021;147:205-212.

138. Esserman LJ, Thompson IM, Reid B, et al. Addressing overdiagnosis and overtreatment in cancer: a prescription for change. *Lancet Oncol*. 2014;15(6):e234-42.

139. Kooby DA, Antonescu CR, Brennan MF, Singer S. Atypical lipomatous tumor/well-differentiated liposarcoma of the extremity and trunk wall: importance of histological subtype with treatment recommendations. *Ann Surg Oncol*. 2004;11(1):78-84.

140. Epstein JI, Amin MB, Reuter VR, Mostofi FK, The Bladder Consensus Conference Committee. The World Health Organization/International Society of Urological Pathology Consensus Classification of Urothelial (Transitional Cell) Neoplasms of the Urinary Bladder. *Am J Surg Pathol*. 1998;22(12):1435.

141. Ploussard G, Beauval JB, Lesourd M, et al. Performance of systematic, MRI-targeted biopsies alone or in combination for the prediction of unfavourable disease in MRI-positive low-risk prostate cancer patients eligible for active surveillance. *World J Urol*. 2020;38(3):663-671.

142. Netto GJ, Amin MB, Compérat EM, et al. Prostate Adenocarcinoma Grade Group 1: Rationale for Retaining a Cancer Label in the 2022 World Health Organization Classification. *Eur Urol*. Published online October 4, 2022. doi:10.1016/j.eururo.2022.09.015

143. Brierley JD. *TNM Classification of Malignant Tumors*. UICC International Union Against Cancer; 2017.

144. Brizmohun Appayya M, Adshead J, Ahmed HU, et al. National implementation of multi-parametric magnetic resonance imaging for prostate cancer detection - recommendations from a UK consensus meeting. *BJU Int*. 2018;122(1):13-25.

145. Kim TH, Woo S, Han S, et al. The Diagnostic Performance of the Length of Tumor Capsular Contact on MRI for Detecting Prostate Cancer Extraprostatic Extension: A Systematic Review and Meta-Analysis. *Korean J Radiol*. 2020;21(6):684-694.

146. Barentsz JO, Weinreb JC, Verma S, et al. Synopsis of the PI-RADS v2 Guidelines for Multiparametric Prostate Magnetic Resonance Imaging and Recommendations for Use. *Eur Urol*. 2016;69(1):41-49.

147. van der Kwast TH, Amin MB, Billis A, et al. International Society of Urological Pathology (ISUP) Consensus Conference on Handling and Staging of Radical Prostatectomy Specimens. Working group 2: T2 substaging and prostate cancer volume. *Mod Pathol*. 2011;24(1):16-25.

148. Echle A, Rindtorff NT, Brinker TJ, Luedde T, Pearson AT, Kather JN. Deep learning in cancer pathology: a new generation of clinical biomarkers. *Br J Cancer*. 2021;124(4):686-696.

149. Lipkova J, Chen RJ, Chen B, et al. Artificial intelligence for multimodal data integration in oncology. *Cancer Cell*. 2022;40(10):1095-1110.

150. Abels E. Computational pathology defnitions, best practices, and recommendations for regulatory guidance: a white paper from the Digital Pathology Association. *J Pathol*. 2019;249:286-294.

151. Kelly CJ, Karthikesalingam A, Suleyman M, Corrado G, King D. Key challenges for delivering clinical impact with artificial intelligence. *BMC Med*. 2019;17(1):195.

152. McKinney SM, Sieniek M, Godbole V, et al. International evaluation of an AI system for breast cancer screening. *Nature*. 2020;577(7788):89-94.

153. Campanella G, Hanna MG, Geneslaw L, et al. Clinical-grade computational pathology using weakly supervised deep learning on whole slide images. *Nat Med*. 2019;25(8):1301-1309.

154. De Bel T, Hermsen M, Kers J, Van Der Laak J, Litjens GJ. Stain-transforming cycle-consistent generative adversarial networks for improved segmentation of renal histopathology. *Proc International Conference on Medical Imaging with Deep Learning, Proceedings of Machine Learning Research*. 2019;102:151-163.

155. Liu Y, Kohlberger T, Norouzi M, et al. Artificial Intelligence-Based Breast Cancer Nodal Metastasis Detection: Insights Into the Black Box for Pathologists. *Arch Pathol Lab Med*. 2019;143(7):859-868.

156. Tellez D, Litjens G, Bándi P, et al. Quantifying the effects of data augmentation and stain color normalization in convolutional neural networks for computational pathology. *Med Image Anal*. 2019;58:101544.

157. Pohjonen J, Stürenberg C, Föhr A, Pitkänen E, Rannikko A, Mirtti T. Exposing and addressing the fragility of neural networks in digital pathology. *arXiv [eessIV]*. Published online June 30, 2022. http://arxiv.org/abs/2206.15274

158. Cho H, Lim S, Choi G, Min H. Neural Stain-Style Transfer Learning using GAN for Histopathological Images. *arXiv [csCV]*. Published online October 23, 2017. http://arxiv.org/abs/1710.08543

159. Anowczyk A, Basavanhally A, Madabhushi A. Stain Normalization using Sparse AutoEncoders (StaNoSA): application to digital pathology. *Comput Med Imaging Graph*. 2017;57:50-61.

160. Tarek Shaban M, Baur C, Navab N, Albarqouni S. StainGAN: Stain Style Transfer for Digital Histological Images. *arXiv [csCV]*. Published online April 4, 2018. http://arxiv.org/abs/1804.01601

161. Zheng Y, Jiang Z, Zhang H, et al. Stain Standardization Capsule for Application-Driven Histopathological Image Normalization. *IEEE J Biomed Health Inform*. 2021;25(2):337-347.

162. Kleppe A, Skrede OJ, De Raedt S, Liestøl K, Kerr DJ, Danielsen HE. Designing deep learning studies in cancer diagnostics. *Nat Rev Cancer*. 2021;21(3):199-211.

163. Kather JN, Krisam J, Charoentong P, et al. Predicting survival from colorectal cancer histology slides using deep learning: A retrospective multicenter study. Butte AJ, ed. *PLoS Med*. 2019;16(1):e1002730.

164. Courtiol P, Maussion C, Moarii M, et al. Deep learning-based classification of mesothelioma improves prediction of patient outcome. *Nat Med*. 2019;25(10):1519-1525.

165. Staartjes VE, Kernbach JM. Significance of external validation in clinical machine learning: let loose too early? *Spine J*. 2020;20(7):1159-1160.

166. A central repository of digital pathology slides to boost the development of artificial intelligence. Accessed January 15, 2023. https://bigpicture.eu/

167. Nationell valideringsplattform för AI inom mammografiscreening (VAI-B). Accessed January 15, 2023. https://cancercentrum.se/samverkan/vara-uppdrag/forskning/forsknings--och-innovationsprojekt/tre-projekt-for-att-stodja-anvandandet-av-ai/nationell-valideringsplattform-for-ai-inom-mammografiscreening-vai-b/

168. Nagendran M, Chen Y, Lovejoy CA, et al. Artificial intelligence versus clinicians: systematic review of design, reporting standards, and claims of deep learning studies. *BMJ*.

2020;368:m689.

169. Fraggetta F, L'Imperio V, Ameisen D, et al. Best Practice Recommendations for the Implementation of a Digital Pathology Workflow in the Anatomic Pathology Laboratory by the European Society of Digital and Integrative Pathology (ESDIP). *Diagnostics (Basel)*. 2021;11(11). doi:10.3390/diagnostics11112167

170. Hufnagl P, Zwönitzer R, Haroske G. *Guidelines Digital Pathology for Diagnosis on (and Reports Of) Digital Images Version 1*.

171. Pantanowitz L, Sinard JH, Henricks WH, et al. Validating whole slide imaging for diagnostic purposes in pathology: guideline from the College of American Pathologists Pathology and Laboratory Quality Center. *Arch Pathol Lab Med*. 2013;137(12):1710-1722.

172. Evans AJ, Brown RW, Bui MM, et al. Validating Whole Slide Imaging Systems for Diagnostic Purposes in Pathology: Guideline Update from the College of American Pathologists in Collaboration with the American Society for Clinical Pathology and the Association for Pathology Informatics. *Arch Pathol Lab Med*. Published online 2021.

173. Cross S, Furness P, Igali L, Snead D, Treanor D, Williamson L. Best practice recommendations for implementing digital pathology January 201.

174. Goacher E, Randell R, Williams B, Treanor D. The Diagnostic Concordance of Whole Slide Imaging and Light Microscopy: A Systematic Review. *Arch Pathol Lab Med*. 2017;141(1):151-161.

175. Azam AS, Miligy IM, Kimani PKU, et al. Diagnostic concordance and discordance in digital pathology: a systematic review and meta-analysis. *J Clin Pathol*. 2021;74(7):448-455.

176. Center for Devices, Radiological Health. Use of International Standard ISO 10993-1, "Biological evaluation of medical devices - Part 1: Evaluation and testing within a risk management process." U.S. Food and Drug Administration. Accessed January 15, 2023. https://www.fda.gov/regulatory-information/search-fda-guidance-documents/use-international-standard-iso-10993-1-biological-evaluation-medical-devices-part-1-evaluation-and

177. Gillessen S, Bossi A, Davis ID, et al. Management of Patients with Advanced Prostate Cancer. Part I: Intermediate-/High-risk and Locally Advanced Disease, Biochemical Relapse, and Side Effects of Hormonal Treatment: Report of the Advanced Prostate Cancer Consensus Conference 2022. *Eur Urol*. 2023;83(3):267-293.

178. Rebello RJ, Oing C, Knudsen KE, et al. Prostate cancer. *Nat Rev Dis Primers*. 2021;7(1):9.

179. D'Amico AV, Whittington R, Malkowicz SB, et al. Biochemical outcome after radical prostatectomy or external beam radiation therapy for patients with clinically localized prostate carcinoma in the prostate specific antigen era. *Cancer*. 2002;95(2):281-286.

180. Kane CJ, Eggener SE, Shindel AW, Andriole GL. Variability in outcomes for patients with intermediate-risk prostate cancer (Gleason score 7, international society of urological pathology Gleason group 2-3) and implications for risk stratification: A systematic review. *Eur Urol Focus*. 2017;3(4-5):487-497.

181. Epstein JI, Zelefsky MJ, Sjoberg DD, et al. A Contemporary Prostate Cancer Grading System: A Validated Alternative to the Gleason Score. *Eur Urol*. 2016;69(3):428-435.

182. Ventimiglia E, Seisen T, Abdollah F, et al. A systematic review of the role of definitive local

treatment in patients with clinically lymph node-positive prostate cancer. *Eur Urol Oncol*. 2019;2(3):294-301.

183. Albertsen PC. Observational studies and the natural history of screen-detected prostate cancer. *Curr Opin Urol*. 2015;25(3):232-237.

184. Thomsen FB, Brasso K, Klotz LH, Røder MA, Berg KD, Iversen P. Active surveillance for clinically localized prostate cancer--a systematic review. *J Surg Oncol*. 2014;109(8):830-835.

185. Tosoian JJ, Mamawala M, Epstein JI, et al. Active surveillance of grade group 1 prostate cancer: Long-term outcomes from a large prospective cohort. *Eur Urol*. 2020;77(6):675-682.

186. Hamdy FC, Donovan JL, Lane JA, et al. 10-year outcomes after monitoring, surgery, or radiotherapy for localized prostate cancer. *N Engl J Med*. 2016;375(15):1415-1424.

187. Inoue LYT, Trock BJ, Partin AW, Carter HB, Etzioni R. Modeling grade progression in an active surveillance study. *Stat Med*. 2014;33(6):930-939.

188. Kalalahti I, Kilpeläinen T, Rannikko A. Aktiivinen vai passiivinen eturauhassyövän seuranta?: Kevyempi hoito vähemmin haitoin vaarantamatta syövänhallintaa. *Duodecim*. 2022;138(7):561-562.

189. Bill-Axelson A, Holmberg L, Garmo H, et al. Radical prostatectomy or watchful waiting in early prostate cancer. *N Engl J Med*. 2014;370(10):932-942.

190. Gleicher S, Basin MF, Arens L, Jacob J, Byler T, Ferry E. Management of Localized T1c Prostate Cancer among men 75 years and older: A National Cancer Database Study. *Clin Genitourin Cancer*. Published online October 12, 2022. doi:10.1016/j.clgc.2022.10.004

191. Harmenberg U, Hamdy FC, Widmark A, Lennernäs B, Nilsson S. Curative radiation therapy in prostate cancer. *Acta Oncol*. 2011;50 Suppl 1(sup1):98-103.

192. Carlos-Reyes A, Muñiz-Lino MA, Romero-Garcia S, López-Camarillo C, la Cruz ONH de. Biological Adaptations of Tumor Cells to Radiation Therapy. *Front Oncol*. 2021;11. doi:10.3389/fonc.2021.718636

193. Attard G, Murphy L, Clarke NW, et al. Abiraterone acetate and prednisolone with or without enzalutamide for high-risk non-metastatic prostate cancer: a meta-analysis of primary results from two randomised controlled phase 3 trials of the STAMPEDE platform protocol. *Lancet*. 2022;399(10323):447-460.

194. Fizazi K, Gillessen S, ESMO Guidelines Committee. Electronic address: clinicalguidelines@esmo.org. Updated treatment recommendations for prostate cancer from the ESMO Clinical Practice Guideline considering treatment intensification and use of novel systemic agents. *Ann Oncol*. 2023;34(6):557-563.

195. Trewartha D, Carter K, Vanneste BG, Van Limbergen EJ, Van Lin EN. Prostate cancer radiation therapy: what do clinicians have to know? *Nat Rev Drug Discov*. 2013;12.

196. Matzinger O, Duclos F, van den Bergh A, et al. Acute toxicity of curative radiotherapy for intermediate- and high-risk localised prostate cancer in the EORTC trial 22991. *Eur J Cancer*. 2009;45(16):2825-2834.

197. Zaffuto E, Gandaglia G, Fossati N, et al. Early Postoperative Radiotherapy is Associated with

Worse Functional Outcomes in Patients with Prostate Cancer. *J Urol*. 2017;197(3 Pt 1):669-675.

198. Boorjian SA, Karnes RJ, Crispen PL, Rangel LJ, Bergstralh EJ, Blute ML. Radiation therapy after radical prostatectomy: impact on metastasis and survival. *J Urol*. 2009;182(6):2708-2714.

199. Parker CC, Clarke NW, Cook AD, et al. Timing of radiotherapy after radical prostatectomy (RADICALS-RT): a randomised, controlled phase 3 trial. *Lancet*. 2020;396(10260):1413-1421.

200. Kneebone A, Fraser-Browne C, Duchesne GM, et al. Adjuvant radiotherapy versus early salvage radiotherapy following radical prostatectomy (TROG 08.03/ANZUP RAVES): a randomised, controlled, phase 3, non-inferiority trial. *Lancet Oncol*. 2020;21(10):1331-1340.

201. Spratt DE, Dai DLY, Den RB, et al. Performance of a Prostate Cancer Genomic Classifier in Predicting Metastasis in Men with Prostate-specific Antigen Persistence Postprostatectomy. *Eur Urol*. 2018;74(1):107-114.

202. Cimino S, Reale G, Castelli T, et al. Comparison between Briganti, Partin and MSKCC tools in predicting positive lymph nodes in prostate cancer: a systematic review and meta-analysis. *Scand J Urol*. 2017;51(5):345-350.

203. Briganti A, Larcher A, Abdollah F, et al. Updated nomogram predicting lymph node invasion in patients with prostate cancer undergoing extended pelvic lymph node dissection: the essential importance of percentage of positive cores. *Eur Urol*. 2012;61(3):480-487.

204. Gandaglia G, Fossati N, Zaffuto E, et al. Development and internal validation of a novel model to identify the candidates for extended pelvic lymph node dissection in prostate cancer. *Eur Urol*. 2017;72(4):632-640.

205. Fossati N, Willemse PPM, Van den Broeck T, et al. The benefits and harms of different extents of lymph node dissection during radical prostatectomy for prostate cancer: A systematic review. *Eur Urol*. 2017;72(1):84-109.

206. Haglind E, Carlsson S, Stranne J, et al. Urinary incontinence and erectile dysfunction after robotic versus open radical prostatectomy: A prospective, controlled, nonrandomised trial. *Eur Urol*. 2015;68(2):216-225.

207. Ilic D, Evans SM, Allan CA, Jung JH, Murphy D, Frydenberg M. Laparoscopic and robotic-assisted versus open radical prostatectomy for the treatment of localised prostate cancer. *Cochrane Database Syst Rev*. 2017;9(9):CD009625.

208. Bolla M, Van Tienhoven G, Warde P, et al. External irradiation with or without long-term androgen suppression for prostate cancer with high metastatic risk: 10-year results of an EORTC randomised study. *Lancet Oncol*. 2010;11(11):1066-1073.

209. Vale CL, Burdett S, Rydzewska LHM, et al. Addition of docetaxel or bisphosphonates to standard of care in men with localised or metastatic, hormone-sensitive prostate cancer: a systematic review and meta-analyses of aggregate data. *Lancet Oncol*. 2016;17(2):243-256.

210. Fizazi K, Foulon S, Carles J, et al. Abiraterone plus prednisone added to androgen deprivation therapy and docetaxel in de novo metastatic castration-sensitive prostate cancer (PEACE-1): a multicentre, open-label, randomised, phase 3 study with a 2 × 2 factorial design. *Lancet*. 2022;399(10336):1695-1707.

211. Smith MR, Hussain M, Saad F, et al. Darolutamide and Survival in Metastatic, Hormone-Sensitive

Prostate Cancer. *N Engl J Med*. 2022;386(12):1132-1142.

212. Gillessen S, Attard G, Beer TM, et al. Management of Patients with Advanced Prostate Cancer: Report of the Advanced Prostate Cancer Consensus Conference 2019. *Eur Urol*. 2020;77(4):508-547.

213. Ashrafizadeh M, Ahmadi Z, Mohamadi N, et al. Chitosan-based advanced materials for docetaxel and paclitaxel delivery: Recent advances and future directions in cancer theranostics. *Int J Biol Macromol*. 2020;145:282-300.

214. de Bono JS, Oudard S, Ozguroglu M, et al. Prednisone plus cabazitaxel or mitoxantrone for metastatic castration-resistant prostate cancer progressing after docetaxel treatment: a randomised open-label trial. *Lancet*. 2010;376(9747):1147-1154.

215. de Wit R, de Bono J, Sternberg CN, et al. Cabazitaxel versus Abiraterone or Enzalutamide in Metastatic Prostate Cancer. *N Engl J Med*. 2019;381(26):2506-2518.

216. Scher HI, Fizazi K, Saad F, et al. Increased survival with enzalutamide in prostate cancer after chemotherapy. *N Engl J Med*. 2012;367(13):1187-1197.

217. Parker C, Nilsson S, Heinrich D, et al. Alpha emitter radium-223 and survival in metastatic prostate cancer. *N Engl J Med*. 2013;369(3):213-223.

218. Morris MJ, Corey E, Guise TA, et al. Radium-223 mechanism of action: implications for use in treatment combinations. *Nat Rev Urol*. 2019;16(12):745-756.

219. de Bono JS, Logothetis CJ, Molina A, et al. Abiraterone and increased survival in metastatic prostate cancer. *N Engl J Med*. 2011;364(21):1995-2005.

220. Ryan CJ, Smith MR, de Bono JS, et al. Abiraterone in metastatic prostate cancer without previous chemotherapy. *N Engl J Med*. 2013;368(2):138-148.

221. Beer TM, Armstrong AJ, Rathkopf DE, et al. Enzalutamide in metastatic prostate cancer before chemotherapy. *N Engl J Med*. 2014;371(5):424-433.

222. Hussain M, Mateo J, Fizazi K, et al. Survival with Olaparib in Metastatic Castration-Resistant Prostate Cancer. *N Engl J Med*. 2020;383(24):2345-2357.

223. Kantoff PW, Schuetz TJ, Blumenstein BA, et al. Overall survival analysis of a phase II randomized controlled trial of a Poxviral-based PSA-targeted immunotherapy in metastatic castration-resistant prostate cancer. *J Clin Oncol*. 2010;28(7):1099-1105.

224. Graff JN, Chamberlain ED. Sipuleucel-T in the treatment of prostate cancer: an evidence-based review of its place in therapy. *Core Evid*. 2015;10:1-10.

225. Kantoff PW, Gulley JL, Pico-Navarro C. Revised Overall Survival Analysis of a Phase II, Randomized, Double-Blind, Controlled Study of PROSTVAC in Men With Metastatic Castration-Resistant Prostate Cancer. *J Clin Oncol*. 2017;35(1):124-125.

226. Gulley JL, Borre M, Vogelzang NJ, et al. Phase III Trial of PROSTVAC in Asymptomatic or Minimally Symptomatic Metastatic Castration-Resistant Prostate Cancer. *J Clin Oncol*. 2019;37(13):1051-1061.

227. Antonarakis ES, Piulats JM, Gross-Goupil M, et al. Pembrolizumab for Treatment-Refractory Metastatic Castration-Resistant Prostate Cancer: Multicohort, Open-Label Phase II KEYNOTE-199

Study. *J Clin Oncol*. 2020;38(5):395-405.

228. Tucker MD, Zhu J, Marin D, et al. Pembrolizumab in men with heavily treated metastatic castrate-resistant prostate cancer. *Cancer Med*. 2019;8(10):4644-4655.

229. Karzai F, VanderWeele D, Madan RA, et al. Activity of durvalumab plus olaparib in metastatic castration-resistant prostate cancer in men with and without DNA damage repair mutations. *J Immunother Cancer*. 2018;6(1):141.

230. Lotan TL, Tomlins SA, Bismar TA, et al. Report From the International Society of Urological Pathology (ISUP) Consultation Conference on Molecular Pathology of Urogenital Cancers. I. Molecular Biomarkers in Prostate Cancer. *Am J Surg Pathol*. 2020;44(7):e15-e29.

231. Stopsack KH, Gerke T, Zareba P, et al. Tumor protein expression of the DNA repair gene BRCA1 and lethal prostate cancer. *Carcinogenesis*. 2020;41(7):904-908.

232. Sartor O, de Bono J, Chi KN, et al. Lutetium-177-PSMA-617 for Metastatic Castration-Resistant Prostate Cancer. *N Engl J Med*. 2021;385(12):1091-1103.

233. Afshar-Oromieh A, Hetzheim H, Kratochwil C, et al. The Theranostic PSMA Ligand PSMA-617 in the Diagnosis of Prostate Cancer by PET/CT: Biodistribution in Humans, Radiation Dosimetry, and First Evaluation of Tumor Lesions. *J Nucl Med*. 2015;56(11):1697-1705.

234. Partin AW, Yoo J, Carter HB, et al. The use of prostate specific antigen, clinical stage and Gleason score to predict pathological stage in men with localized prostate cancer. *J Urol*. 1993;150(1):110-114.

235. Partin AW, Mangold LA, Lamm DM, Walsh PC, Epstein JI, Pearson JD. Contemporary update of prostate cancer staging nomograms (Partin Tables) for the new millennium. *Urology*. 2001;58(6):843-848.

236. Cagiannos I, Karakiewicz P, Eastham JA, et al. A preoperative nomogram identifying decreased risk of positive pelvic lymph nodes in patients with prostate cancer. *J Urol*. 2003;170(5):1798-1803.

237. D'amico AV, Whittington R, Malkowicz SB, Schultz D, Blank K, Broderick GA. Biochemical outcome after radical prostatectomy, external beam radiation therapy, or interstitial radiation therapy for clinically localized prostate cancer. *J Clin Oncol*. 2007;25(3):305-311.

238. Škerl D, Tomaževič D, Likar B, Pernuš F. Evaluation of similarity measures for reconstruction-based registration in image-guided radiotherapy and surgery. *Int J Radiat Oncol Biol Phys*. 2006;65(3):943-953.

239. Canes D. Re: A comparison of the incidence and location of positive surgical margins in robotic assisted laparoscopic radical prostatectomy and open retropubic radical prostatectomy. *J Urol*. 2008;180(1):410-411.

240. Nyberg T, Frost D, Barrowdale D, et al. Prostate cancer risk by BRCA2 genomic regions. *Eur Urol*. 2020;78(4):494-497.

241. D'Amico AV, Whittington R, Malkowicz SB, et al. Biochemical outcome after radical prostatectomy, external beam radiation therapy, or interstitial radiation therapy for clinically localized prostate cancer. *JAMA*. 1998;280(11):969-974.

242. Brajtbord JS, Leapman MS, Cooperberg MR. The CAPRA score at 10 years: Contemporary perspectives and analysis of supporting studies. *Eur Urol*. 2017;71(5):705-709.

243. Bruzzese D, Mazzarella C, Ferro M, et al. Prostate health index vs percent free prostatespecific antigen for prostate cancer detection in men with "gray" prostate-specific antigen levels at first biopsy: systematic review and meta-analysis. *Transl Res*. 2014;164:444-451.

244. Tomlins SA, Day JR, Lonigro RJ, et al. Urine TMPRSS2:ERG plus PCA3 for individualized prostate cancer risk assessment. *Eur Urol*. 2016;70(1):45-53.

245. Haese A, de la Taille A, van Poppel H, et al. Clinical utility of the PCA3 urine assay in European men scheduled for repeat biopsy. *Eur Urol*. 2008;54(5):1081-1088.

246. Mugoni V, Ciani Y, Nardella C, Demichelis F. Circulating RNAs in prostate cancer patients. *Cancer Lett*. 2022;524:57-69.

247. Ström P, Nordström T, Aly M, Egevad L, Grönberg H, Eklund M. The Stockholm-3 model for prostate cancer detection: Algorithm update, biomarker contribution, and reflex test potential. *Eur Urol*. 2018;74(2):204-210.

248. Lebastchi∗ AH, Russell CM, Helfand AM, et al. MICHIGAN PROSTATE SCORE (MIPS): AN ANALYSIS OF A NOVEL URINARY BIOMARKER PANEL FOR THE PREDICTION OF PROSTATE CANCER AND ITS IMPACT ON BIOPSY RATES. *J Urol*. 2017;197(Supplement):e128.

249. Klein EA, Cooperberg MR, Magi-Galluzzi C, et al. A 17-gene assay to predict prostate cancer aggressiveness in the context of Gleason grade heterogeneity, tumor multifocality, and biopsy undersampling. *Eur Urol*. 2014;66(3):550-560.

250. Yonover P, Steyaert S, Cohen JJ, et al. Clinical utility study of confirms mdx for prostate cancer in a community urology practice. *J Clin Orthod*. 2019;37(7_suppl):94-94.

251. Health Quality Ontario. Prolaris Cell Cycle Progression Test for Localized Prostate Cancer: A Health Technology Assessment. *Ont Health Technol Assess Ser*. 2017;17(6):1-75.

252. Legisi L, DeSa E, Qureshi MN. Use of the Prostate Core Mitomic Test in Repeated Biopsy Decision-Making: Real-World Assessment of Clinical Utility in a Multicenter Patient Population. *Am Health Drug Benefits*. 2016;9(9):497-502.

253. Punnen S, Pavan N, Parekh DJ. Finding the Wolf in Sheep's Clothing: The 4Kscore Is a Novel Blood Test That Can Accurately Identify the Risk of Aggressive Prostate Cancer. *Rev Urol*. 2015;17(1):3-13.

254. McDunn JE, Li Z, Adam KP, et al. Metabolomic signatures of aggressive prostate cancer. *Prostate*. 2013;73(14):1547-1560.

255. Jairath NK, Dal Pra A, Vince R Jr, et al. A Systematic Review of the Evidence for the Decipher Genomic Classifier in Prostate Cancer. *Eur Urol*. 2021;79(3):374-383.

256. Tukachinsky H, Madison RW, Chung JH, et al. Genomic Analysis of Circulating Tumor DNA in 3,334 Patients with Advanced Prostate Cancer Identifies Targetable BRCA Alterations and AR Resistance Mechanisms. *Clin Cancer Res*. 2021;27(11):3094-3105.

257. van Buuren S, Groothuis-Oudshoorn K. mice : Multivariate Imputation by Chained Equations in R. *J Stat Softw*. 2011;45(3):1-60.

258. Team RC. R: A language and environment for statistical computing. R Foundation for Statistical Computing, Vienna, Austria. Published 2018. Accessed 2018. https://www.R-project.org/

259. R Core Team. R: a language and environment for statistical computing. Published online 2021. https://www.R-project.org/

260. Kuhn M, Wing J, Weston S, et al. *CARET: Classification and Regression Training; 2017*.; 2019. https://CRAN.R-project.org/package=caret

261. Therneau TM. *A Package for Survival Analysis in R*.; 2021. https://CRAN.R-project.org/package=survival

262. de Rooij M, Hamoen EHJ, Witjes JA, Barentsz JO, Rovers MM. Accuracy of Magnetic Resonance Imaging for Local Staging of Prostate Cancer: A Diagnostic Meta-analysis. *Eur Urol*. 2016;70(2):233-245.

263. Morlacco A, Sharma V, Viers BR, et al. The Incremental Role of Magnetic Resonance Imaging for Prostate Cancer Staging before Radical Prostatectomy. *Eur Urol*. 2017;71(5):701-704.

264. Grivas N, Hinnen K, de Jong J, et al. Seminal vesicle invasion on multi-parametric magnetic resonance imaging: Correlation with histopathology. *Eur J Radiol*. 2018;98:107-112.

265. Gupta RT, Faridi KF, Singh AA, et al. Comparing 3-T multiparametric MRI and the Partin tables to predict organ-confined prostate cancer after radical prostatectomy. *Urologic Oncology: Seminars and Original Investigations*. 2014;32(8):1292-1299.

266. Gupta RT, Brown AF, Silverman RK, et al. Can Radiologic Staging With Multiparametric MRI Enhance the Accuracy of the Partin Tables in Predicting Organ-Confined Prostate Cancer? *American Journal of Roentgenology*. 2016;207(1):87-95.

267. Feng TS, Sharif-Afshar AR, Wu J, et al. Multiparametric MRI Improves Accuracy of Clinical Nomograms for Predicting Extracapsular Extension of Prostate Cancer. *Urology*. 2015;86(2):332-337.

268. Nishida K, Yuen S, Kamoi K, et al. Incremental value of T2-weighted and diffusion-weighted MRI for prediction of biochemical recurrence after radical prostatectomy in clinically localized prostate cancer. *Acta radiol*. 2011;52(1):120-126.

269. Kasel-Seibert M, Lehmann T, Aschenbach R, et al. Assessment of PI-RADS v2 for the Detection of Prostate Cancer. *Eur J Radiol*. 2016;85:726-731.

270. Jäderling F, Akre O, Aly M, et al. Preoperative staging using magnetic resonance imaging and risk of positive surgical margins after prostate-cancer surgery. *Prostate Cancer Prostatic Dis*. Published online 2019. doi:10.1038/s41391-018-0116-z

271. Valentin B, Arsov C, Ullrich T, et al. Comparison of 3 T mpMRI and pelvic CT examinations for detection of lymph node metastases in patients with prostate cancer. *Eur J Radiol*. 2022;147:110110.

272. Gandaglia G, Ploussard G, Valerio M, et al. A Novel Nomogram to Identify Candidates for Extended Pelvic Lymph Node Dissection Among Patients with Clinically Localized Prostate Cancer Diagnosed with Magnetic Resonance Imaging-targeted and Systematic Biopsies. *Eur Urol*. 2019;75(3):506-514.

273. Panebianco V, Barchetti G, Simone G, et al. Negative Multiparametric Magnetic Resonance Imaging for Prostate Cancer: What's Next? *Eur Urol*. 2018;74(1):48-54.

274. Venderink W, van Luijtelaar A, van der Leest M, et al. Multiparametric magnetic resonance imaging and follow-up to avoid prostate biopsy in 4259 men. *BJU Int*. 2019;124(5):775-784.

275. Lee D, Fontugne J, Gumpeni N, et al. Molecular alterations in prostate cancer and association with MRI features. *Prostate Cancer Prostatic Dis*. 2017;20(4):430-435.

276. Li P, You S, Nguyen C, et al. Genes involved in prostate cancer progression determine MRI visibility. *Theranostics*. 2018;8(7):1752-1765.

277. Purysko A, Magi-Galluzzi C, Mian O, et al. mp28-04 Correlation between MRI phenotypes and a genomic classifier of prostate cancer. *Journal of Urology*. 2019;201(Supplement 4). doi:10.1097/01.ju.0000555709.00017.09

278. Sadun TY, Houlahan KE, Salmasi A, et al. PD05-03 Molecular hallmarks of mpmri visibility in prostate cancer. *Journal of Urology*. 2019;201(Supplement 4). doi:10.1097/01.ju.0000555063.11964.56

279. Langer DL, van der Kwast TH, Evans AJ, et al. Prostate tissue composition and MR measurements: investigating the relationships between ADC, T2, K(trans), v(e), and corresponding histologic features. *Radiology*. 2010;255(2):485-494.

280. Miyai K, Mikoshi A, Hamabe F, et al. Histological differences in cancer cells, stroma, and luminal spaces strongly correlate with in vivo MRI-detectability of prostate cancer. *Mod Pathol*. 2019;32(10):1536-1543.

281. Pachynski RK, Kim EH, Miheecheva N, et al. Single-cell Spatial Proteomic Revelations on the Multiparametric MRI Heterogeneity of Clinically Significant Prostate Cancer. *Clin Cancer Res*. 2021;27(12):3478-3490.

282. Andersen MK, Rise K, Giskeødegård GF, et al. Integrative metabolic and transcriptomic profiling of prostate cancer tissue containing reactive stroma. *Sci Rep*. 2018;8(1):14269.

283. Barron DA, Rowley DR. The reactive stroma microenvironment and prostate cancer progression. *Endocr Relat Cancer*. 2012;19(6):R187-204.

284. De Vivar AD, Sayeeduddin M, Rowley D, et al. Histologic features of stromogenic carcinoma of the prostate (carcinomas with reactive stroma grade 3). *Hum Pathol*. 2017;63:202-211.

285. Shah RB, Shore KT, Yoon J, Mendrinos S, McKenney JK, Tian W. PTEN loss in prostatic adenocarcinoma correlates with specific adverse histologic features (intraductal carcinoma, cribriform Gleason pattern 4 and stromogenic carcinoma). *Prostate*. 2019;79(11):1267-1273.

286. Su Q, Zhang B, Zhang L, et al. Jagged1 upregulation in prostate epithelial cells promotes formation of reactive stroma in the Pten null mouse model for prostate cancer. *Oncogene*. 2017;36(5):618-627.

287. Jaramillo D. Radiologists and Their Noise: Variability in Human Judgment, Fallibility, and Strategies to Improve Accuracy. *Radiology*. 2022;302(3):511-512.

288. Tolonen TT, Kujala PM, Tammela TL, Tuominen VJ, Isola JJ, Visakorpi T. Overall and worst Gleason scores are equally good predictors of prostate cancer progression. *BMC Urol*. 2011;11.

doi:10.1186/1471-2490-11-21

289. Chandramouli S, Leo P, Lee G, et al. Computer extracted features from initial H&E tissue biopsies predict disease progression for prostate cancer patients on active surveillance. *Cancers*. 2020;12(9):1-11.

290. Mobadersany P, Yousefi S, Amgad M, et al. Predicting cancer outcomes from histology and genomics using convolutional networks. *Proc Natl Acad Sci U S A*. 2018;115(13):E2970-E2979.

291. Elmarakeby HA, Hwang J, Arafeh R, et al. Biologically informed deep neural network for prostate cancer discovery. *Nature*. 2021;598(7880):348-352.

292. Diao JA, Wang JK, Chui WF, et al. Human-interpretable image features derived from densely mapped cancer pathology slides predict diverse molecular phenotypes. *Nat Commun*. 2021;12(1):1613.

10 Original publications